

الجمهورية الجزائرية الديمقراطية الشعبية  
PEOPLE'S DEMOCRATIC REPUBLIC OF ALGERIA  
وزارة التعليم العالي والبحث العلمي  
MINISTRY OF HIGHER EDUCATION AND SCIENTIFIC RESEARCH  
جامعة سعد دحلب البليدة (1)  
UNIVERSITY OF SAAD DAHLEB BLIDA (1)  
كلية العلوم- دائرة الفيزياء  
Faculty of Science- Department of Physics



**MASTER DIPLOMA THESIS  
IN PHYSICS**

Branch: Nano-Physics

**THEME**

**DESIGN OF TEMPERATURE SENSOR BASED ON SAW  
TRANSDUCER**

**Conception d'un Capteur de Température à Base de  
Transducteur SAW**

**Presented by: BEHLOULI ASSIA**

*Presented on 25 / 09 / 2022 to the jury composed of*

Dr. AMRANE Amine	MCB	USDB	President
Dr. SERHANE Rafik	DR	CDTA	Thesis Director
Dr. HASSEIN BEY Abdelkader	MCB	USDB	Examiner

September 2021/2022



## ملخص

في هذا العمل، قمنا بنمذجة دراسة تجريبية لمستشعر درجة حرارة الموجة الصوتية السطحية عن طريق محاكاة عددية باستخدام طريقة العناصر المحدودة (FEM) تحت أداة Comsol متعددة الفيزياء، يعتمد هذا المستشعر على المادة الكهرضغطية وهي AIN على ركيزتين Pt/AIN/Si و Pt/AIN/Pt/Si، تعمل مستشعرات درجة الحرارة هذه في درجات حرارة تصل إلى 500 درجة مئوية. أظهرت النتائج أن التردد المركزي للرنان في درجة حرارة الغرفة هو 445 ميغاهرتز، ويتغير هذا التردد خطياً مع درجة الحرارة. قيمة معامل درجة الحرارة للتردد (TCF) هي -40.54 جزء في المليون/درجة مئوية. هذا يظهر حساسية جيدة لدرجة الحرارة، ويجعلها مناسبة لتطبيقات قياس درجة الحرارة. يزداد معامل الاقتران الكهروميكانيكي ( $k^2$ ) مع درجة الحرارة ويلاحظ وجود علاقة خطية. معامل درجة الحرارة  $k^2$  هو 821 جزء في المليون / درجة مئوية محسوبة من المطابقة الخطية. تبلغ قيمة  $k^2$  0.35% عند درجة حرارة الغرفة، وترتفع إلى 0.37% عند 500 درجة مئوية. لقد بحثنا أيضاً في تكوين خط تأخير SAW يعمل في المجال الزمني بهدف استخدامه في تطبيقات أجهزة الاستشعار اللاسلكية.

الكلمات الدلالية: مستشعرات، MEMS، التصميم، محولات SAW.

## Resumé

Dans ce travail, nous avons modélisé une étude expérimentale d'un capteur de température à ondes acoustiques de surface par une simulation numérique en utilisant la méthode des éléments finis (FEM) sous l'outil Comsol multiphysique, ce capteur à base du matériau piézoélectrique qui est l'AIN avec deux configurations Pt/AIN/Si et Pt/AIN/Pt/Si, ces capteurs de température fonctionnent aux températures, allant jusqu'à 500 °C. Les résultats montrent que la fréquence centrale du résonateur à température ambiante est de 445 MHz, la variation de cette fréquence avec la température est linéaire, et la valeur du coefficient de température pour la fréquence (TCF) est de -40.54 ppm/°C. Ce qui montre une bonne sensibilité à la température, et le rend appropriée pour les applications de détection et de mesure de la température. Le coefficient de couplage électromécanique ( $k^2$ ) augmente avec la température et une relation linéaire est observée. le coefficient de température de  $k^2$  est 821 ppm/°C calculé à partir de l'ajustement linéaire. La valeur de  $k^2$  est 0.35% à température ambiante, et il augmente à 0.37% à 500°C. Nous avons également étudié une configuration d'une ligne à retard SAW fonctionnant dans le domaine temporel dans la perspective de son utilisation dans les applications de capteurs sans fil.

**Mots clés :** Capteurs, MEMS, Conception, Transducteurs SAW.

## Abstract

In this work, we modeled an experimental study of a surface acoustic wave temperature sensor by a numerical simulation using the finite element method (FEM) under the Comsol multiphysics tool, this sensor based on the piezoelectric material which is AIN with two configurations Pt/AIN/Si and Pt/AIN/Pt/Si, these temperature sensors operate at temperatures up to 500°C. The results show that the central frequency of the resonator at room temperature is 445 MHz, the variation of this frequency with temperature is linear, and the value of the temperature coefficient for frequency (TCF) is -40.54 ppm/°C. This shows good temperature sensitivity, and makes it suitable for temperature sensing and measurement applications. The electromechanical coupling coefficient ( $k^2$ ) increases with temperature and a linear relationship is observed. the temperature coefficient of  $k^2$  is 821 ppm/°C calculated from the linear fit. The value of  $k^2$  is 0.35% at room temperature, and it increases to 0.37% at 500°C. We have also investigated a configuration of a SAW delay line operating in the time domain with a view to its use in wireless sensor applications.

**Keywords:** Sensors, MEMS, Design, SAW Transducers

## *Dedication*

*I dedicate this work:*

*To my father;*

*To my mother;*

*To my sister;*

*To my Husband;*

*And of course, to my little prince, my son ADEM*

*And to all my Family and my friends.*

# *Acknowledgements*

*This work was performed within the "MEMS & Sensors" team of the Microelectronics and Nanotechnology Division (D.M.N.) of the Center for the Development of Advanced Technologies (C.D.T.A.).*

*The realization of this thesis was possible thanks to the help of several people to whom I would like to express my gratitude.*

*First, I would like to express my gratitude to the director of this thesis, **Dr. SERHLANE RAFIK** for his patience, his availability and especially his judicious advices, which contributed to feed my reflection. A big thanks for his advices concerning my writing style, they greatly facilitated my work.*

*I would also like to thank all professors of the University of Saad dahleb who provided me with the necessary tools for the success of my university studies.*

*I would especially like to thank the president of this jury **Dr. Amrane Amine** and the head of this speciality **Dr. Abdelkader Hassen-Bey**, who was the first to introduce me to the field and the subject and who also guided me throughout my thesis.*

*I would like to express my gratitude to the friends and colleagues who gave me their moral and intellectual support throughout my process.*

*I will never forget that this work would not have been possible without the support of my small and large family, who have all given me their encouragement and support in the most difficult moments. I thank especially my parents, my sister: Imene, my husband: Ayoub and my child: Adam for their support*

# Summary

## LIST OF FIGURES

## LIST OF TABLES

<b>General Introduction</b> .....	12
<b>Chapter 1: State of the art and Generality: from SAW transducer to temperature sensor.</b>	<b>14</b>
<b>1. Introduction</b> .....	<b>15</b>
<b>2. MEMS Technology</b> .....	<b>15</b>
<b>3. Surface acoustic waves and transducer (SAW and IDT)</b> .....	<b>17</b>
3.1. Surface acoustic waves (SAW) .....	17
3.1.1. Types of SAW .....	17
3.1.1.1. Raleigh waves.....	18
3.1.1.2. Bleustein-Gyilave waves .....	18
3.1.1.3. STW waves (Surfae Transverse waves) .....	19
3.1.2. SAW resonator .....	20
3.1.3. Operating principale of SAW .....	20
3.2. Interdigital transducers (IDTs).....	21
3.2.1. Operating prancipale of the (IDT) .....	22
<b>4. Surface acoustic wave transducers</b> .....	<b>23</b>
<b>5. SAW devices</b> .....	<b>24</b>
<b>6. SAW sensors</b> .....	<b>26</b>
6.1. Operating principales of SAW sensors.....	26
6.2. SAW temperature sensor .....	27
<b>7. State of the art on the modeling and simulation of surface acoutic wave sensor by the finite element method(FEM)</b> .....	<b>28</b>
<b>8. Piezoelectricity</b> .....	<b>29</b>
8.1. What is the Piezoelectricity ? .....	29
8.2. Piezoelectricity Materials .....	30
8.3. Piezoelectricity Equations.....	33
8.4. Field of applications.....	32
8.5. Aluminum Nitride (AlN) .....	32
8.5.1. The material AlN .....	32
8.5.2. The crystalline structure of AlN .....	33
8.5.3. Mechanical propertes.....	34
8.5.4. Coefficient of elasticity.....	34
8.6. Aluminum nitride (AlN): Piezoelectric thin film material contact .....	35

8.7. Applications of AlN .....	35
<b>9. Conclusion.....</b>	<b>36</b>
<b>Chapter 2: The Theory of SAW .....</b>	<b>37</b>
1. Introduction .....	38
2. The history of Impulse Response test method .....	38
3. Definition of Impulse Response .....	39
3.1. Why is it useful?.....	39
3.2. Impulse Response Theory .....	40
4. Relationship between Transducer Geomerty and Transducer Impulse Response .....	41
4.1. Frequency resonance of IDT .....	42
5. Thermal strain effect .....	45
5.1. TCF constant and sensivity of the sensor .....	47
5.2. Parameters to be considered in simulation of a SAW temperature sensor .....	48
6. Conclusion .....	50
<b>Chapter 3: Simulation with Comsol Software .....</b>	<b>51</b>
1. Introduction .....	52
2. physical modeling finit elements.....	52
2.1. Presentation of COMSOL Multiphysics software .....	54
3. 2D simulation of SAW (modal and harmonic study of cell).....	92
3.1. Modal study of a cell .....	92
3.2. Geomety of the SAW structure .....	96
4. Study of the global structure of the SAW resonator .....	60
4.1. Simulation procedure of the SAW by Comsol .....	60
4.2. Choise of the dimension of the simulation space .....	60
4.3. Choice of physics .....	60
4.3.1. Geometric parameters of the model .....	60
4.3.2. The geometry of the SAW Structure .....	61
4.3.3. Materials constituting the structure .....	62
4.3.3.1. Silicone (Si).....	62
4.3.3.2. Platinuim (Pt) .....	63
4.3.3.3. Alumium nitride (AlN).....	63
4.3.3.4. IDTs electrodes with Pt on Ti.....	64
4.3.3.4.1. Platimum (Pt) .....	64
4.3.3.4.2. Titanum (Ti).....	65
4.3.4. Electrical boundary condition (grounded, Terminal) .....	65
4.3.5. Mechanical Boundary condition.....	65

5. Meching of the structure .....	66
6. Definition of the frequency rang of the study.....	67
7. The electrical and mechanical response of SAW resonator.....	67
8. Conclusion.....	68
<b>Chapter 4: Results and Descusion.....</b>	<b>69</b>
1. Introduction.....	70
2. Structure ( <i>Pt/AlN/Pt/Si</i> ).....	70
2.1. Total mechanical displacement field .....	70
2.2. The electrical admittance.....	71
2.3. The $S_{11}$ -Scattering parameter.....	72
2.4. The electromechanical coupling factor ( $K^2eff$ ).....	75
2.5. Quality factor (Q-factor) of Pt/AlN/Pt/Si SAW structure.....	77
2.6. Sensitivity of the sensor .....	78
3. Structure ( <i>Pt/AlN/Pt/Si</i> ).....	79
4. Total mechanical displacement field.....	79
4.1. The electrical admittance $Y_{11}$ .....	80
4.2. The $S_{11}$ -Scattering paramter.....	80
4.3. The electromechanical coupling factor ( $K^2eff$ ) .....	81
4.4. Quality factor (Q-factor) .....	82
4.5. Sensitivity of the sensor .....	83
5. Copmaraison of the literature and the experimental results (Chuian Li) and our theoretical results (Simulation).....	84
6. Dlay line -type SAW sensor .....	88
6.1. What does delay line mean.....	88
6.2. Simulation of ( <i>Pt/Aln/Si</i> ) SAW delay line.....	89
7. Conclusion.....	90
<b>General Conclusion.....</b>	<b>95</b>
<b>Appendix (A).....</b>	<b>96</b>
<b>Bibliographical Reference.....</b>	<b>97</b>



# LIST OF FIGURES

## Chapter 1

<b>Figure 1.1:</b> The four families of MEMS .....	17
<b>Figure 1.2:</b> Propagation and polarization of the Rayleigh wave.....	18
<b>Figure 1.3:</b> displacement of particles during the propagation of a Bleustein-Gulyaev wave .....	19
<b>Figure 1.4:</b> Propagation of shear waves shear horizontal-SAW [SH-SAW].....	20
<b>Figure 1.5:</b> (a)- Configuration of a two-port SAW resonator, (b)- one-port SAW resonator .....	21
<b>Figure 1.6:</b> a typical design of a one-port SAW resonator .....	22
<b>Figure 1.7:</b> Geometrical characteristics of a SAW device $\lambda$ = wave length, $W$ = aperture, $L$ = length..	23
<b>Figure 1.8:</b> Principle and characteristics of an acoustic wave device.....	24
<b>Figure 1.9 :</b> A SAW resonator /filter uses interdigital transducers mountes on a piezoelectric substrate to generate surface acoustic waves in the space between the transducers ; producing frequency dependent responce at the output Image Source (Digi-key electronics) .....	24
<b>Figure 1.10:</b> (a)-SAW delay line, (b)and(e) One-port SAW resonator, (d)ow-port resonator .....	26
<b>Figure 1.11:</b> Setup for mesuring SAW sensor characterstic using network analyzer .....	28
<b>Figure 1.12:</b> The piezo-electronic generation of charge due to mechanical stress (direct effect, leftt) And strain caused by the application of an electric field (convers effect, right).....	30
<b>Figure 1.13:</b> Hexagonal mesh composed of silicon atomes and oxygen atomes before and after a mechanical stress.....	31
<b>Figure 1.14:</b> (a)Aluminum Nitrid nano pawder,(b) and aluminum nitrid powder .....	34
<b>Figure 1.15:</b> Structure wurzite (a) and Zn blende of aluminum nitride.....	34
<b>Figure 1.16:</b> 2H hexagonal structure of aluminum nitride: the aluminum atomes (in yellow) and the nitrogen atomes (in grey) both have a tetrahedral environement.....	35

## Chapter 2

<b>Figure 2.1 :</b> Impulse response diagram .....	40
<b>Figure 2.2:</b> Impulse response (time domain response) and transfer function (frequency response) ..	41
<b>Figure 2.3:</b> Transfer function.....	41
<b>Figure 2.4:</b> Symbolic diagram of a SAW .....	43
<b>Figure 2.5:</b> Impulse response, (a) of the IDT electrode system (b)-of the entire SAW delay line .....	44
<b>Figure 2.6:</b> Impulse response of an IDT .....	45
<b>Figure 2.7:</b> $S_{11}$ resturn loss (reflection) $S_{21}$ insertion loss (transmission).....	47

## Chapter 3

<b>Figure 3.1:</b> Comsol multiphysics software interface .....	56
<b>Figure 3.2:</b> Add for comsol multiphysics .....	56
<b>Figure 3.3:</b> Unit cell SAW Structure. ....	57
<b>Figure 3.4:</b> Geomety of a SAW resonator cell, with the periodicity condition.....	59
<b>Figure 3.5:</b> Mechanical displacement field in SAW unit cell (symmetric an antisymmetric raylight mode) .....	59
<b>Figure 3.6:</b> The SAW mechanical displacement composed ( $u_k$ , $u_z$ ) detaild by a cut line in the strucure	60
<b>Figure 3.7:</b> The different parts constituating the simulated SAW structure .....	62
<b>Figure 3.8:</b> Assignmment of Si to the substrate region .....	63
<b>Figure 3.9:</b> Assignmment of Pt as buffer layer between Si and AlN .....	64
<b>Figure 3.10:</b> Assignmment of AlN to the substrate region.....	65

<b>Figure 3.11:</b> Assignment of Pt electrode .....	66
<b>Figure 3.12:</b> Assignment of Ti electrode.....	66
<b>Figure 3.13:</b> Definition of the mechanical boundary condition PML .....	67
<b>Figure 3.14:</b> Mesh of the structure .....	68

## Chapter 4

<b>Figure 4.1:</b> Geometry the SAW structure $Pt/AlN/Pt/Si$ ( $N_b=50, N_p=50$ ) .....	70
<b>Figure 4.2:</b> Mechanical displacement field of the SAW structure $Pt/AlN/Pt/Si$ at 445 MHz .....	71
<b>Figure 4.3:</b> ( $Y_{11}$ ) electrical admittance amplitude of the SAW temperature sensor for different temperature.....	72
<b>Figure 4.4:</b> Extraction of $S_{11}(f)$ from $Y_{11}(f)$ . ( $S_{11}$ ) from ( $Y_{11}$ ) .....	72
<b>Figure 4.5:</b> ( $S_{11}$ ) electrical response of the temperature sensor for different values of temperature ...	73
<b>Figure 4.6:</b> Characteristic of SAW resonator at room temperature .....	74
<b>Figure 4.7:</b> Parametric sweep Pt, Cijkl.....	74
<b>Figure 4.8 :</b> Parametric sweep Si,Cijkl .....	75
<b>Figure 4.9:</b> Parametric sweep AlN,Cijkl .....	75
<b>Figure 4.10:</b> The electromechanical coupling coefficient formula .....	76
<b>Figure 4.11:</b> The electromechanical coupling of the sensor for different values of temperature.....	76
<b>Figure 4.12:</b> Variation of $k^2$ versus temperature for SAW resonator.....	77
<b>Figure 4.13:</b> The Quality factor of the temperature sensor for different values of temperature.....	77
<b>Figure 4.14:</b> Quality factor versus temperature for SAW resonator .....	78
<b>Figure 4.15:</b> Resonance frequency variation versus temperature for SAW sensor .....	78
<b>Figure 4.16:</b> Geometry of the SAW structure $Pt/AlN/Si$ ( $N_b=50, N_p=50$ ).....	79
<b>Figure 4.17:</b> Mechanical displacement field of structure $Pt/AlN/Si$ at 418.7 MHz .....	79
<b>Figure 4.18:</b> ( $Y_{11}$ ) electrical admittance of the temperature sensor for different values of $T^\circ$ .....	80
<b>Figure 4.19:</b> ( $S_{11}$ ) electrical response of the $T^\circ$ sensor for different values of $T^\circ$ .....	80
<b>Figure 4.20:</b> ( $S_{11}$ ) performance at room temperature ( $N_b=10$ ) .....	81
<b>Figure 4.21:</b> The electromechanical coupling of the $T^\circ$ sensor for different values of $T^\circ$ .....	82
<b>Figure 4.22:</b> Relative variation of $K^2$ versus $T^\circ$ measured on SAW resonator of the structure $Pt/AlN/Si$ .....	82
<b>Figure 4.23:</b> The quality factor of the Temperature .....	82
<b>Figure 4.24:</b> Quality factor variation versus Temperature for SAW resonator .....	83
<b>Figure 4.25:</b> Resonance frequency variation versus temperature for $Pt/AlN/Si$ SAW sensor .....	83
<b>Figure 4.26:</b> Comparison of our simulated results to experimental data of Chuin Li <i>et al.</i> of the structure $Pt/AlN/Pt/Si$ .....	84
<b>Figure 4.27:</b> Influence of $T^\circ$ on coupling coefficient of the structure $Pt/AlN/Si$ .....	85
<b>Figure 4.28:</b> Influence of $T^\circ$ on coupling coefficient of the structure $Pt/AlN/Pt/Si$ .....	85
<b>Figure 4.29:</b> A schematic layout of reflective delay line surface acoustic wave sensor (a) and the Corresponding impulse response of the sensor (b).....	86
<b>Figure 4.30:</b> Integration principle of the SAW sensor. ....	87
<b>Figure 4.31:</b> SAW structure $Pt/AlN/Si$ delayline by comsol software .....	88
<b>Figure 4.32:</b> Mechanical displacement of delay line SAW sensor .....	89
<b>Figure 4.33:</b> Simulated ( $S_{11}$ ) in the frequency domain was obtained by comsol .....	90
<b>Figure 4.34:</b> Simulated ( $S_{11}$ ) in time domain using Matlab program .....	90
<b>Figure 4.35:</b> Resume of delay line SAW sensor .....	91
<b>Figure 4.36:</b> The mechanical displacement for different $N_b$ of Bragg's reflector .....	92

# **LIST OF TABLS**

## **Chapter 1**

**Table (1.1):** Areas of application according to their working frequency ..... 32

## **Chapter 2**

**Table (2.1):** (AlN) and (Si) physical parameters used in the temperature sensing model. .... 49

## **Chapter 3**

**Table (3.1):** Region defining the piezoelectric layer AlN ..... 57

**Table (3.2):** Region defining the Si substrate layer ..... 57

**Table (3.3):** Region defining the electrode with Pt ..... 57

**Table (3.4):** Region defining the electrode with Ti ..... 57

**Table (3.5):** Region defining the Pt layer ..... 57

**Table (3.6):** Geometrical parameters of the SAW model ..... 61

**Table (3.7):** physical properties of Si ..... 63

**Table (3.8):** physical properties of Pt ..... 63

**Table (3.9):** physical properties of Ti ..... 65

## **Chapter 4**

**Table (4.1):** The new parameters for delay line ..... 88

# General Introduction

MEMS or microelectromechanical systems are technologies that benefit from infinitely light weight, high performance, ease of mass production, and low cost.

Surface Acoustic Wave (SAW) devices are considered as type of this system due to the continuous electrical and mechanical interactions that occur during wave propagation on the surface of piezoelectric substrate. In addition to being small, simple, and rugged, surface acoustic wave devices have the advantage of being passive. (No battery required), remote access (wireless), cheap if manufactured on a large scale.

Since its first explanation by Rayleigh in 1885[1], SAWs have found wide applications in industries and common life. Particularly in the field of sensor, SAW devices have been fabricated for multiple purposes, including chemical and physical sensors working in gas and liquid phases, temperature sensors, pressure sensors, biology sensors, and so on.

Over the last few years, applications of SAW devices for sensing require devices with lot of performances, like higher frequency response, good stability and lower insertion loss, together with realizing the wireless transmission, wireless passive sensing.

Piezoelectric sensors for high-or less temperatures application are in great demand, particularly in the automotive, aerospace, and energy industries [2]. For these reasons, SAW devices are well suited for wireless temperature measurements.

In this study, we reporte a new SAW temperature sensor based on AlN piezoelectric material and a scilisium (Si) as substrate. This sensor can perform measurements in environments with temperatures as high as 400 °C [3].

This work confirms that these materials are good candidates for manufacturing SAW based temperature sensors, due to their high acoustic velocity and suitable electromechanical coupling coefficient and its quality factor. Moreover they make possible to achieve a hight value of Temperature Coefficient of Frequency (TCF) to enhance the sensitivity of the sensor to the temperature changes.

This work is based on the evaluation of the  $S_{11}$  scattering parameter of the sensor, which is characterized by the shift in the central frequency while the

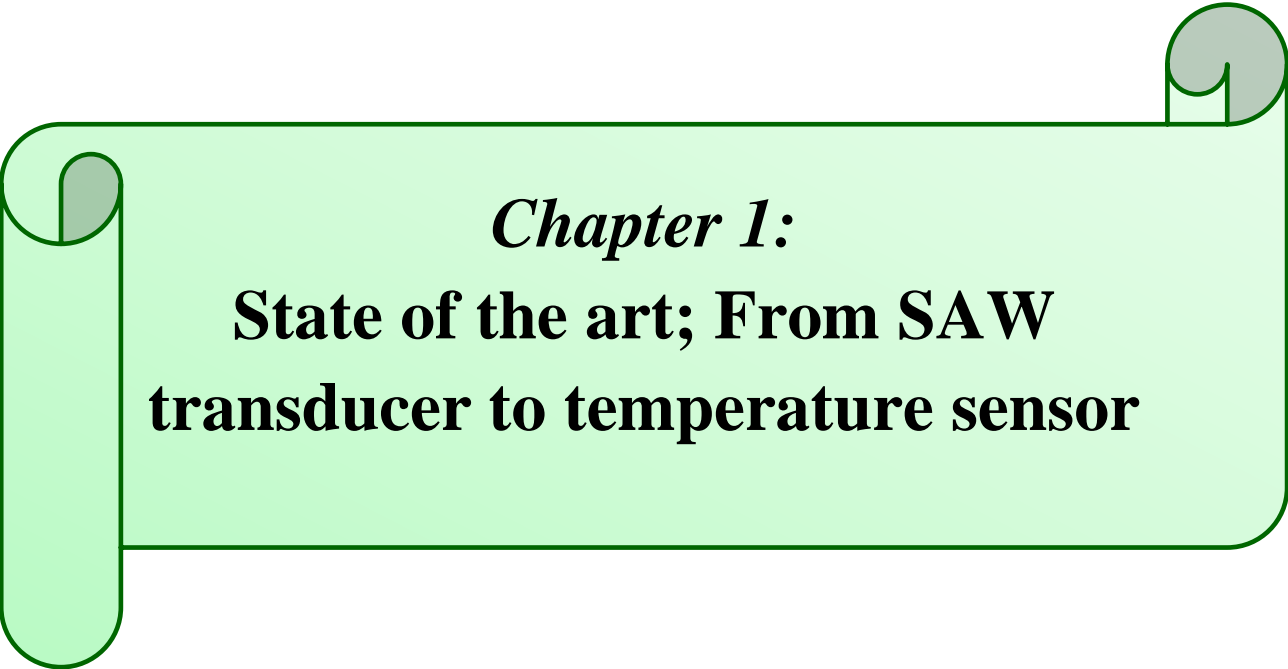
temperature changes. The decay of frequency when varying the temperature is highlighted, and demonstrate the origin of the temperature sensing, we also, investigate the electromechanical coupling factor ( $k^2$ ). The performances of the (SAW) device in terms of sensitivity, quality factor are studied under variation of the temperature in the range of -25 °C to 200 °C. The studied SAW resonator has a center frequency situated in the ISM (Industrial, Scientific and Medical) frequency bands; this frequency resulted from the chosen design parameters. This modelisation is realized by the finite element method (FEM), 2D simulations under COMSOL multiphysics software.

In addition to the general introduction, this thesis is divided into four chapters with a general conclusion. The first chapter (1) provides the reader with the basic knowledge necessary for understanding the subject of our work. Since the historical approach is often the best way to understand the state of the art of an already mature technology, we have chosen to approach the SAW technology from this point of view, trying to highlight the major innovations that have marked the history of SAW devices and have gradually led to the development of the sensors studied today, without forgetting to present some generalities of the important piezoelectric material used in this study, which is the AlN (Aluminum nitride).

Chapter (2) presents the theoretical study of SAW and briefly explains the impulse response in signal processing, using the inverse Fourier transform.

Chapter (3) is reserved to the development of the SAW temperature sensor model, coupled to the 2D finite elements method simulation. We perform a modal study on the SAW unit cell and a harmonic study on the whole SAW structure, to determine the response of the sensor. Then, we make a comparison with the experimental data from literature.

In chapter (4), we determine the response of the sensor and its sensitivity, we discuss all obtained results and we conclude by the important points that we have obtained. Finally, we finish the manuscript with a general conclusion and some perspectives.



*Chapter 1:*  
**State of the art; From SAW  
transducer to temperature sensor**

## 1. Introduction

In order to realize a sensor function, MEMS has been identified as one of the most promising technologies for the 21<sup>st</sup> Century, the use of microsystems has been developed because of their small size in parallel with a high sensitivity and precision linked to miniaturization, comprising one or more mechanical functions and using electricity as a power source.

SAW devices considered to be the earliest type of MEMS since they use mechanical acoustic waves, which are launched and detected electrically. Surface acoustic wave devices and technology started in 1965 with the concept of a thin metal interdigital transducer IDT on a polished piezoelectric substrate [4].

Since this technology is based on transducers IDT, we will present their operating principle, their different types, and their frequency response. All this will be described it in the first part of this chapter, the second and third parts present a bibliographical study approach of the piezoelectricity concept and the main materials used as piezoelectric active area. We review the main configurations adopted for the different types of SAW sensors.

## 2. MEMS Technology:

MEMS devices are beginning to touch almost every area of science and technology. It's a technology that's growing more and more significant in a number of industries. [6] such as wireless communication, automotive design, and entertainment and light wave systems. MEMS devices have a number of desirable attributes to offer to the systems architect such as small size, high speed, low power, and a high degree of functionality. In particular, many researchs believe that the size scale at which these machines work well make them a particularly good match to optics problems where the devices, structures, and relevant wavelengths range in size from one to several hundred microns.

These devices or systems have the ability to sense, control and actuate on the micro scale [7].

The experience gained from the early MEMS applications has made it an enabling technology for new biomedical applications (often referred to as bio-MEMS) and wireless communications comprised of both optical, also referred to as micro-optoelectromechanical systems (MOEMS), and radio frequency (RF) MEMS.

Advances in MEMS micro-technology (based on the principle of photolithography) have led to an explosion of applications and a segmentation of the field. There are four families associated with their application frameworks that is

showing in **figure 1.1**.

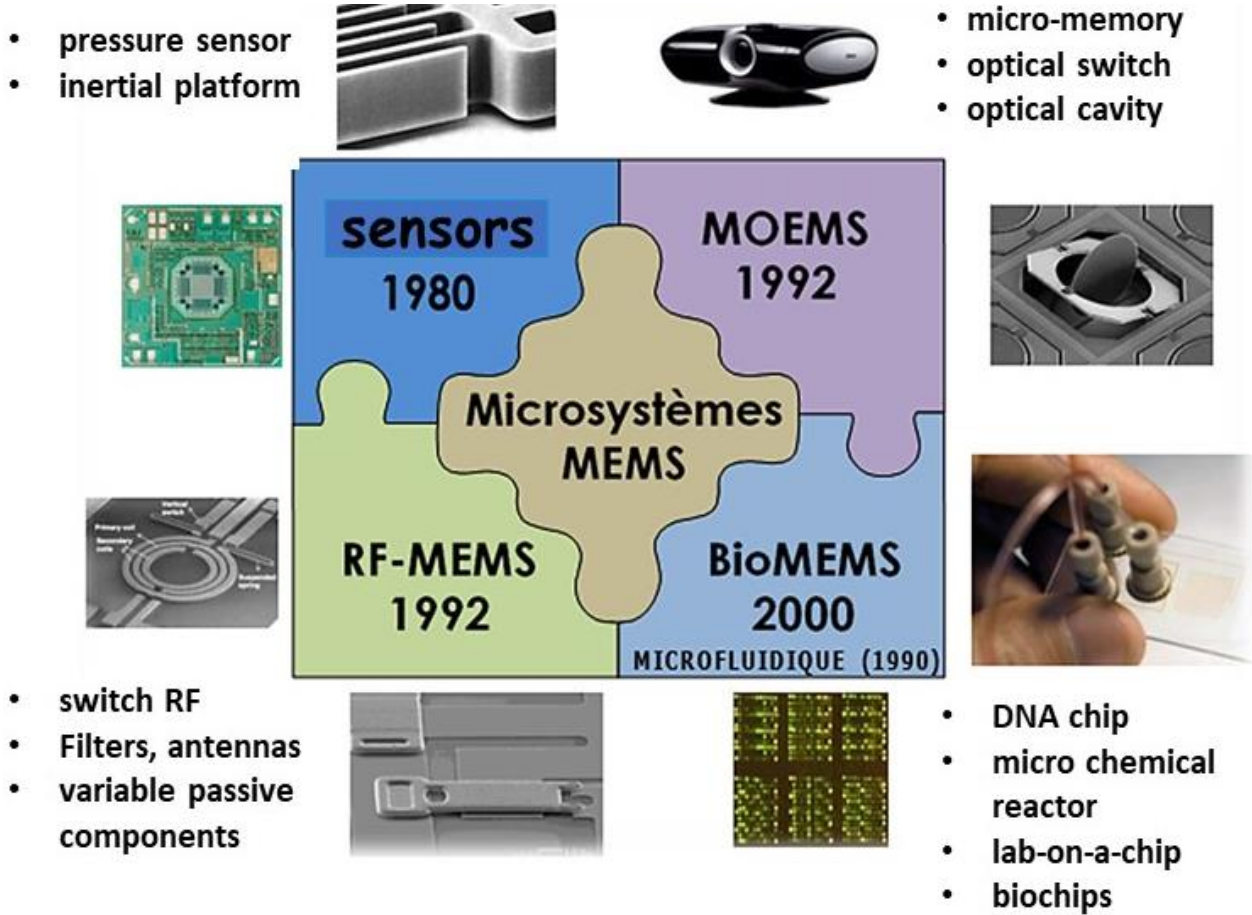


**Figure 1.1:** The four families of MEMS.



### **3. Surface Acoustic waves and transducers (SAW and IDT):**

#### **3.1. Surface acoustic waves (SAW):**

The microelectromechanical systems (MEMS) industry has seen phenomenal growth and a subsequent increase in the demand for high quality components. Surface acoustic wave (SAW) devices form an important part of MEMS family. A SAW is an acoustic wave traveling along the surface of a material exhibiting elasticity. The amplitude of these waves is higher at the surface and decreases exponentially along the depth of the substrate. The basic principle behind SAW generation and detection is the well-known piezoelectricity. In piezoelectric materials, electrical charge is produced when mechanically strained and vice versa. The SAW devices exhibit a frequency response according to the properties of surface acoustic waves propagating over their substrate.

SAW devices are one of the major components in many communication systems such as satellite receivers, remote control units, keyless entry system, radio frequency identification (RFID), television sets, and mobile phones...etc. SAW devices are also used as micro actuators such as SAW nano-stepping motors and SAW micro pumps. Sensors based on SAWs find diverse applications ranging from gas and vapor detection to strain and pressure measurement. Onboard antennas can be integrated within the SAW devices and applied in sensors for remote and inaccessible locations [8]. There is always a need for SAW sensors such as improvement in sensitivity, selectivity, and fabrication techniques.

##### **3.1.1. Types of surface acoustic waves:**

Three modes of surface can be distinguished, *Rayleigh wave*, *Bleustein Gulyaev wave* (SH-SAW: shear Horizontal SAW), and *STW* (*Surface Transverse Wave*). Of these three types, the first two are distinct from the third. Indeed, the Rayleigh and Bleustein-Gulyaev waves propagate freely along the surface, while the STW waves are guided by engraved grooves or metallic strips deposited on the surface [9].

### 3.1.1.1. Rayleigh waves:

Discovered by Lord Rayleigh in 1885, the Rayleigh wave propagates in a semi-infinite medium [10]. The depth of penetration of this type of wave in the substrate, so the distance at which the acoustic displacements are zero, is of the order of  $2\lambda$  (are guided along the surface of the material and their amplitude fully decreases with the distance of penetration). This is why Rayleigh waves are also known as surface waves SAW.

Rayleigh Wave

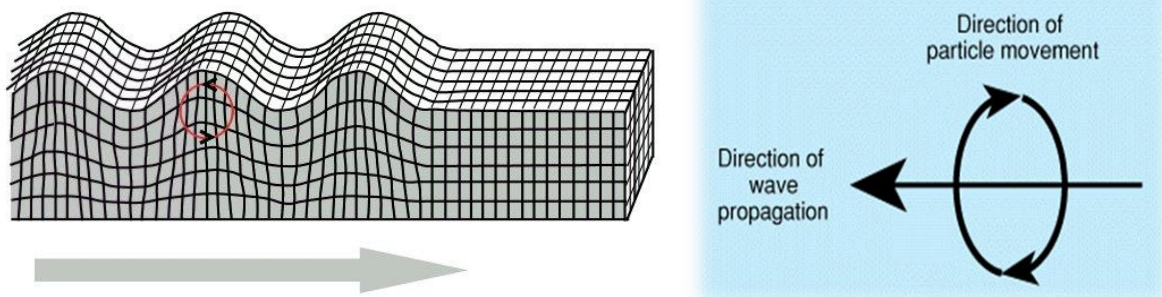


**Figure 1.2:** Propagation and polarization of the Rayleigh wave

In an isotropic medium, the polarization of Rayleigh waves is "elliptical" like the seismic wave: where the acoustic displacement on the ground rolls in an elliptical motion, similar to ocean waves. In a homogeneous half-space, the polarization is always retrograde, i.e., the rolling motion is in the opposite direction to the Rayleigh wave propagation. [figure 1.2.](#)

In an anisotropic medium, the acoustic displacements occur in a plane that is tilted with respect to the sagittal plane, the polarization is said to be "quasi-elliptical".

### 3.1.1.2. Bleustein-Gulyaev waves:

A strongly piezoelectric material with certain symmetries can guide a purely horizontal transverse surface horizontal surface wave called Bleustein-Gulyaev wave [11]. The depth penetration is greater than in the case of a Rayleigh wave, of the order of  $100\lambda$ . In addition, the more piezoelectric the material, the more confined the Bleustein-Gulyaev wave in the surface ([Figure 1.3](#)) [12]. These waves are also known under the name "SH-SAW" (Shear Horizontal Surface Acoustic Wave), for "transverse horizontal surface acoustic wave" [see figure 1.4.](#)

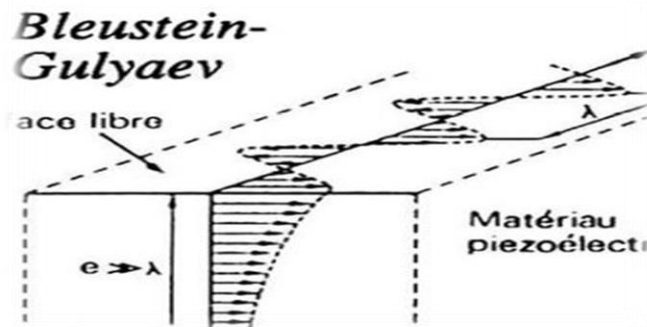


**Figure 1.3:** Displacement of particles during the propagation of a Bleustein-Gulyaev wave.

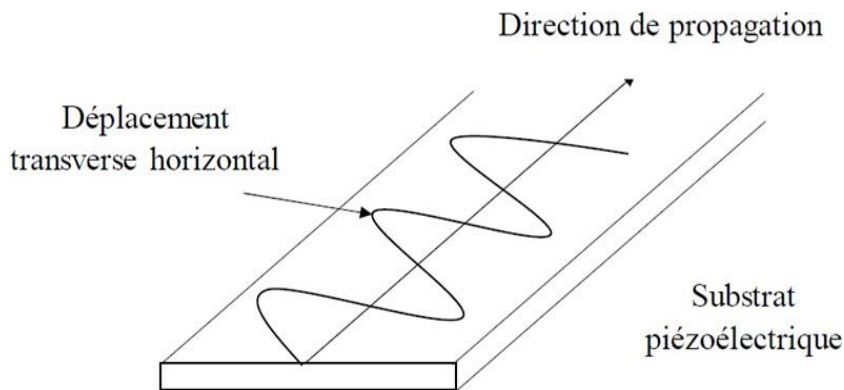


**Figure 1.4 :** Propagation of shear waves shear horizontal-SAW [SH-SAW].

### 3.1.1.3. STW waves (Surface Transverse Wave):

Surface Transverse Wave (STW) waves are to be differentiated from other types of waves, insofar as their propagation requires a trapping on the surface. It is sometimes possible to generate a wave, especially in a quartz substrate of simple cut rotation [13]. This wave, which tends to go towards the volume of the material, is called SSBW (Surface Skimming Bulk Wave), for "subsurface creeping bulk wave" Therefore, it is not strictly a surface wave.

However, if the propagation path is, a periodic pattern of grooves etched or engraved on the substrate, or if metal strips are deposited on the surface, they will be captured on the surface. Can then get the wave surface guide, this is the STW wave.

### 3.1.2. SAW resonator:

SAW resonators are devices that can be **one-port** (single/mono port) or **two-port** (dual/bi port). One-port devices consist of a single IDT to generate and receive the acoustic wave, with two reflector arrays on each end. These two gratings reflect the surface acoustic wave and generate a standing wave. **Figure 1.5(a)** shows a typical configuration of a single-port SAW resonator. Single ports are mainly used in oscillator circuits, such as VCO or Colpitts oscillators.

The two-port SAW resonators consist of an input IDT that generates the surface wave, and an output IDT that recovers this wave. As with single-port resonators, two reflector arrays are installed on the edges to reflect and confine the wave between the two IDTs. The configuration is shown in **figure 1.4(b)** Dual-port devices are primarily used as band pass filters.

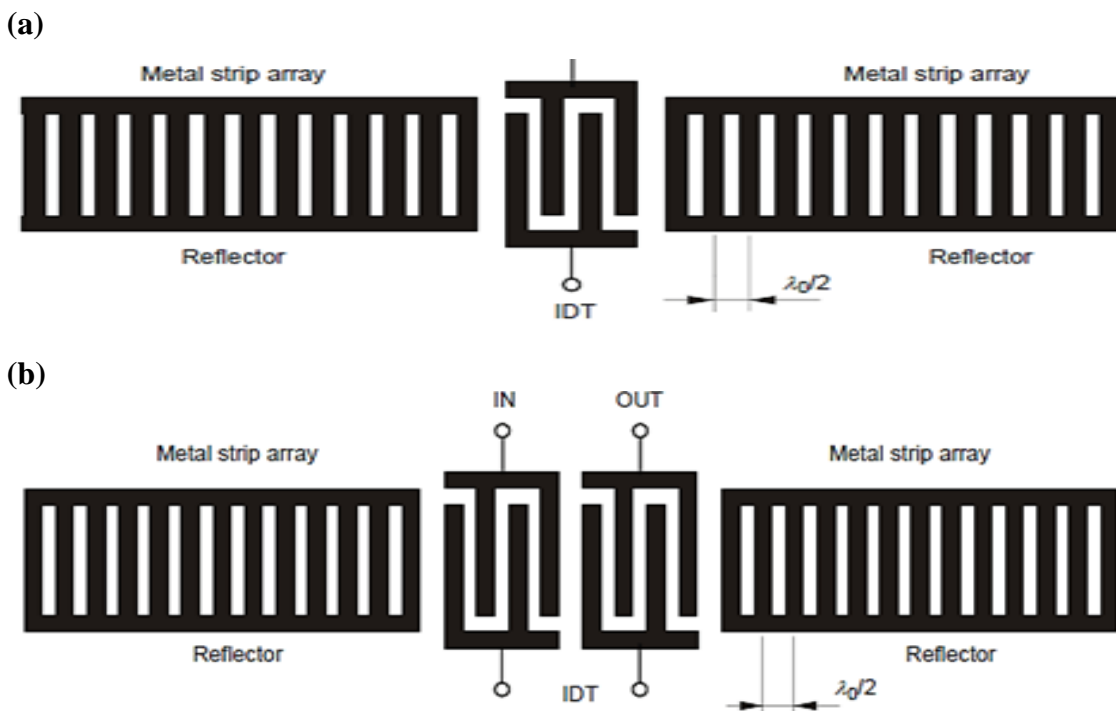


**Figure 1.5:** (a) Configuration of a one-port SAW resonator, (b) Configuration of a two-port SAW resonator,

### 3.4 Operating principle of SAW devices

SAW devices are made of piezoelectric materials on which a periodic comb-shaped interdigital transducer (IDT) pattern is developed by a photolithographic or other process. These electrodes are generally made of inert metals or alloys, for example Au, Cr/Au/Cr, Al, Pt, etc.

When an AC voltage is applied to these IDTs, an acoustic wave is generated which travels across the crystal surface, however, perpendicular to the IDTs but in an away direction. The velocity of surface waves is  $10^{-5}$  times that of light waves. These acoustic waves are confined to the substrate surface, having penetration depths of a few wavelengths. This indicates that they possess high surface energy. Lord Raleigh was the first to explain the propagation of waves along the plane surface of elastic solids in his classical paper [13].

A typical SAW resonator is shown in Figure 1(a). In this configuration there are specially designed grating reflectors having a period of  $\lambda/2$ , which are used to reflect back the surface waves towards the IDTs for resonance. A single port SAW device contains only one set of IDTs, but two reflectors on each side of the crystal for obtaining suitable resonance signals.

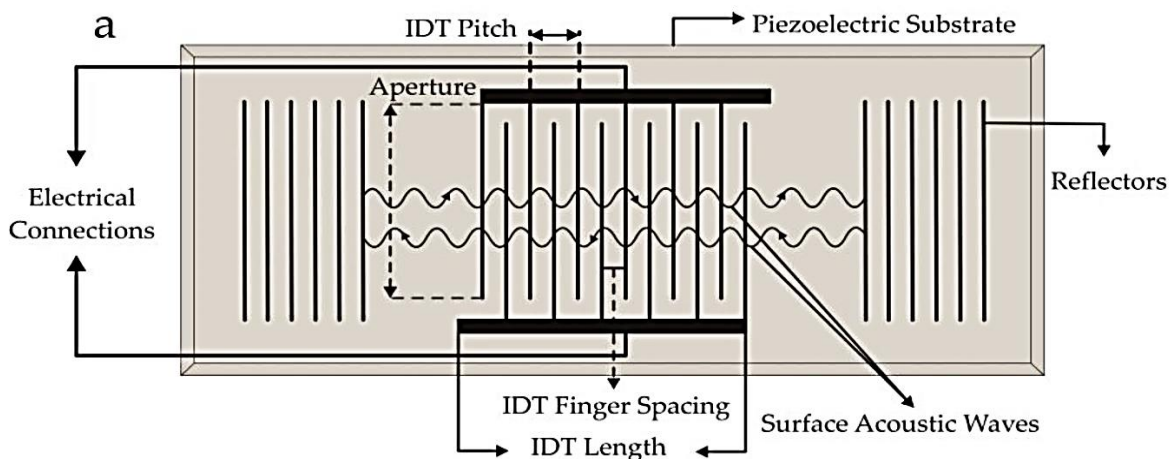


**Figure 1.6:** A typical design of a one-port SAW resonator.

Single port SAWs are usually considered for making oscillating circuits whereas two port devices are useful for developing special frequency filters.

### 3.2. Interdigital transducers (IDTs):

At the University of California in 1965, *White et al.* [13] discovered the principle of generating and detecting surface acoustic waves using an Inter Digital Transducers (IDT) disposed on the surface of a piezoelectric material.

The basic principle is as follows. The Inter Digital Transducer is deposited as a thin metal layer of approximately 100 nanometers on a piezoelectric substrate.

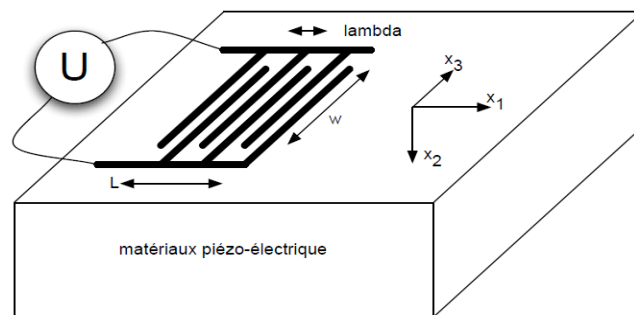


**Figure 1.7:** Excitation of surface acoustic waves using interdigitated combs [14] (Lambda = periodicity of combs, W = aperture, L = length).

#### 3.2.1. Operating principle of the (IDT):

The generation of acoustic waves is done by means of two parallel and coplanar electrodes deposited on the surface of the piezoelectric substrate. A cumulative effect can be obtained from an interdigital assembly constituting the transducer. By applying an alternating voltage to the input transducer, an alternation of compressions and expansions can propagate along the substrate **figure 1.7**.

The system being reversible, an identical set serves as a receiver and allows to collect the signal in electrical form. The received signal is delayed and attenuated compared to the transmitted signal, Hence, the name of delay line. It is possible to increase the quality coefficient  $Q$  of the system, by increasing the number of fingers constituting each electrode, within the limits of technological feasibility.

The distance between the fingers is determined in order to obtain a cumulative phenomenon of constructive waves at a given frequency. **Figure 1.8** gives the main characteristics of a1 surface acoustic wave device.

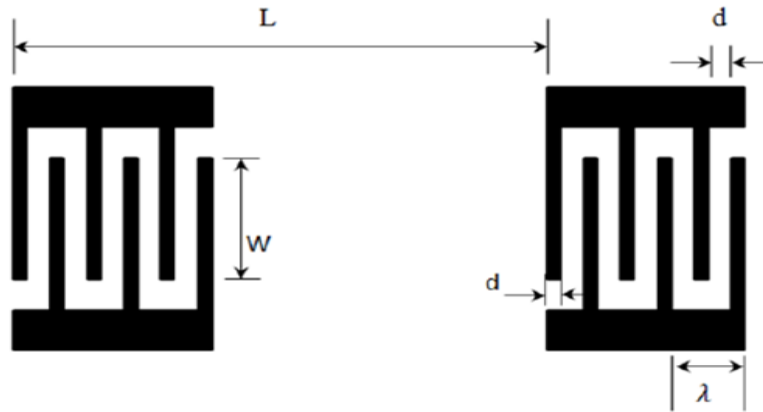


**Figure 1.8:** Geometrical characteristics of a SAW device.  $W$ = acoustic aperture,  $L$ =distance between IDTs,  $\lambda=2\pi(V/\omega)$  Wavelength,  $d = \lambda/4$  electrode spacing and electrode width.

#### 4. Surface acoustic wave transducers:

In the field of bio-receptor technology, SAW sensors can be used to determine the presence of specific molecules in the environment [15]. The SAW device is fabricated using a photolithography technology similar to the technology used in the semiconductor industry. Periodic metallic interdigital transducers (IDTs), deposited on uniformly polarized piezoelectric crystals, act as an electrical input or output.

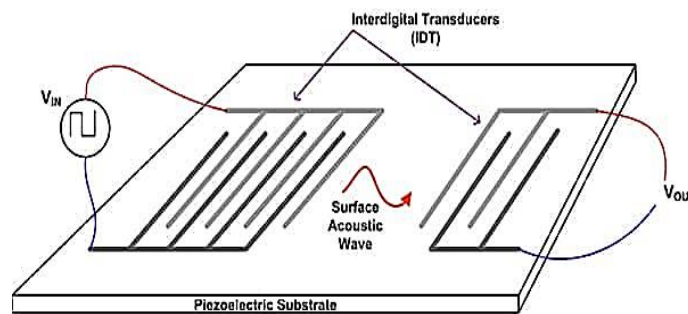


**Figure 1.9:** SAW resonator/filter uses interdigital transducers mounted on a piezoelectric substrate to generate surface acoustic waves in the space between the transducers, producing a frequency-dependent response at the output. (Image source: Digi-Key Electronics).

The application of a signal to the IDT produces a deformation of the surface of the material causing the launch of a SAW that propagates along the piezoelectric surface with a phase velocity given by the physical properties of the material figure (1.9). These surface waves can then be converted back to an electrical signal by a receiving IDT.

The resonance frequency of the SAW device is given by the following formula:

$$f = \frac{V_p}{\lambda} \quad (1.1)$$

$$\lambda = 2p \quad (1.2)$$

Where  $\lambda$  is the wavelength (spatial periodicity of the IDT fingers),  $V_p$ : The phase velocity in the material,  $p$ : the period

## 5. SAW devices:

Devices based on SAW are usually developed on piezoelectric substrates such as lithium niobate, lithium tantalate, langasite, and quartz, ZnO, AlN..etc. Non piezoelectric materials such as silicon dioxide and diamond are usually coated with piezoelectric substrates and SAW devices are realized. The two basic configuration of SAW devices are the SAW delay line and SAW resonator.

The SAW delay line consists of two IDTs on the surface of the substrate separated by a few wavelengths. **Figure 1.10 (a)** shows the elements of a SAW delay line device. The transmitter IDT excites and receiver IDT detects the SAW over the substrate.



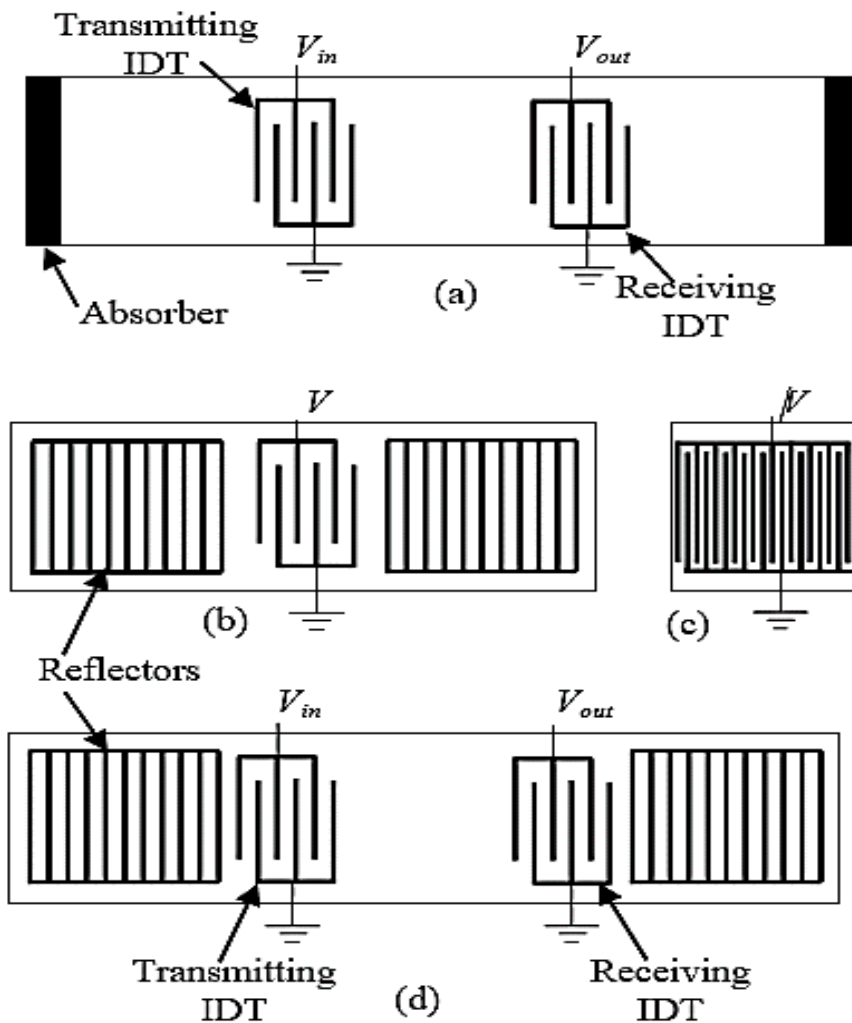


**Figure 1.10:** (a) SAW delay line, (b) & (c) One-port SAW resonators, and (d) Two-port SAW resonator.

In case of one port resonator, two sets of reflectors are fabricated in the either side of the bidirectional IDT as shown in [figure 1.10 \(b\)](#) [16]. These reflectors could be made of shorted metal strips or grooves. At the Bragg frequency, such that the periodicity of reflector electrodes equals half the wavelength, reflections from individual strips have the same phase so they add coherently, as in a single electrode of an IDT. Strong reflections are obtained when  $N |r_s| > 1$ , where  $N$  is the number of strips and  $r_s$  is the reflection coefficient of one strip. One port SAW resonator action can be achieved by single long IDT as shown in [figure 1.10 \(c\)](#), where multiple reflections within the IDT lead to standing waves and resonate in a particular frequency. SAW resonators can be used as a controlling element for a high stability oscillator. For this purpose, a two-port SAW resonator can be used as shown in the [figure 1.10\(d\)](#).

## 6. SAW sensors:

### 6.1. Operating principles of SAW sensors:

Acoustic wave devices are sensitive to any disturbance that may affect the speed, the travel distance or even the modes of wave propagation. A disturbance results in a variation of the electrical response of the device (frequency, amplitude, delay, phase..etc.). SAW systems are no exception to this rule and are sensitive to three main types of disturbances: **Temperature variation, deformation and deposition of Gaseous, Liquid or Solid species on the surface.**

Temperature changes and deformation cause changes in velocity (changes in elasticity modulus, density and piezoelectric coefficients).

The speed of the waves changes also under the deposition (adsorption/absorption) of gaseous species. This can produce a change in the mechanical inertia at the surface (increase of the moving mass), a change in the elasticity modulus (after diffusion of adsorbed species on the propagation medium), or from a perturbation of the surface electric field.

The deposition of liquid or solid species modifies the mode of propagation of the waves. The addition of a layer of liquid or a viscoelastic film on the surface can cause the appearance of guided modes at particular frequencies. The speed of these modes depends on the physical parameters of the guiding layer and it is thus possible to measure them by following the evolution of the frequency response of the devices. These parameters are viscosity, density, stiffness, thickness etc...

All SAW sensors on the market use one of these three kinds of sensitivities. The other sensor configuration is the resonator type, [figure 1.10\(b\)](#) shows a one-port SAW resonator, where the sensing film is coated over the entire acoustic path. Thus, change in properties of sensing medium will alter the resonance frequency of the SAW resonator.

[Figure \(1. 11\)](#) shows a block diagram of a measurement scheme that can be used in measuring the characteristics of SAW sensor. The IDTs can be excited using network analyzer and from the scattering parameters of the device one can characterize the SAW sensor.

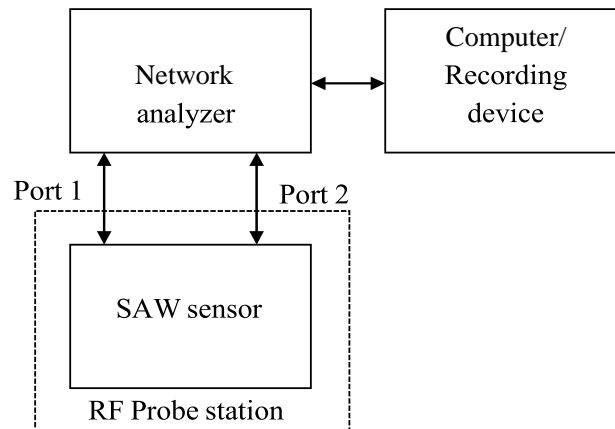


**Figure 1.11:** Setup for measuring SAW sensor characteristics using network analyzer.

## 6.2. SAW temperature sensor:

The development of SAW sensors for temperature measurement is not an easy task, but is nevertheless a very promising research avenue. If successful, the economic benefits could be very significant. Thanks to the original combination of four fundamental properties, namely high robustness over a wide temperature range, small size, the ability to be interrogated from distance and the absence of on-board electronics, the number of (potential) industrial applications for 'high temperature' SAW sensors is indeed very important. Applications are notably envisaged in the automotive, nuclear, mining and petroleum industries, as well as in the mining and oil industry as well as, of course, in the steel industry.

One of the main problems in the development of 'high temperature' SAW sensors is the choice or development of the basic components of the sensor element. Although materials such as AlN is well known today and have proven to be well suited for high or even very high temperature measurements, they still have major limitations for operating in harsh environments for a long period of time or for operating at high frequencies and thus obtaining high accuracy.

Although bilayer structures have many advantages (robustness,  $k^2$ , very high frequency operation...), new problems arise precisely because of their particular structure. In particular, the different thermal expansion of the two layers generates stress fields that can significantly influence the TCD of the structure.

SAW devices can be modeled using various techniques such as the delta function model, equivalent circuit model, coupling of mode (**COM**) method, and can be

simulated using techniques such as the finite element method (**FEM**). In the next part of this chapter FEM simulation of SAW devices such as SAW resonator, SAW device model to simulate a temperature sensor are discussed.

## 7. State of the art on the modeling and the simulation of surface acoustic wave sensors by the finite elements method (FEM):

As previously cited, surface acoustic wave (SAW) devices are widely used in communication equipment [17], including as electronic actuators [18,19], modulators [20], RF filters [21], and as biochemical and gas sensors [22-23]. Early researchers rely on experiments to design and develop SAW devices. There were frequent discrepancies in actual function of devices. Basic design of SAW transducers has to be optimized with the help of modeling techniques. Nowadays computer aided simulation helps in designing SAW devices and studying the characteristics of these devices made on new piezoelectric substrates. So, Simulations are therefore very necessary to design, optimize and develop these high-performance devices. They allow reducing production time and costs, as well as a better understanding of the physics and helping in estimating and visualizing the SAW device response before fabricating these devices.

A number of simulation techniques and methods have therefore been developed and applied to acoustic modeling, but significant improvements are still needed. Methods used to model and analyze interdigital transducers (IDTs) include the delta function model, the equivalent circuit model [24], the P-matrix model which analyzes SAW devices using mathematical methods and mode coupling theory. However, these methods require some approximations, and considerable computational resources, especially for complex geometries. These techniques are more suitable for RF applications for filter and SAW resonator design.

*The finite element method (FEM)*, which can be implemented via commercial software, such as **ANSYS** or **COMSOL Multiphysics®**, has proven to be a better alternative to model and analyze SAW sensors. The FEM uses simple methods to analyze complex geometries (such as those of surface acoustic wave devices) and to understand the associated physical phenomena, before their realization in a clean room [25].

## 8. Piezoelectricity:

### 8.1. What is the piezoelectricity?

The qualitative observation of the piezoelectric phenomenon was made by a French mineralogist abbot R. HAÜY (in 1817). However, the discovery of piezoelectricity is attributed to the brothers Pierre Curie and Jacques Curie (1880). Piezo is a Greek prefix which means pressure. Some crystals have the property to polarize under the influence of a mechanical constraint (or stress): it is the direct piezoelectric effect schematized on [figure 1.12](#) The piezoelectric effect is reversible: these same crystals deform when they are subjected to an external electric field. This phenomenon is only observed in non-conductive materials. The displacement of charges is done in a privileged direction under the forces of or compression in the crystalline structure of the ceramic.

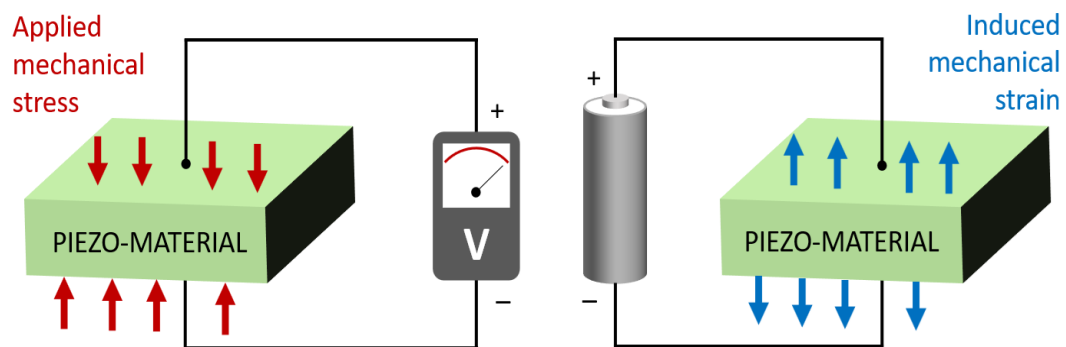


**Figure 1.12:** The piezo-electric effect: Generation of charges due to mechanical stress (direct effect, left), and strain caused by the application of an electric field (converse effect, right).

In the [figure 1.13](#) we can easily imagine an exemple of piezoelectric crystal structure, made up of hexagonal arrangements of ions, all lined up in an orderly matrix throughout the bulk of the crystal volume. When the crystal is compressed, each hexagon would contribute to a net polarization across the crystal.

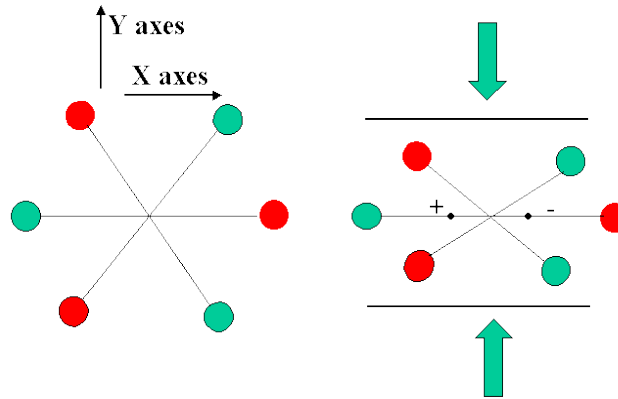


**Figure 1.13:** Hexagonal mesh composed of silicon atoms and oxygen atoms before and after a mechanical stress.

### 8.2. Piezoelectric Materials:

Since their discovery in the 19th century, piezoelectric materials have been used for a variety of applications, from power sources to actuators. Piezoelectric materials can be classified into four main categories: **crystalline, ceramic (AlN or ZnO based thin films), polymers** and **piezoelectric composites**. These materials differ in their physical, thermal, optical, mechanical, electrical and elastic properties.

Each of these properties is associated with specific constants and coefficients, Such as elasticity Modulus and electromechanical coupling modulus. The choice of properties and type of piezoelectric material depends mainly on the intended use. In the SAW sensor area, the important parameters are the surface wave propagation velocity, the acoustic impedance, the electromechanical coupling factor and the temperature coefficient for frequency.

### 8.3. Piezoelectric equations:

- The electromechanical coupling factor ( $k^2$ ): characterizes the efficiency of conversion of electrical energy into mechanical energy and vice versa. It is calculated from the relation (Eq. 1.2) and is expressed in %:

$$k^2 = \frac{\text{Stored electrical energy}}{\text{Mechanical energy supplied}} \quad (1.3)$$

- The temperature coefficient of frequency (TCF): Temperature Coefficient of Frequency) reflects the shift of the resonance frequency under the effect of temperature.

➤ The relationship between the stress  $T$ , strain  $S$ , electric field  $E$ , and electric Displacement  $D$  of the piezoelectric material is given by the following equation:

$$\left[ \begin{array}{l} T_{ij} = C_{ijkl}^E S_{kl} - e_{kij} E_k \\ D_j = e_{jkl} S_{kl} - \epsilon_{jk}^S E_k \end{array} \right. \quad \begin{array}{l} (1.4) \\ (1.5) \end{array}$$

Where  $e_{kij}$  is piezoelectric constant matrix,  $E_k$  is electric field components,  $C_{ijkl}$  is elasticity matrix,  $S_{kl}$  is strain tensor,  $\epsilon_{jk}^S$  is dielectric permittivity matrix.

The simple structure, fast response time, and easy integration make the High Temperature Piezoelectric Sensor (HTPE) advantageous and especially interesting. Various piezoelectric materials such as quartz ( $\text{SiO}_2$ ), lithium niobate ( $\text{LiNbO}_3$ , LN), gallium ortholthic gallium ( $\text{GaPO}_4$ ), langasite, and aluminum nitride (AlN) have been widely studied for high temperature applications. Each of these materials has its own strengths and weaknesses for use with HT sensors.

So, the choice of the piezoelectric substrate, which is an essential part of SAW devices, is one of the challenges to face to realize such sensors. Indeed, there are very few piezoelectric materials capable of withstanding high temperatures above  $400^\circ\text{C}$  [27]. Piezoelectric materials conventionally used in SAW industry are limited in elevated temperatures because of various physical phenomena including:

- ✓ Phase transition that leads to a change and instability of piezoelectric properties with temperature.
- ✓ Electrical resistivity that decreases strongly with temperature leading to increase the acoustic propagation losses.
- ✓ Temperature dependence of electromechanical properties
- ✓ Decomposition [28].

Therefore, in this work we studied a SAW sensor based on (AlN) layer which has a high melting point and a good piezoelectric property in high temperature.

#### 8.4. Fields of applications:

The fields of application of piezoelectricity are numerous. They depend on the frequency of use (table 1.1). The applications concern the electroacoustic transduction for medical imaging and non-destructive testing in the MHz frequency range, but also Sensors, actuators, motor elements, or filters. The design and transducers and ultrasound systems therefore require the knowledge of the electromechanical tensors of all the constituent materials [29].

**Table 1.1:** Areas of application according to their working frequency [30].

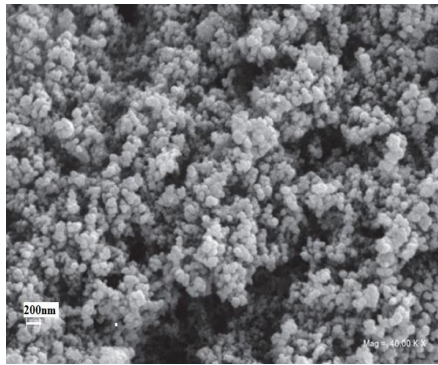
Frequency	Application
10-50 kHz	Cleaning, welding, machining, gluing
10-100 kHz	Underwater, acoustics, analysis of the subsoil.
1-20 MHz	Medical acoustics, ultrasound
100 MHz – 10 GHz	Acoustic-optics, Acoustic-electric
10- 100 GHz	Study of the material

#### 8.5. Aluminum Nitride (AlN):

##### 8.5.1. The material AlN:

**Aluminum nitride or AlN** is a wide band gap semiconductor (6.2 eV). It is an electrical insulator with a high thermal conductivity of  $320 \text{ W}\cdot\text{m}^{-1}\text{K}^{-1}$ , and high resistivity of  $10^{13} \Omega\cdot\text{cm}$ , AlN is also a refractory material with good resistance to oxidation [31] and abrasion. It has potential applications as a substrate in optoelectronics in the ultraviolet field and in electronics for the manufacture of microwave power transistors. Currently, many researches are conducted to produce UV emission diodes using gallium aluminum nitride. Some experiments have made it possible to reach wavelengths of the order of 210 nm [32], the gap of the aluminum nitride would allow emissions up to 200 nm in principle. However, further research will be necessary before such electronic compounds are available on the market. such electronic compounds.





(a)



(b)

**Figure 1.14:** (a)-Aluminum Nitride Nano powder, (b)-Aluminum Nitride powder.

AlN has two polytype crystal structures: a Würtzite (hexagonal) structure and a Zinc Blende (cubic) structure (Figure 1.15).

### 8.5.2. The Crystalline structure of AlN

The Würtzite structure (Fig.1.15(a)) is composed of two hexagonal sub-lattices of nitrogen and aluminum atoms shifted from each other by a vector  $0.3869 \times (0,0,1)$ .

The Zinc Blende form (Fig. 1.15(b)) consists of two face-centered cubic sublattices of nitrogen and aluminum atoms shifted by a quarter of a vector  $1/4 \times (1,1,1)$ . The thermodynamically stable structure is the hexagonal phase [34].

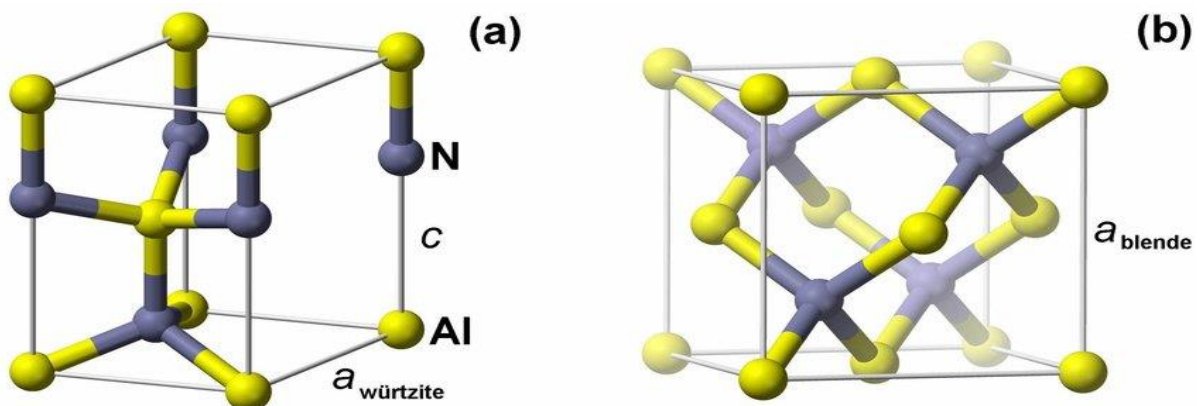


**Figure (1.15):** Aluminum nitride; (a) Würtzite structure and (b) Zinc Blende structure [35]

The AlN Würtzite structure (space group P63mc) is of type 2H according to the nomenclature used for SiC polytypes (Figures 1.15 and 1.16). The corresponding mesh parameters are  $a=3.11\text{\AA}$  and  $c=4.98\text{\AA}$ .

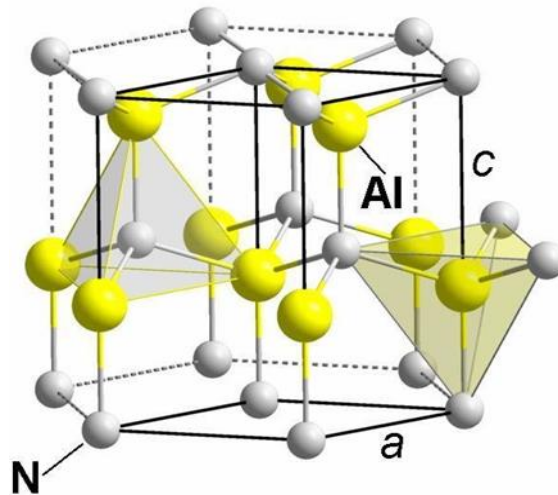


**Figure 1.16:** 2H hexagonal structure of aluminum nitride: the aluminum atoms (in yellow) and the nitrogen atoms (in grey) both have a tetrahedral environment [35].

### 8.5.3. Mechanical properties:

It is important to know the mechanical properties of AlN when performing epitaxial deposition on different substrates. Indeed, a modification even local of the crystal lattice can lead to changes in physical properties such as the gap width. Essential properties are the coefficients of elasticity and Thermal expansion as well as hardness.

### 8.5.4. Coefficient of elasticity:

The stresses and strains of the crystal lattice are related by the laws of Hooke's:

$$\boldsymbol{\sigma} = \mathbf{E} \cdot \boldsymbol{\varepsilon} \quad (1.6)$$

where  $\boldsymbol{\sigma}$  is the stress (in Pa),  $\mathbf{E}$ , the Young's modulus (in Pa) and  $\boldsymbol{\varepsilon}$  the strain or relative elongation.

$$\sigma_{ij} = C_{ijkl} \cdot \varepsilon_{kl} \quad (1.7)$$

where  $\sigma_{ij}$  is the stress tensor (in Pa).  $C_{ijkl}$ , the tensor of elasticity constants (in Pa) and  $\varepsilon_{kl}$  the strain tensor. With the simplifications related to the symmetries of the hexagonal lattice of the 6mm crystal class to which the space group P63mc belongs, the generalized Hooke's law is written according to equation (1.7).

$$\begin{pmatrix} \sigma_1 \\ \sigma_2 \\ \sigma_3 \\ \sigma_4 \\ \sigma_5 \\ \sigma_6 \end{pmatrix} \times \begin{pmatrix} C_{11} & C_{12} & C_{13} & 0 & 0 & 0 \\ C_{12} & C_{11} & C_{33} & 0 & 0 & 0 \\ C_{13} & C_{13} & C_{33} & 0 & 0 & 0 \\ 0 & 0 & 0 & C_{44} & 0 & 0 \\ 0 & 0 & 0 & 0 & C_{44} & 0 \\ 0 & 0 & 0 & 0 & 0 & \frac{(C_{11}-C_{12})}{2} \end{pmatrix} \times \begin{pmatrix} \varepsilon_1 \\ \varepsilon_2 \\ \varepsilon_3 \\ \varepsilon_4 \\ \varepsilon_5 \\ \varepsilon_6 \end{pmatrix} \quad (1.8)$$

The elasticity coefficients of hexagonal aluminum nitride are collected in [table \(2.1\)](#) Coefficients of elasticity  $C_{11}$   $C_{12}$   $C_{13}$   $C_{44}$  .

## 8.6. Aluminum Nitride (AlN): piezoelectric thin film material contact

Aluminum nitride (AlN) is a piezoelectric thin film material currently used for the realization of sensors (ultrasound transducers, pressure sensors, actuators, in micropump, etc. and also of components for signal processing by surface elastic waves. The speed of acoustic waves in AlN is one of the fastest among all materials, which is an advantage for high frequency applications. AlN is deposited at low temperature, which makes it compatible with the integrated circuit manufacturing CMOS process, hence the possibility of making a sensor with integrated electronics to reduce production costs.

Moreover, AlN has a high breakdown electric field and good resistance to chemicals, physical characteristics useful for sensors and actuators. Currently physical etching tests and characterization of AlN are being carried out.

## 8.7. Applications of AlN:

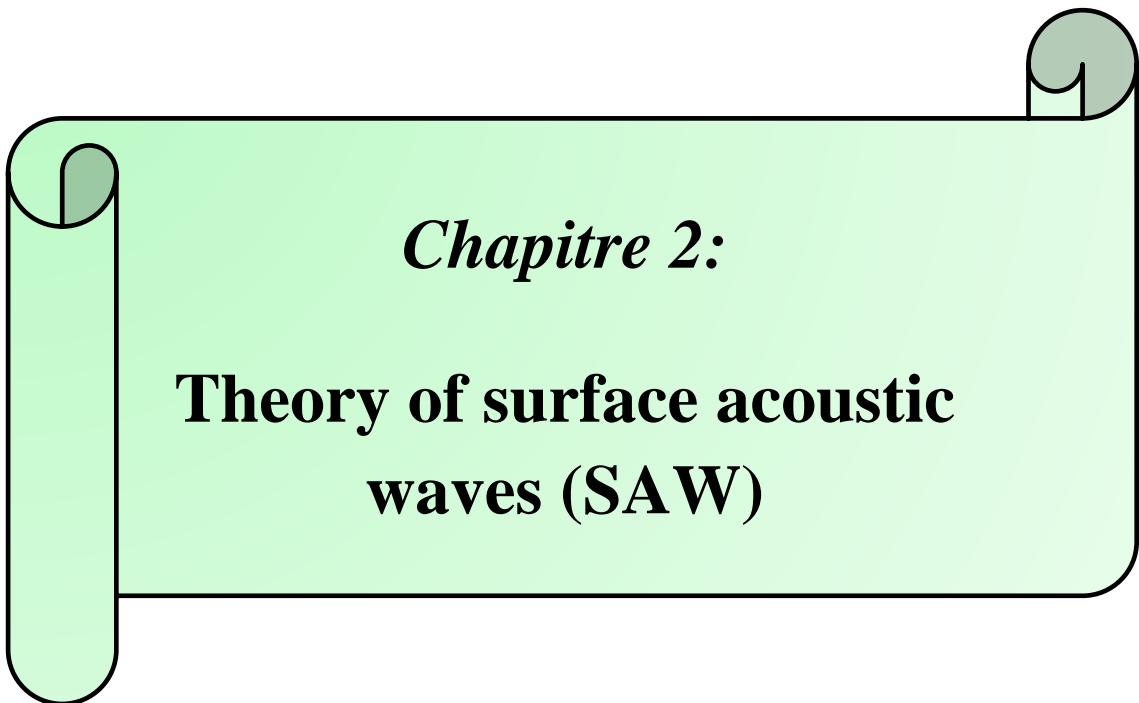
We have seen that AlN is a refractory compound, electrically insulating, with a high hardness and a high thermal conductivity. In addition, it has a good resistance to oxidation. AlN is one of the few materials that is both electrically insulating and a good thermal conductor. AlN is therefore an interesting material for various applications in the form of sintered ceramics.

It can be used in thin layers as an anti-abrasion and anti-corrosion coating [36,37] to protect the surface of cutting tools and certain heating elements. In microelectronics, polycrystalline nitride films are used as dielectrics in **MIS** (Metal Insulator Semiconductor) or **MNOS** (Metal Nitride Oxide Semiconductor) structures. It acts as an anti-diffusion barrier for boron or phosphorus doping elements in semiconductors.

It is also used as a coating layer to protect semiconductors during annealing. Single crystals obtained by heteroepitaxy are used in acoustic wave devices in the high frequency range. An important point is the elaboration of multilayer compounds (AlN-semiconductor-II-VI compound) on substrates that allow the simultaneous processing of acoustic, electronic and optical signals [38, 39]. In the field of power electronics (high temperature, high voltage and high frequency), AlN is sought after for its electrical insulation and high thermal conductivity. Moreover, polycrystalline AlN is also used as a substrate in cooling devices using copper layers in the form of DBC (Direct Bonding Copper) or AMB (Active Metal Bonding).

## 9. Conclusion:

The first part of this bibliographic chapter was devoted to present generalities on the MEMS technology and SAW devices before focusing our interest on the SAW sensors based on transducers, we have given some information about the temperature sensor, and we also talk about the principal of piezoelectricity and their equations, and the principle of generation of acoustic waves using interdigital transducers (IDTs). Without forgetting to introduce the main materials used in our temperature sensors



*Chapitre 2:*

**Theory of surface acoustic  
waves (SAW)**

## **1. Introduction:**

Surface acoustic wave sensors rely on the fact that mechanical vibrations propagate under piezoelectric solid surfaces when surface acoustic waves (SAWs) are excited by an electrical signal at the resonant frequency. This chapter presents an extension of this analysis technique for modeling the effects of diffraction on the impulse response of a complete SAW device. The current work also considers the implications of the twodimensional nature of the mathematical formulation of the model, and how the results of this formulation influence the validity of the model. Comparison is made between theoretical and experimentally observed device performance.

Experimental determination of various forms of the frequency response function has been applied for many years in order to characterize the structural response of a diversity of constructions and a comprehensive review is given by Ewins ~1984.

So, at first, we will describe the impulse response, Secondly, we present the equation that used as an approximation to the scalar two-dimensional impulse response of an ideal point source and that it is assumed that this function is valid for all frequencies, and for the reasonably short separations from the source under consideration. Taking the inverse Fourier transform yields a time domain. At the end we combin

e the relationship between transducer geometry and impulse response and also the frequency response of the SAW.

## **2. The History of Impulse response test method:**

The impulse response test method is a nondestructive, stress wave test, used to evaluate structural components and elements. Its application to concrete structures is less well known than its application to mechanical structures, and the method has received far less publicity than the recently developed impact-echo test [40]. Both methods are described in the American Concrete Institute (ACI) report (1998). Experimental determination of various forms of the frequency response function has been applied for many years in order to characterize the structural response of a diversity of constructions and a comprehensive review is given by Ewins (1984). The method was first adopted in the aviation industry as reported by Kennedy and Panco

(1947) harmonic loadings with different angular frequencies are applied at different locations, and measurement of the response enables one to identify the eigenfrequencies and the eigenmodes.

## 2. Definition of Impulse response:

The impulse response of a system is its response to a very short input signal (Dirac pulse/delta function), a pulse is a signal with amplitude of 1 at  $t=0$  and zero elsewhere. Using a pulse to excite a system provides “infinite” frequency content, i.e., the impulse response tells us how the system will behave for inputs at all frequencies [41].

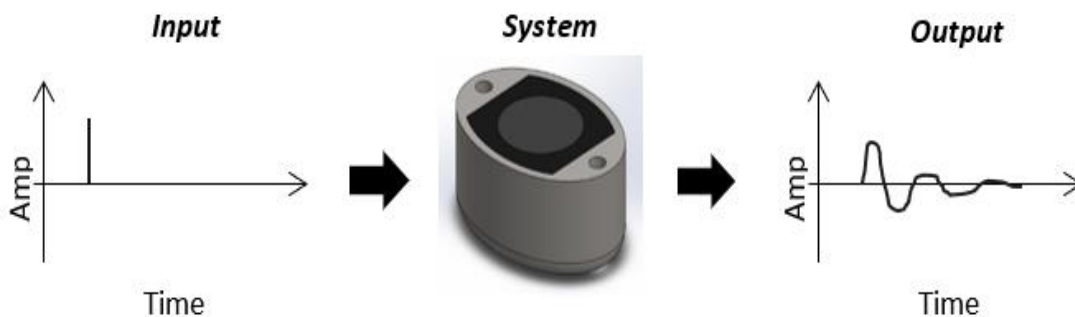


Figure 2.1: Impulse response diagram [42].

### 3.1. Why is it useful?

Impulse response method is a great tool for simulating transducers because many transducer drive signals are wideband.

Finite element analysis (FEA) models cannot support infinite frequency content because the maximum frequency is limited by the size of the mesh. It is possible, though, to simulate an impulse response within a certain frequency band of interest.

In comsol software it is possible to calculate the impulse response across a wide band of interest (band-limited impulse response) using a time-domain response simulation approach. The response to this impulse will allow us to calculate the response to a range of drive signals such as ramps, steps, squares or sinusoidal signals in post-processing. Calculating the impulse response allows users to assess various arbitrary drive functions in one cost-effective model.

### 3.3. Impulse response theory:

The only time-domain signal that contains all single-frequency elements with unit magnitude is an impulse (delta function). In the time domain, putting an impulse into a system gives you a time-domain output signal. Time-domain signals can be converted into the frequency domain using the fast Fourier transform (FFT).

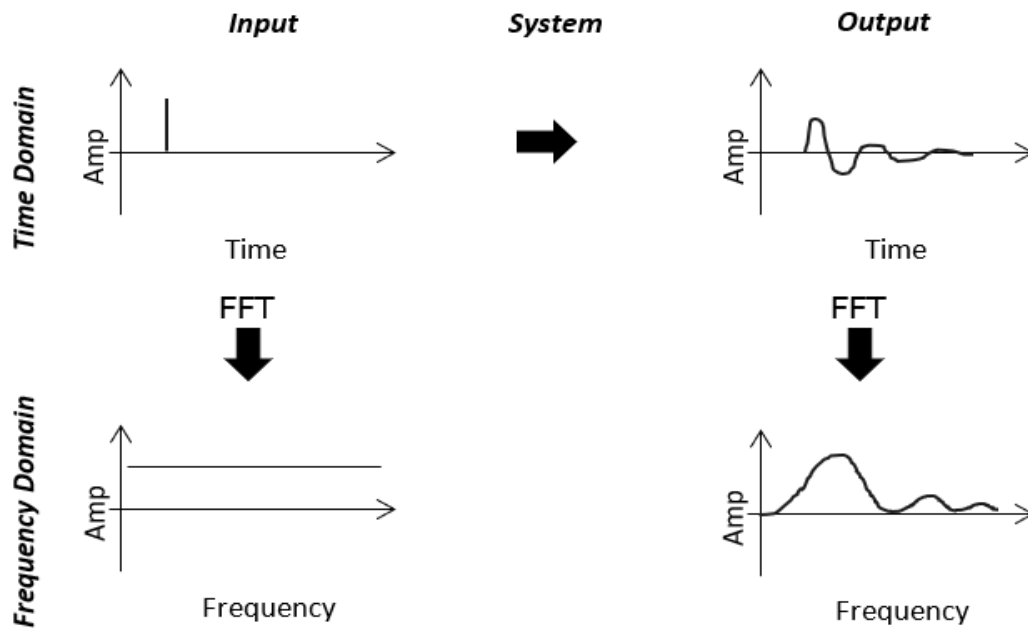


**Figure 2.2:** Impulse response (time domain response) and transfer function (frequency response) [42].

For any other input excitation  $x(t)$ , the output signal  $y(t)$  is considered as the convolution of two functions; the input signal  $x(t)$  and the impulse response  $y(t)$ . In other words, the transfer function  $Y(\omega)$  is given by the simple product of the input signal  $X(\omega)$  and the transfer function of the device  $H(\omega)$ . Where  $X(\omega)$ ,  $H(\omega)$  and  $Y(\omega)$  are respectively the Fourier transform of  $x(t)$ ,  $h(t)$  and  $y(t)$ .

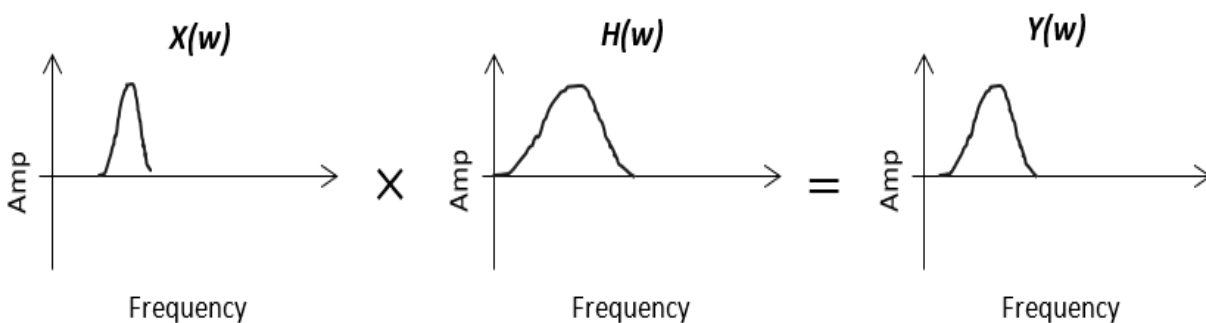


**Figure 2.3:** Transfer function [42].



The Fourier transform of the convolution of two functions is the simple product of the two Fourier transforms. As such, in the time domain the FFT of the convolution of two signals is the product of their frequency spectra

#### **4. Relationship Between Transducer Geometry and Transducer Impulse Response:**

The input transducer  $T_1$  generates a periodic electric field with a periodicity determined by the spacing of the adjacent electrodes. This field generates surface waves through the piezoelectric effect with maximum efficiency at the frequency  $f_0$ . The generated surface wave propagates to the output transducer  $T_2$ , which converts the mechanical displacement of the incident SAW wave to an output electric field by the mean of the inverse piezoelectric effect.

The filtering properties of these devices are completely determined by the processes for conversion of the electrical signal to acoustic energy, and vice versa, at the input and output transducers, respectively. This is shown in [Figure 2.4](#), which schematically describes the device as two frequency selective transfer functions,  $H_1(\omega)$  and  $H_2(\omega)$ , connected by a delay function expressed by  $\exp\left(-\frac{j\omega l}{v}\right)$ . Here  $l$  is the distance between the centers of the two transducers as shown in [Fig 1.8](#) and  $v$  is the surface-wave propagation velocity. The total transfer function of the device is then given by:

$$\frac{V_2(\omega)}{V_1(\omega)} \approx H_1(\omega) \cdot \exp\left(-\frac{j\omega l}{v}\right) \cdot H_2(\omega) \quad (2.1)$$

The transfer functions  $H_i(\omega)$  can be calculated from the impulse responses. This impulse response  $h(t)$  is a waveform which has a particularly simple relationship to the transducer geometry and materials since each electrode pair constitutes a tap on the acoustic delay line whose relative time delay is given by the position of the input and output IDT electrodes on the surface-wave substrate, and whose strength is directly proportional to the amount of overlap  $w(z)$  between adjacent electrodes.

From filter theory it is known that the impulse response  $h(t)$ , and the frequency response  $H(\omega)$ , are a Fourier transform pair [\[42\]](#), and thus the frequency response can be calculated by the mean of a Fourier transform integral given by:

$$H(\omega) = \int_{-\infty}^{\infty} h(t) \exp(-j\omega t) dt \quad (2.2)$$

#### 4.1. Frequency response of an IDT:

In order to define the response of the SAW, an electrical excitation  $U(t)$  of finite duration (assimilated a sinusoid of frequency  $f_0 = V_r/2d$  is applied on the electrode system (input IDT (1)) [43]. Let us introduce the function  $h(t)$  which is the impulse response of the system whose square represents the elastic power density per unit width of the Rayleigh wave beam emitted in each of the two propagation directions  $x_1$  and  $-x_2$ .

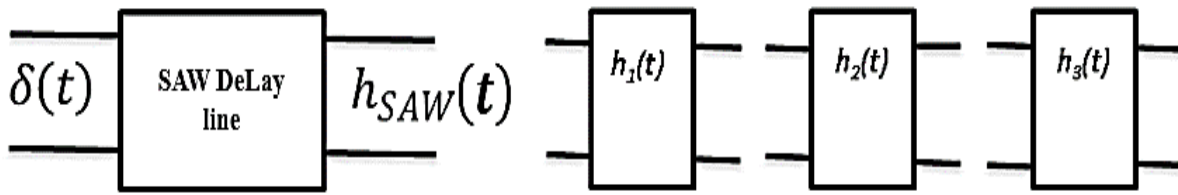


Figure (2.4): Symbolic diagram of a SAW [44].

$$h_{SAW}(t) = h_1(t) \underset{t}{*} h_2(t) \underset{t}{*} h_3(t) \quad (2.3)$$

With,  $h_{SAW}(t)$  is the impulse response of the SAW delay line,  $h_1(t)$  is the impulse response of IDT(1),  $h_2(t)$  is the impulse response of region causing delay (the acoustic path), and  $h_3(t)$  is the impulse response of IDT(2),  $\underset{t}{*}$  denotes the time convolution product operator.

$$h_2(t) = \delta(t - \tau) \quad (2.4)$$

$h_2(t)$  : is the impulse response of the wave path between IDTs that sets the delay  $\tau = \frac{L_{CC}}{V_R}$  (Of the SAW delay line), with slight attenuation.  $L_{CC}$  Represents the distance between the two centers of the IDTs (1 and 2). For a SAW delay line that is symmetrical, (i.e IDT (1) and IDT (2) are identical), then:

$$h_1(t) = h_3(t) \quad (2.5)$$

Their respective Fourier transforms are:

$$H_1(f) = H_2(f) \quad (2.6)$$

Let's take the input IDTs (1), having  $N$  pairs of fingers. The frequency response  $H_1(f)$  of this transducer is deduced from its impulse response  $h_1(t)$ . By

applying on the electrodes, a pulse  $U(t)$  of duration shorter than the travel time of the surface wave between two fingers, we simultaneously polarize all the parts of the transducer (comb (1) at the potential  $U(t)$  while the comb (2) is grounded). Since at each finger interval the electric field reverses. The spatial period of the wave is  $2d$  [45]. As for its duration  $\theta$ , it is equal to the ratio of the length  $L$  of the IDT (1) transducer to the propagation speed of the surface wave  $V_R$ :

$$\theta = \frac{L}{V_R} = \frac{2.d.N}{V_R} \quad (2.7)$$

Knowing that the frequency of this surface wave is:  $f_0 = \frac{V_R}{\lambda}$

$$\theta = \frac{N}{f_0} \quad (2.8)$$

The frequency response is obtained by taking the Fourier transform  $H_1(f)$  of the impulse response  $h_1(t)$  of the IDT.

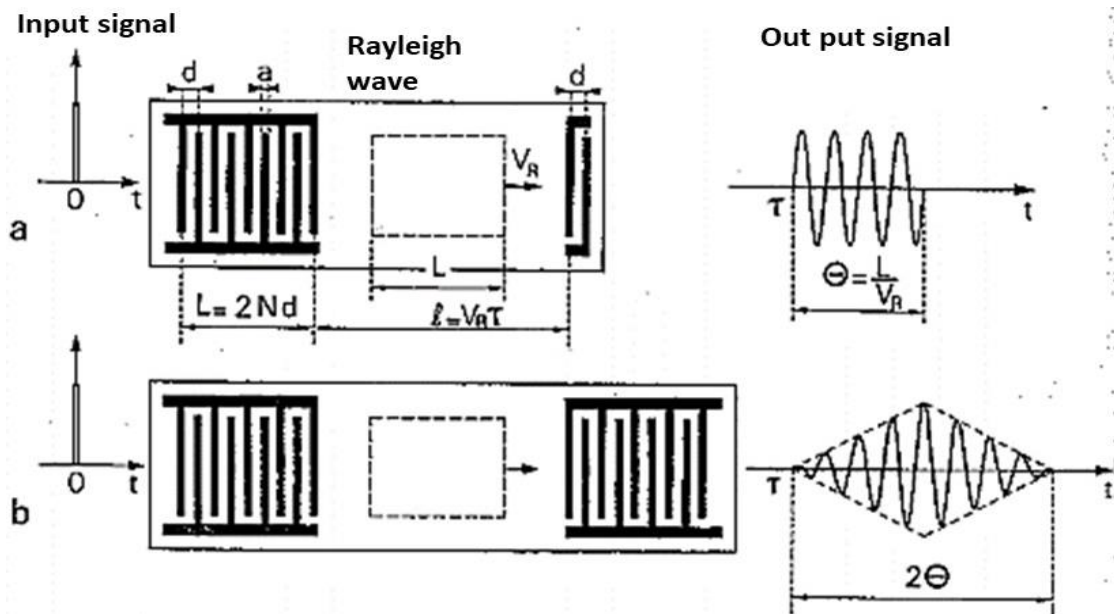


**Figure 2.5:** Impulse response, (a) -of the IDT electrode system (1), (b)-of the entire SAW delay line [46].

The response  $h_1(t)$  is the response of the input IDT to a Dirac pulse of unit voltage  $U(t)=\delta(t)$ , at the out put of the first IDT system  $h_1(t)$  is given by a sinusoid of frequency  $f_0 = \frac{V_R}{\lambda}$  and duration  $\theta = \frac{N}{f_0}$ , Figure 2.6.

$$h_1(t) = \begin{cases} a_0 \cdot \sin(2\pi f_0 t), & \text{for } -\frac{\theta}{2} < t < \frac{\theta}{2} \\ 0 & \text{elsewhere} \end{cases} \quad (2.9)$$

$t$  : is the time and  $a_0$  its amplitude.

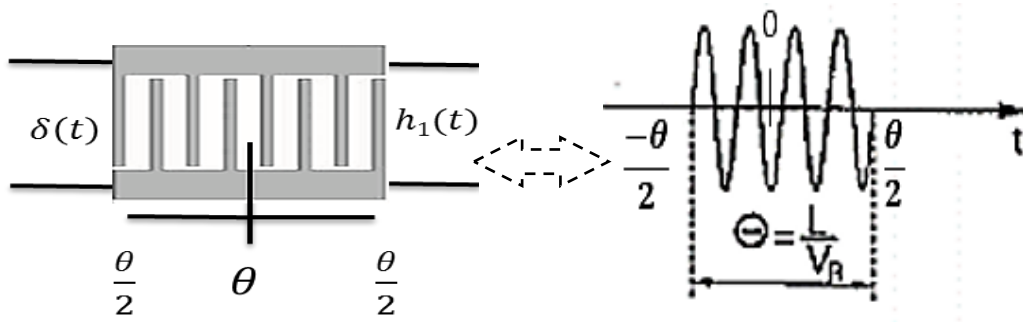


**Figure 2.6:** Impulse response of an IDT [47].

The frequency response or transfer function is deduced by taking the Fourier transform of the impulse response  $h_1(t)$ , that is:

$$H_1(f) = TF\{h_1(t)\} \quad (2.10)$$

Or

$$H_1(f) = \int_{-\infty}^{+\infty} h_1(t) e^{-j2\pi ft} dt \quad (2.11)$$

The impulse response of the (2.7) can be represented as a product of two functions, the sine function and a rectangular window, so its Fourier transform can be written as follows:

$$H_1(f) = TF(\Pi(t) \times \sin(2\pi f_0 t)) \quad (2.12)$$

$$H_1(f) = TF\{\Pi(t)\}_f^* TF\{\sin(2\pi f_0 t)\} \quad (2.13)$$

Now, the Fourier transform of the sine function is:

$$TF\{\sin(2\pi f_0 t)\} = \delta(f - f_0) \quad (2.14)$$

$\delta(f - f_0)$  : is the neutral element of the convolution product.

$$H_1(f) = TF\{\Pi(t)\}, \text{ centered in } f_0. \quad (2.15)$$

$$H_1(f) = \int_{-\frac{\theta}{2}}^{\frac{\theta}{2}} 0 * e^{-j2\pi(f-f_0)t} dt + \int_{\frac{\theta}{2}}^{\frac{\theta}{2}} 1 * e^{-j2\pi(f-f_0)t} dt + \int_{\frac{\theta}{2}}^{+\infty} 0 * e^{-j2\pi(f-f_0)t} dt \quad (2.16)$$

$$H_1(f) = \int_{-\frac{\theta}{2}}^{\frac{\theta}{2}} 1 \times e^{-j2\pi(f-f_0)t} dt \quad (2.17)$$

$$H_1(f) = \frac{1}{-\pi(f-f_0)} \left[ \frac{e^{-j(f-f_0)2\pi\theta/2} - e^{+j2\pi(f-f_0)\theta/2}}{2j} \right] \quad (2.18)$$

$$H_1(f) = \frac{1}{\pi(f-f_0)} \sin(\pi(f-f_0)\theta) \quad (2.19)$$

$$H_1(f) = \frac{1}{\pi(f-f_0)\frac{L}{V_R}} \sin\left(\pi(f-f_0)\frac{L}{V_R}\right) \quad (2.20)$$

$H_1(f) = \theta \left[ \frac{\sin(\pi(f-f_0)\theta)}{(\pi(f-f_0)\theta)} \right]$ , using the (2.6), we obtain

$$H_1(f) = \theta \left[ \frac{\sin\left(\pi(f-f_0)\frac{L}{V_R}\right)}{\left(\pi(f-f_0)\frac{L}{V_R}\right)} \right] = \theta \cdot \text{sinc}\left(\pi(f-f_0)\frac{L}{V_R}\right) \quad (2.21)$$

With  $\text{sinc}(X) = \sin(X)/X$  is the cardinal sine function.

$$H_{saw}(f) = h_1(t)_t * h_2(t)_t * h_3(t) \quad (2.22)$$

$$H_{saw}(f) = TF\{h_{saw}(t)\} \quad (2.23)$$

$$H_{saw}(f) = TF\{h_1(t)_t * h_2(t)_t * h_3(t)\} \quad (2.24)$$

Using the property of the Fourier transform on the convolution product gets the simple product of Fourier transform:

$$H_{SAW}(f) = TF\{h_1(t)\} * TF\{h_2(t)\} * TF\{h_3(t)\} \quad (2.25)$$

$$H_{SAW}(f) = H_1(f) \cdot H_2(f) \cdot H_3(f)$$

But:  $H_1(f) = H_3(f)$

$$H_{saw}(t) = H_1^2(f) \cdot H_2(f) \quad (2.26)$$

$$H_{saw}(t) = \theta^2 \{ [\sin^2 \pi f \theta] / (\pi f \theta)^2 \} e^{-\eta l_{cc}} \quad (2.27)$$

$$H_{saw}(t) = \theta^2 \{ [\sin^2 \pi f \theta] / (\pi f \theta)^2 \} e^{-\eta l_{cc}} \quad (2.28)$$

We represent, also in [figure 2.7](#), the electrical response in terms of return loss

expressed by the  $S_{11}$  Scattering parameter, and in term of insertion losses by the  $S_{21}$  scattering parameter

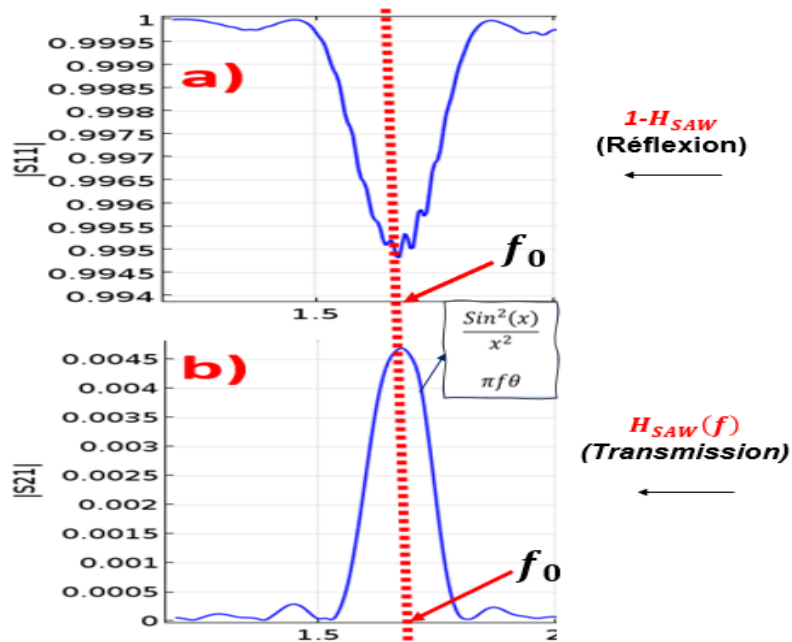


**Figure 2.7:**  $S_{11}$  return loss (Reflection),  $S_{21}$  insertion loss (Transmission)

### 5. Thermal strain effect:

This section discusses the analytical expersion for the TCF constant of a thickness (TE) surface acoustic wave (SAW) resonator and will emphaze the difficulty and the importance to achieve temperature mesurement.

The wave velocity and consequently the resonance frequency shifts of resonators are related to changes in stiffness coefficiets witht temperature and the thermal expansion, which affects not only the dimensions of the resonators, but also the density of the material, the velocity of the excited SAW is given by [10 and 11] as:

$$v = \sqrt{\frac{C_{ij}^D}{\rho}} \tag{2.30}$$

Where  $C_{ij}^D$  refers to the stiffness constants measures at constant displacement and to the density  $\rho$ . The fundamental resonance frequency for a TE resonator, also refereed to the parallel resonance, it is given by [10]:

$$f_p = \frac{v}{2d\pi} \sqrt{\pi^2 - 8k^2} \tag{2.31}$$

where  $d$  refers to the thickness of the piezoelectric substrate and  $k^2$  to the electromechanical coupling constant.

When the piezoelectric contribution in (2.31) is neglected, we can deduce the series resonance frequency of (2.32) given by:

$$f_{res} \cong \frac{v}{2d} \quad (2.32)$$

### 5.1.TCF constant and sensitivity of the sensor

The change of the resonance frequency due to temperature changes is described by the temperature coefficient of frequency (TCF). TCF is one of the key parameters of a temperature sensor; it allows to evaluate the SAW's resonance frequency normalized shift (in ppm, part per million) for a variation of 1°C of temperature. In the case of SAW based temperature sensors, a large value of the TCF constant is recommended because it is itself the standard sensitivity  $S$  [ppm/°C] of the sensor, contrary to the other application (filters, resonators, gas sensing, .ect.) where TCF must be around zero to ensure the stability of the device to the temperature.

The relation between TCF and the sensitivity is given by:

$$S = \frac{1}{f_0} \frac{\partial f_0}{\partial T} = TCF \quad (2.33)$$

The temperature coefficient of frequency for the low coupling approximation of the TE resonance is given as :

$$TCE = \frac{1}{f} \frac{\partial f}{\partial T} = \frac{1}{v} \frac{\partial v}{\partial T} - \frac{1}{d} \frac{\partial d}{\partial T} = \frac{1}{v} \frac{\partial v}{\partial T} - \alpha_z \quad (2.34)$$

Where  $\alpha_z$  corresponds to the thermal expansion of the substrate. Using (2.33) in (2.34) the TCF leads to

$$TCF = \frac{1}{2} \left[ \frac{1}{c_{ij}^D} \frac{\partial c_{ij}^D}{\partial T} - \frac{1}{\rho} \frac{\partial \rho}{\partial T} \right] - \alpha_z \quad (2.35)$$

The second order temperature dependence of the elasticity coefficients is :

$$c_{ij}(T_0)(1 + TC_{ij}\Delta T) + TC_{ij}\Delta T^2 \quad (2.36)$$

Where  $T_0$  refers to the reference temperature of the material,  $\Delta T$  to the

environment temperature change.  $C_{ij}$  is the elasticity constants of materials, and  $TC_{ij}^D$  the relative variation of the elasticity constant per unit of temperature.

The temperature dependence of the density  $\rho$  is in first order given by

$$\rho(T) = \rho(T_0)(1 - (\alpha_{11} + \alpha_{22} + \alpha_{33})\Delta T) \quad (2.37)$$

Using (2.36) and (2.37) in (2.34) leads to the first order formulation of the TCF for a TE resonator, as

$$TCF = \frac{1}{2} [TC_{ij} - (\alpha_{11} + \alpha_{22} + \alpha_{33})] - \alpha_z \quad (2.38)$$

TCF constant is related to materials parameters as  $\alpha_{11}$ ,  $\alpha_{22}$  and  $\alpha_{33}$ , which represent the effective thermal expansion coefficients of the piezoelectric layer in the x, y and z directions respectively and  $\alpha$  that of the substrate according to (2.38).

## 5.2. Parameters to be considered in simulation of a SAW temperature sensor:

The change in the temperature of the surrounding environment and consequently sensor's temperature can cause two major effects, which are a change in the length of the propagation path and interdigital distance  $d$ , added to a change in material's density when it is deformed.

In order to construct a model of the SAW temperature sensor by Finite Element Method (FEM), we consider the variations of the physical parameters cited above and developed in the first order.

### Interdigital distance:

$$d = d(T_0)(1 + \alpha \Delta T) \quad (2.39)$$

### (AIN) thickenss:

$$h_{ALN} = h_{ALN}(T_0)(1 + \alpha_{33}\Delta T) \quad (2.40)$$

### Density of the substrate:

$$\rho(T) = \rho(T_0)[1 - (\alpha_{11} + \alpha_{22} + \alpha_{33})\Delta T] \quad (2.41)$$

### The elastic constants developed in the second order are given by:

$$C_{ij}(T) = C_{ij}(T_0)[1 + TCE_{ij}\Delta T + TCE2_{ij}\Delta T^2] \quad (2.42)$$



For (AlN) and (Si), the constants  $\alpha_{11}$ ,  $\alpha_{22}$ ,  $\alpha_{33}$ ,  $TCE_{ij}$ ,  $TCE2_{ij}$  and  $\alpha$  are given in [table 2.1](#).

**Table 2.1:** (AlN) and (Si) Physical parameters used in the temperature sensing model.

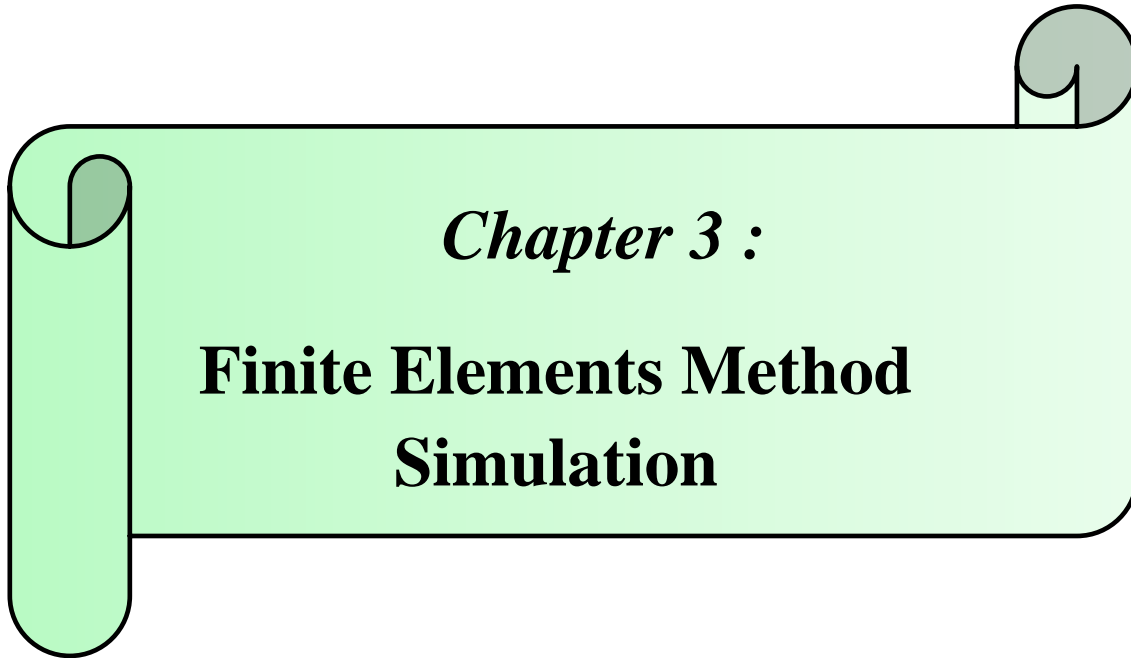
		AlN	Si
<b>elastic constants, <math>c_{ij}</math> [GPa]</b>	C <sub>11</sub>	410.02	165.7
	C <sub>12</sub>	149	34.7
	C <sub>13</sub>	110.1	–
	C <sub>33</sub>	390	–
	C <sub>44</sub>	125	65.5
	C <sub>66</sub>	130.27	–
<b>1st order TCE <math>Tc_{ij}</math> [<math>10^{-6}/K</math>]</b>	Tc <sub>11</sub>	-80e-6	-81e-6
	Tc <sub>12</sub>	180e-6	-110e-6
	Tc <sub>13</sub>	-160e-6	–
	Tc <sub>33</sub>	-100e-6	–
	Tc <sub>44</sub>	-50e-6	–
	Tc <sub>66</sub>	-10.80e-6	-63e-6
<b>2nd order TCE <math>T2c_{ij}</math> [<math>10^{-9}/K^2</math>]</b>	T2c <sub>11</sub>	-20.61e-9	-52e-9
	T2c <sub>12</sub>	-19.51e-9	-52e-9
	T2c <sub>13</sub>	-19.88e-9	–
	T2c <sub>33</sub>	-20.03e-9	–
	T2c <sub>44</sub>	-20.36e-9	-52e-9
	T2c <sub>66</sub>	-57e-9	–
<b>piezoelectric stress coef., <math>e_{ij}</math> [C/m<sup>2</sup>]</b>	e <sub>15</sub>	-0.48	
	e <sub>31</sub>	-0.58	–
	e <sub>33</sub>	1.55	
<b>relative permittivity, <math>\epsilon_{ij}</math></b>	$\epsilon_{11}$	9	11.7
	$\epsilon_{33}$	11	11.7
<b>CTE, <math>\alpha_{ij}</math> [<math>10^{-6}/K</math>]</b>	$\alpha_{11}$	5.27e-6	2.6
	$\alpha_{33}$	4.15e-6	2.6
<b>density, <math>\rho</math> [kg/m<sup>3</sup>]</b>		3260	2329

## 6. Conclusion

At first part of this chapter we have describe the impulse response, its equations taking the inverse Fourier transform yields a time domain, after we combine the relationship between transducer geometry and impulse response and also the frequency response of the SAW.

At the second part in order to construct a model of the SAW temperature sensor by Finite Element Method (FEM), we consider the variations of the physical parameters cited above and developed in the first order.

We finished by taking physical parameters for (AlN) and (Si) used in the temperature model .



*Chapter 3 :*

**Finite Elements Method  
Simulation**

## 1. Introduction :

Finite elements method (FEM) simulation is a computer tool widely used in many fields such as physics, mechanics, thermics or electricity. Other modeling techniques are also used to obtain results more quickly. This method offers a substantial gain in both time and money, and allows to optimize the design of systems such as SAW delay lines, filters or resonators, before their realization in clean room [48,49]. In the field of sensors in particular, these tools have largely proven, and still proving their usefulness for the design to increase sensitive detection devices.

In this study, we use COMSOL Multiphysics for modeling SAW temperature sensor using FEM method, and we attempt to increase the sensitivity of our sensor. The finite element simulation allows us to take into account several multiphysics phenomena; we focus here on the electrical and the mechanical properties of our device, especially, the particle displacement field and electric potential, when surface acoustic waves propagate along the surface of a given piezoelectric material.

We started by the simulation of an existing experimental example in the literature, of a SAW temperature sensor operating at a frequency of 425 MHz, in order to compare calculations (simulations) and experiments. Different configurations were tested and only the one that was in perfect agreement with the experimental results was taken into account. This optimization phase is crucial step because it allows us to estimate the accuracy of our simulations and model and to validate this model method in order to use in the simulation of other new structures we wish to design.

In the first part of this chapter, we briefly introduce the COMSOL Multiphysics simulation software, based on the finite element method. Then we will describe our own model to reproduce the experimental structure of Chuian Li *et al.* and predict the electrical behavior of all SAW transducers for future optimizations.

## 2. Physical modeling by finite elements

The Finite Element Method (FEM) was introduced in 1956 by Turner [50]. The objective was to find an approximate solution to problems that are difficult to solve analytically. Finite element modeling (FEM) is a mathematical tool that has been widely used in simulations of microsystems of several multi-physical domains, thermal, electrical, and in particular mechanical to calculate the deformations as well as the stresses of complex structures [51]. This method is widely used for the design of microstructures, hence the principle which consists in cutting the structure and search

for an approximate solution of the exact solution of the distribution of a physical quantity on a given domain.

In FEM method, the physical domain is divided into several subdomains that we call element. This operation is called a discretization of type finite elements. This is equivalent to splitting a complex problem into several simple problems to solve [52]. The elements are composed of a geometric set of points called nodes that comprise a mathematical graph of energy exchanges within the element and through its nodes. The global evaluated (calculated) field is then defined by a finite number of field values on the nodes. The unknowns at each of the nodes are called nodal variables or degrees of freedom.

### The finite element modeling consists of several steps:

- The choice of the energy domain which allows fixing the nature of the variables (degrees of freedom).
- The discretization of the studied domain into a large number of small elements and nodes. This operation is called meshing [52,53].
- The resolution of the global system of equations.
- The calculation of the quantities associated with the degrees of freedom.

The finite element method allows obtaining a display of quite precise graphs of the structure's behavior, but this method has the drawback of having a long calculation time. Indeed, some complex structures and geometries require a lot of time: several hours or even several days of calculations and simulations. It is therefore difficult to consider parametric studies using this finite element approach.

This approach will be illustrated in this chapter by using COMSOL Multiphysics® modeling software to solve multiphysics problems, such as the study of piezoelectric behavior of a resonator of a SAW device under a temperature changes.

## 2.1. Presentation of COMSOL Multiphysics® software

COMSOL Multiphysics is a software dedicated to finite element modeling and numerical simulation of multiphysical phenomena described by systems of partial differential equations (PDE). It is multiplatform software: Windows, Mac, and GNU/Linux. It has a graphical and interactive interface allowing the user to design his model in 1D, 2D or 3D. It is an advanced and powerful tool that contains powerful solvers to handle and solve problems in physics, mechanics and process engineering problems while quickly getting to the result.

COMSOL allows you to optimize solutions, couple and solve equations from multi-physics domains simultaneously. A very important advantage of COMSOL Multiphysics is that it offers the user the opportunity to focus on the model and not spend time solving the mathematical equations that require writing several lines of programming.

The most important steps of the modeling process on this software, of which a view of the graphical interface is shown in [Figure 3.1](#), proceed as follows:

- ✓ Choose the dimension of the model geometry (1D, 2D and 3D).
- ✓ Choose the physical domain of the study (AC/DC, acoustics, mechanics of structures, heat transfer...).
- ✓ Choose the type of study for the calculation (frequency, time, stationary,...).
- ✓ Build the geometric model of the device to be studied.
- ✓ Define the physical properties of the materials and the boundary conditions.
- ✓ Construct the mesh of the structure.
- ✓ Solve and display the results: Analysis of the results and post processing.

Note that this software allows the simulation of several physical domains at the same time and for the same study [\[54,55\]](#). In addition, it offers the possibility of processing specific applications via its various complementary modules ([Figure 3.2](#)) [\[56\]](#).

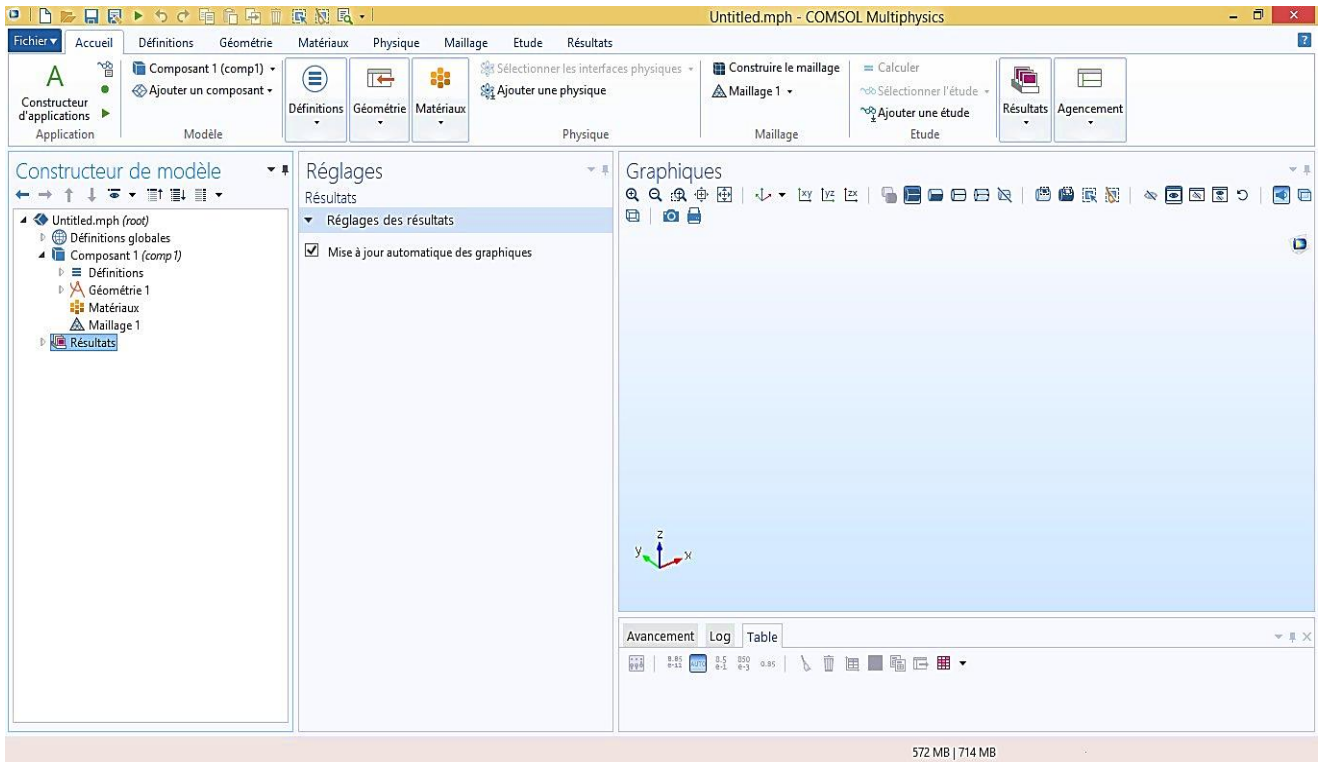


**Figure 3.1:** COMSOL Multiphysics software interface.

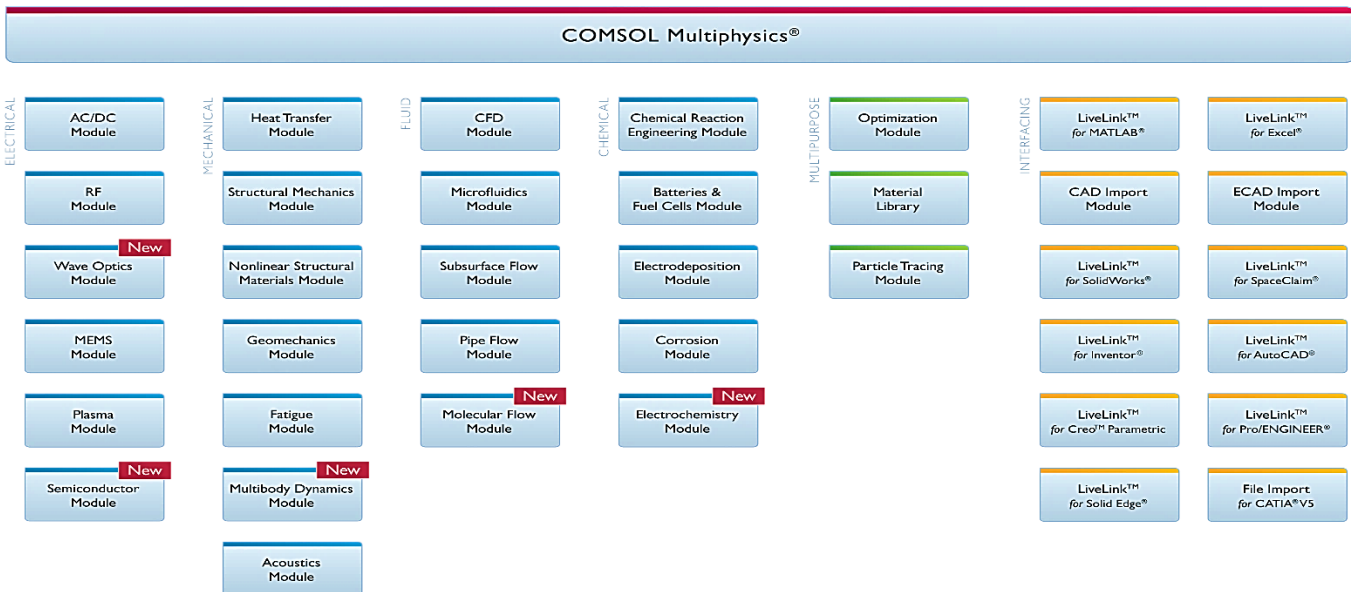


**Figure 3.2:** Add-on modules for COMSOL Multiphysics.

In the rest of this manuscript, we will first present a model of the SAW devices using the COMSOL Multiphysics software. The results obtained will be compared with those obtained from experimental measurements [60]. This will allow us to define a model capable of taking into account and predicting the electrical and mechanical behavior of all the SAW transducers for the subsequent optimization steps.

### 3. 2D simulation of a SAW unit cell:

We consider a two-dimensional (2D) structure, of a SAW transducer in the  $Oxz$  plane, (see figure (3.3)), we are interested in the excitation of the piezoelectric effect through the application of an external electric field on the input inter-digit electrodes.

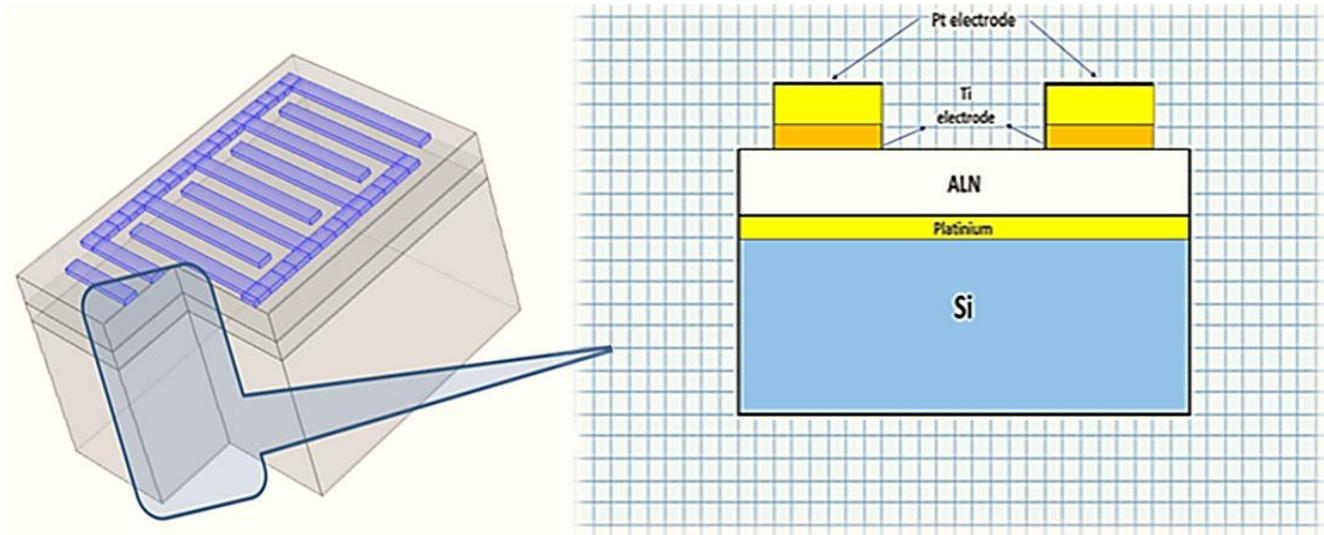


**Figure 3.3:** Unit cell SAW Structure.

First, we perform a modal study on a SAW unit cell (by considering periodicity conditions) in order to deduce the eigenfrequencies of the structure, then we perform a harmonic study of the same cell by sweeping the excitation frequency into the region containing the eigenfrequency of the surface modes, determined from the previous modal study.

#### 3.1. Modal study of a SAW unit cell

#### 3.2. Geometry of the SAW structure

Comsol Multiphysics offers geometric design tools in (1D, 2D and 3D). Geometric operations are always organized in sequences like model tree. The geometry of our structure is a single SAW unit cell (considering the periodicity conditions) which consists of five layers superimposed as follows (Silicon substrate, Platinum intermediate layer, ALN piezoelectric layer and Pt electrodes on a Ti buffer layer). Each of them is delimited by a rectangle (box), the geometrical parameters of each rectangle (characterised by its length, width and the position of its origin) are listed in (tables (3.1), (3.2) and (3.3) (3.4)), respectively, the figure 3.4 shows the geometrie of this structure.



<b>Table 3.1:</b> Region defining the piezoelectric layer AlN		<b>Table 3.2:</b> Region defining the Si substrate layer.	
<i>Name</i>	Value	<i>Name</i>	Value
<i>X Position</i>	$-NB \cdot \lambda / 2$	<i>X Position</i>	0
<i>Y Position</i>	0	<i>Y Position</i>	$-3 \cdot \lambda$
<i>Width</i>	$\lambda$	<i>Width</i>	$\lambda$
<i>Length</i>	$t_{\text{AlN}}$	<i>Length</i>	$h_{\text{SUB}}$

<b>Table 3.3:</b> Region defining the electrode with Pt		<b>Table 3.4:</b> Region defining the electrode with Ti		
<i>Name</i>	Value	Value	Value	Value
<i>Name</i>	Electrode 1	Electrode 2	Electrode 1	Electrode 2
<i>x Position</i>	$\lambda / 8$	$\lambda / 2$	$\lambda / 8$	$\lambda / 8$
<i>y Position</i>	$t_{\text{AlN}} + t_{\text{electrode\_Ti}}$	$t_{\text{AlN}} + t_{\text{electrode\_Ti}}$	$t_{\text{AlN}}$	$t_{\text{AlN}}$
<i>Width</i>	$\lambda / 4$	$\lambda / 4$	$\lambda / 4$	$\lambda / 4$
<i>Length</i>	$t_{\text{electrode\_Pt}}$	$t_{\text{electrode\_Pt}}$	$t_{\text{electrode\_Ti}}$	$t_{\text{electrode\_Ti}}$

<b>Table 3.5:</b> Region defining Pt layer.	
<i>Name</i>	Value
<i>Position x</i>	0
<i>Position y</i>	0
<i>Width</i>	$\lambda$
<i>Length</i>	$t_{\text{Pt layer}}$

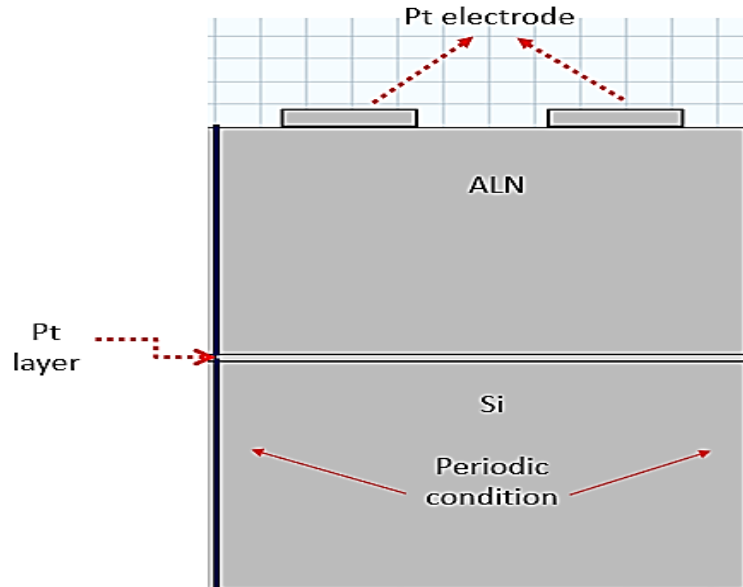


**Figure 3.4:** Geometry of a SAW unit cell, using the periodicity condition.

The applied boundary conditions are illustrated in figure 3.4, considering the continuity periodicity condition: Figure 3.5 represents the simulation results (mechanical response in terms of total mechanical displacement field) showing the different possible vibration modes in the SAW resonator unit cell. for each natural frequency. In color level, Red is associated with maximum intensity, while Blue one is associated with minimum intensity; a natural mode of vibration is associated. These modes are considered to surface modes.

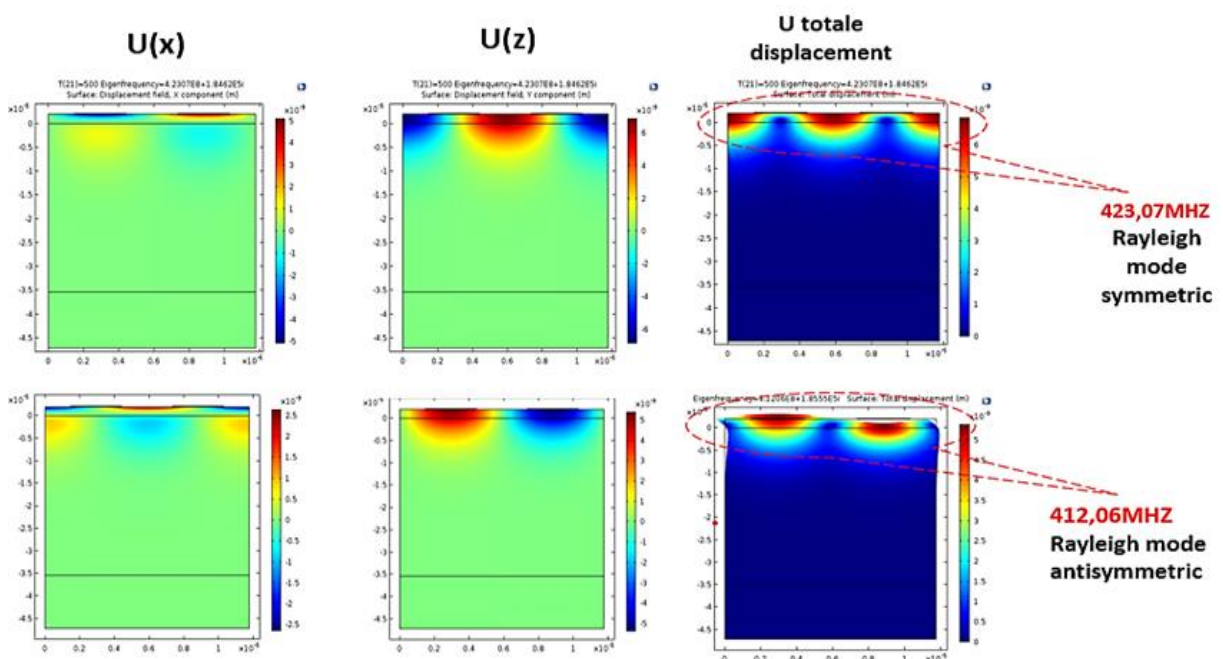


**Figure 3.5:** Mechanical displacement field in SAW unit cell (symmetric and antisymmetric Rayleigh mode).

The visualization on the same figure of the two components ( $u_x, u_z$ ) of the mechanical displacement field shows that for both modes (symmetrical and antisymmetrical), the displacement is localized at the surface of the device. At the frequency 423.07 MHz, both  $u_x, u_z$  and also  $u_{tot}$  of the mechanical displacement field are symmetric with respect to the mediator of the structure (oz axes passing by the centre of the structure). For the frequency 412.06 MHz these components are rather antisymmetric with respect to the mediator.

In **figure (3.6.a)**, we have done a cross section in our structure to given more details about the mechanical displacement components ( $u_x, u_z$ ) variation with depth in the substrate. The maximum of these components are observed at the top surface of the structure and they decrease with the penetration in the depth of the substrate, this is shown in the **figure 3.6.b**, that is explain our intrest mode surface acoustic waves, where the mechanical energy is confined on the top surface of the SAW device.

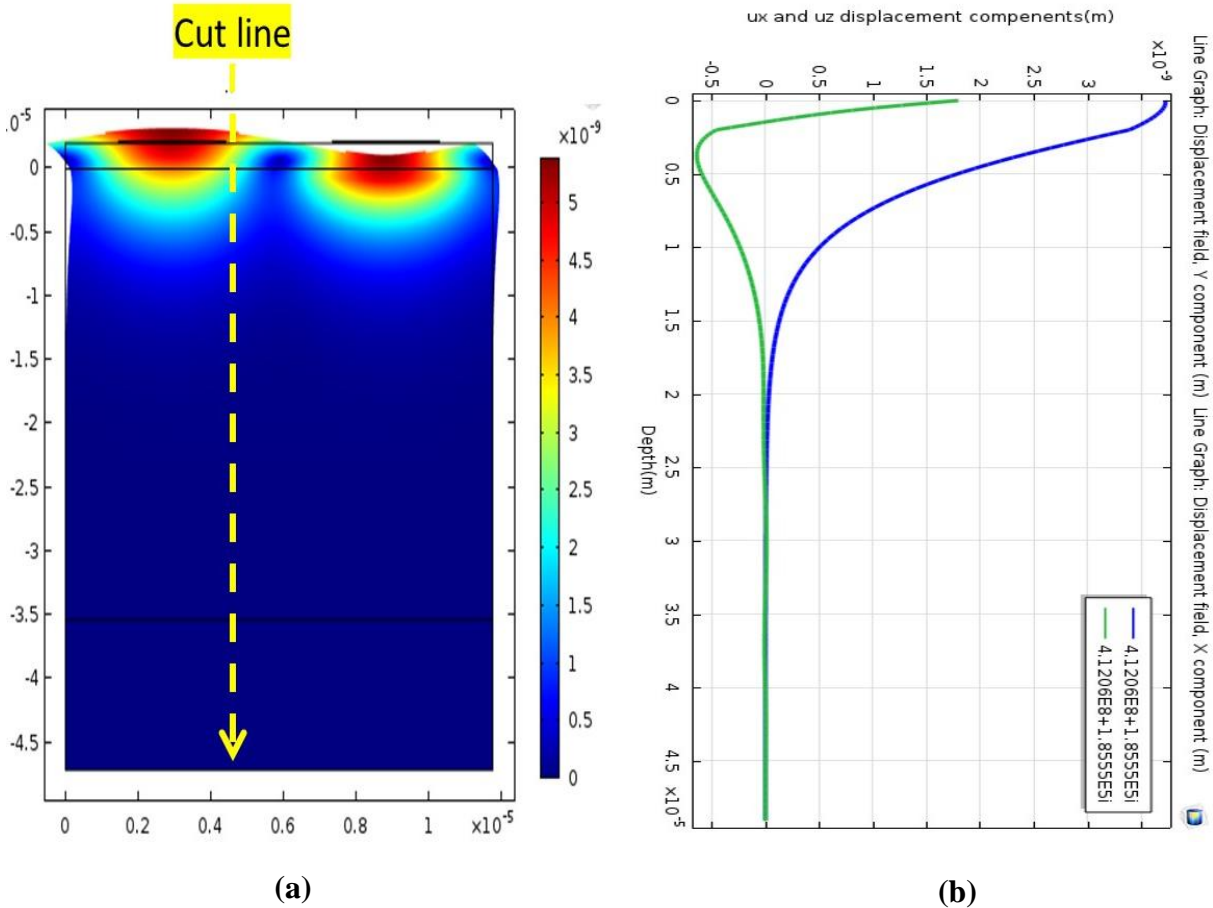


**Figure 3.6:** a)-Mechanical displacement components ( $u_x, u_z$ ) detailed in b)-by a cut line in the depth of structure.

## 4. Study of the global structure of the SAW resonator

### 4.1. Simulation procedure of the whole SAW device by Comsol:

The main simulation steps we will follow to study the piezoelectric SAW resonators by the finite element method are listed as follows:

- 1) Choice of the dimension of the simulation space.
- 2) Selection of the different physics describing our phenomenon to be studied.
- 3) Definition of the geometrical parameters of the model.
- 4) Assignment of materials to the different regions of the resonator.
- 5) Application of boundary conditions (electrical and mechanical) on the different regions, boundaries and interfaces.
- 6) Choice of the appropriate mesh for the SAW structure.
- 7) Definition of the frequency range of the study.
- 8) Launching the calculation.
- 9) Post exploitation and processing of the results.

### 4.2. Choice of the dimension of the simulation space:

In this first step we carry out the choice of the dimension of the problem, we select here to make a two-dimensional simulation (2D), on a section of the SAW ( $Oxz$  plane). We consider that the surface acoustic waves propagate in the ( $Ox$ ) direction, and polarized in ( $Oz$ ) direction.

### 4.3. Choice of physics:

In Comsol software we can simulate several physical phenomena such as electrostatics, electromagnetism, heat diffusion, mechanical deformation, piezoelectric effect, ...etc. Most MEMS devices use one or more phenomena to translate a physical input quantity into an electrical output quantity or vice versa. SAW resonators are mainly based on the direct or inverse piezoelectric effect through an electromechanical coupling. In this second step, we choose to use the physics "Piezoelectric Devices (pzd)", which couples both electrostatic and solid mechanic phenomena.

#### 4.3.1. Geometric parameters of the model:

It is very useful to make a parametrization in a table of the variables of the model and then use them in the different steps of simulation, it is enough to change in the table the value attributed to the variable that we want to modify and this will be taken into account automatically in the whole model. In this simulation, the values of the geometric parameters are listed in [table 3.6](#).

**Table 3.6:** Geometrical parameters of the SAW model.

Name	Expression	Description
$t_{AIN}$	2 [um]	AIN thickness
$\lambda$	$t_{AIN_0}/0.17$	SAW wavelength
$f_0$	440[MHz]	Estimated SAW frequency
$t_{electrode\_Pt}$	140[nm]	electrode thickness Pt
$t_{electrode\_Ti}$	10 [nm]	Electrode thickness Ti
$N_p$	50	Number of electrode pair
$f_i$	340[MHz]	Initial Frequency
$f_f$	500[MHz]	Final Frequency
$df$	$(f_f - f_i)/150$	Frequency step
$LB$	$\lambda/2$	The pitch between IDTs and Bragg reflectors
$NB$	100	Number of Bragg reflectors
$LPML$	$\lambda$	Length of the perfectly matched layer
$h_{SUB}$	$5*\lambda + LPML$	Substrate
$T$	125	Temperature
$T_0$	25	Initial temperature

#### 4.3.2. The geometry of the SAW Structure:

The whole structure (SAW resonator) is divided into three parts; **Figure 3.7:**

- i)- The input inter-digitated electrodes (transmitter/receiver IDT act as electrical access).
- ii)- The reflector systems containing the Bragg mirrors on the both sides of the structure.
- iii)- The PML (Perfectly Matched Layer) regions act as an absorber region.

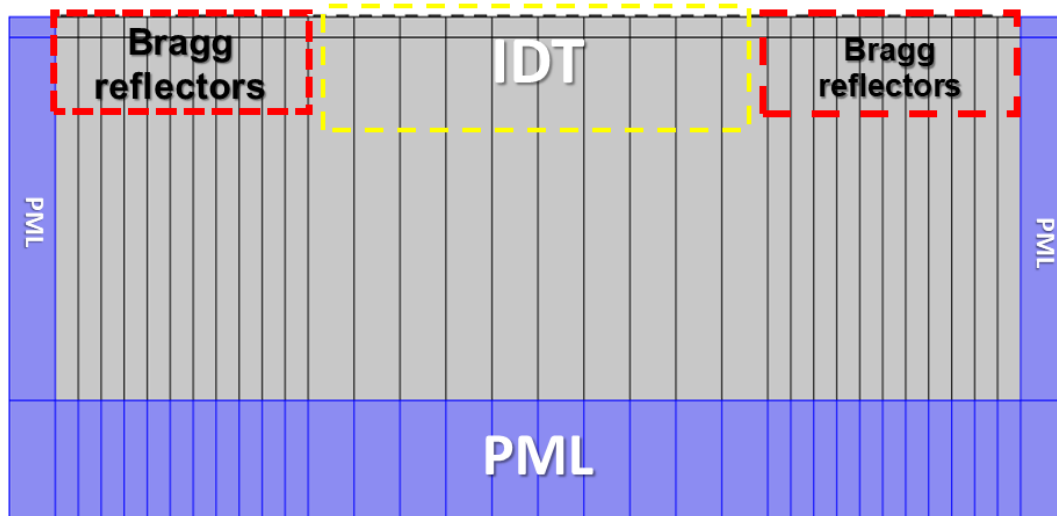


**Figure 3.7:** The different parts constituting the simulated SAW structure.

The part (i), the transmitter/receiver are already described previously in the case of the study of a unit cell except that this time we introduce a finite number of electrodes pairs (according to the [table \(3.6\)](#),  $N_{Pair}=50$ ).

For the parts (ii) we define the Bragg reflectors (Pt strips) witch act as a mirrors reflecting all mechanical energy of the incoming SAW wave, and thus creating an acoustic resonant cavity to forms the SAW resoator.

The PML part contains three regions (two laterals and one in the bottom of the substrate). The side regions contain the following overlapping layers; the Si substrate, a Pt layer and a AlN layer.

### 4.3.3. Materials constituting the structure:

For each chosen physic, a minimum of physical parameters must be defined so that the calculation can be launched. The physical parameters associated with each material, such as the dielectric permittivity, the Young's modulus, the bulk density, the elasticity tensor and the piezoelectric tensor...etc, are defined in each domain of the SAW structure.

#### 4.3.3.1. Silicon (Si)

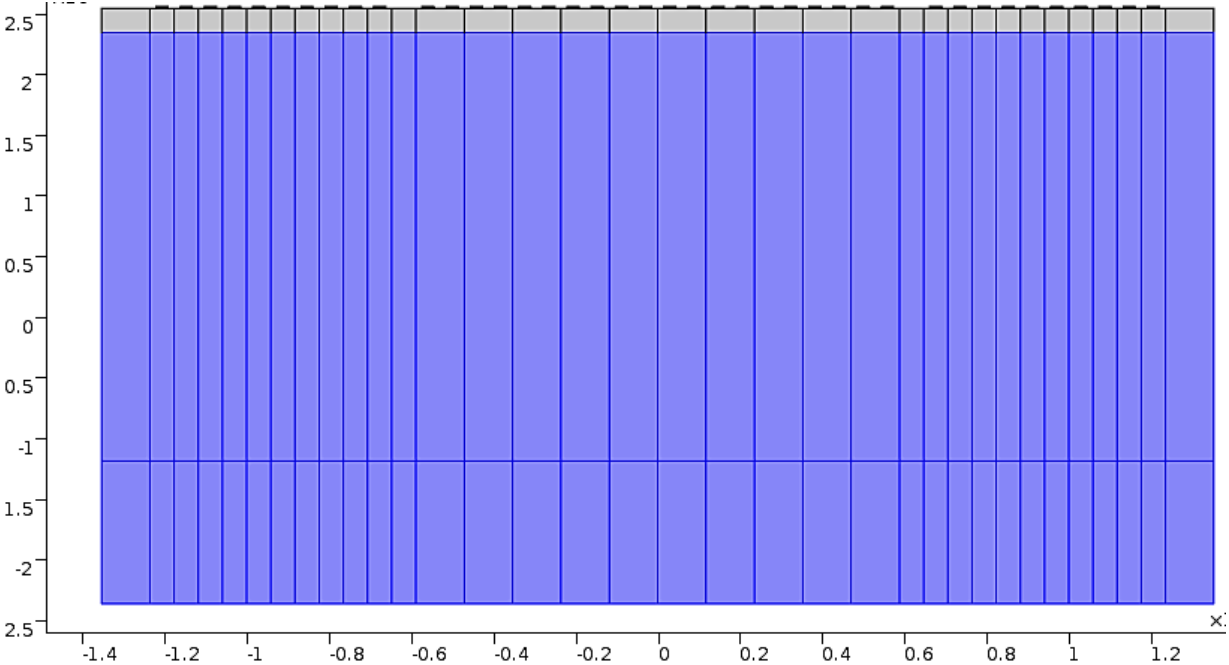
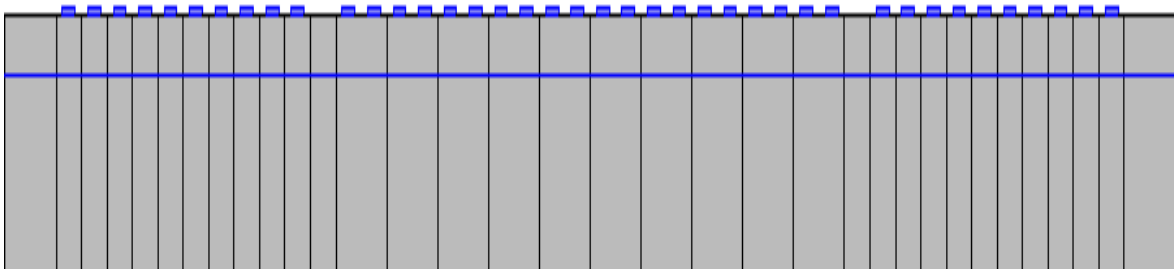


Figure 3.8: Assignment of Si to the substrate region.

**Table 3.7:** Physical properties of Si

<i>Property</i>	<i>Name</i>	Value
<i>Density</i>	<i>Rho</i>	2329 [kg/m <sup>3</sup> ]
<i>relative permittivity Si</i>	$\epsilon_r$	11.7
<i>Poisson's ratio</i>	<i>Nu</i>	0.15
<i>Young's modulus</i>	<i>E</i>	66.3e9 [Pa]

**4.3.3.2. Platinum (Pt) :**



**Figure 3.9:** Assignment of Pt as buffer layer between Si and AlN.

**Table 3.8:** Physical properties of Pt

<i>Property</i>	<i>Name</i>	Value of Pt
<i>Density</i>	<i>Rho</i>	21450 [kg/m <sup>3</sup> ]
<i>Coefficient of thermal expansion</i>	<i>alph_Pt</i>	9e-6 [1/K]
<i>Poisson's ratio</i>	<i>Nu</i>	0.23
<i>Young's modulus</i>	<i>E</i>	168e9[Pa]

### 4.3.3.3. Alumium nitride (AlN) :

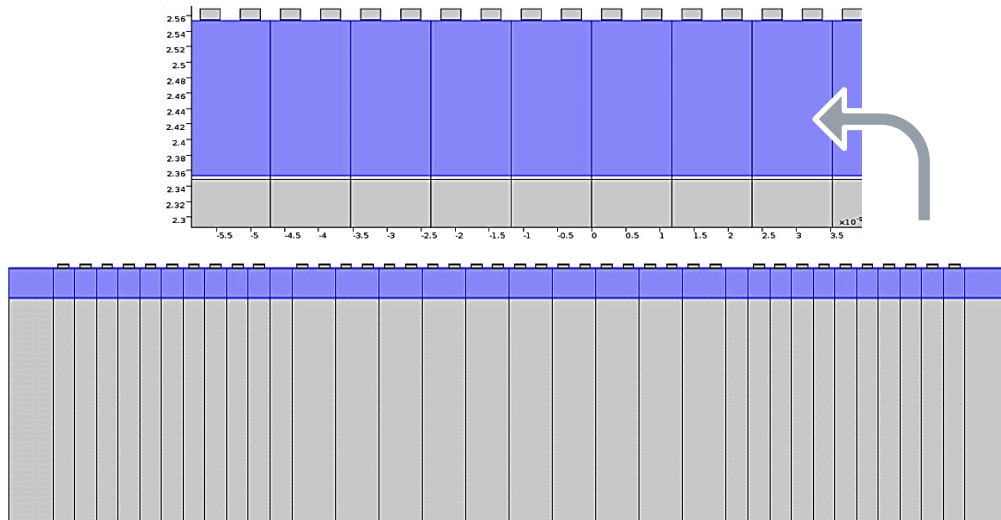


**Figure 3.10:** Assignment of AlN to the substrate region.

AlN is a piezoelectric (and dielectric) material, very interesting as piezoelectric active layer for the SAW device [figure 3.10](#). From the material library, the physical constants of AlN are listed in (Table (2.1) temperature effect). The choice of this material is made on the basis of its relatively good electromechanical coupling coefficient ( $k_{eff}^2$ ), which reflects the ratio of conversion of mechanical energy to electrical energy and vice versa, and also because of the stability of the oscillation frequency of this material. The generation of the wave is done by means of two pair of electrodes (IDTs), deposited on the surface of the piezoelectric layer. The electrical power applied on the transmitter IDTs is converted into an elastic wave that will propagate on the surface of the structure, this wave will be reflected back the same IDTs by the mean of Bragg reflectors acting as mirrors, the reflected energy is converted again into an output electrical power on the same IDTs.

### 4.3.3.4. IDTs electrodes with Pt on Ti :

Platinum thin film electrodes are popular for both low and high-temperature sensors due to their excellent electrical properties, high melting point and outstanding oxidation resistance<sup>[61]</sup>.



#### 4.3.3.4.1. Platinum:

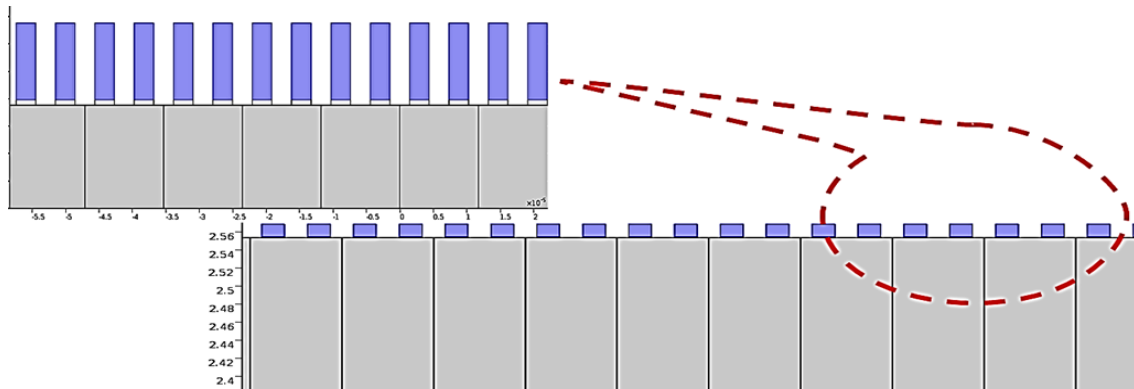


Figure 3.11 : Assignment of Pt electrode.

#### 4.3.3.4.2. Titanium:

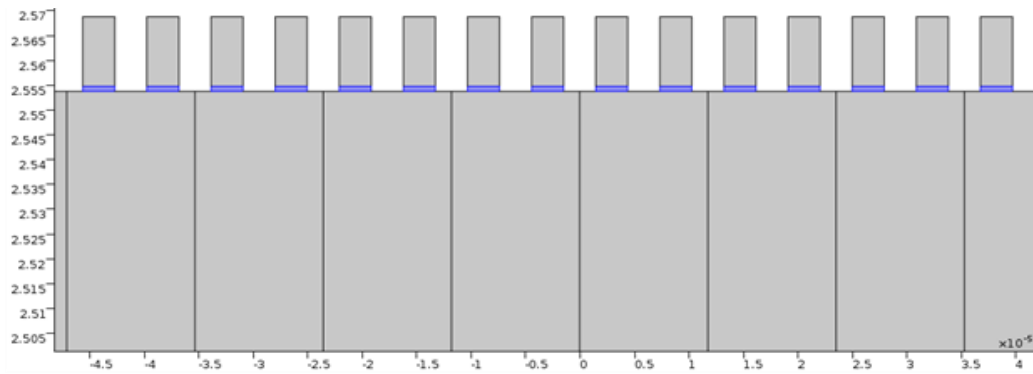


Figure 3.12 : Assignment of Ti electrode.

Table 3.9: Physical properties of Ti

<i>Property</i>	<i>Name</i>	Value
<i>Density</i>	<i>Rho</i>	4506[kg/m <sup>3</sup> ]
<i>Coefficient of thermal expansion</i>	<i>alph_Ti</i>	8.60e-6[1/K]
<i>Poisson's ratio</i>	<i>Nu</i>	0.321
<i>Young's modulus</i>	<i>E</i>	115.7e9[Pa]

#### 4.3.4. Electrical boundary condition (*Grounds, Terminal*):

The electric boundary conditions are due to the fact that the electrodes are connected to an external electric potential (generator). The anode and the cathode of the IDTs (interlaced) electrode system respectively linked to the generator ground ( $V=0$  Volt) and the to the potential  $V= 10 V_{out}$ . We can also apply an electrical power as the case of the characterization by a vector network analyser (VNA), for the determination of the Scatterin parameter  $S_{11}$ .

#### 4.3.5. Mechanical Boundary condition:

Numerical simulation of wave propagation problems in infinite media using the finite element method requires the reduction of the study domain to a limited domain. The method of absorbent layer is considered in this sens by using a perfectly matched Layer (PML) zones, surrounding borders of the structure. These layers are used in order to force the waves to be evanished and prohibit its reflection back the structure. However, the computation time required by a problem coupling the study domain and the absorbing domain becomes more important. **Figure 3.13** shows the PLM absorbing regions in our SAW resonator. In the extremity lateral ends and bottom, we use fixed constraint boundary condition, where the mechanical displacement is kept null ( $u_{tot}=0$ ). All the rest of the structure is free to be vibrating

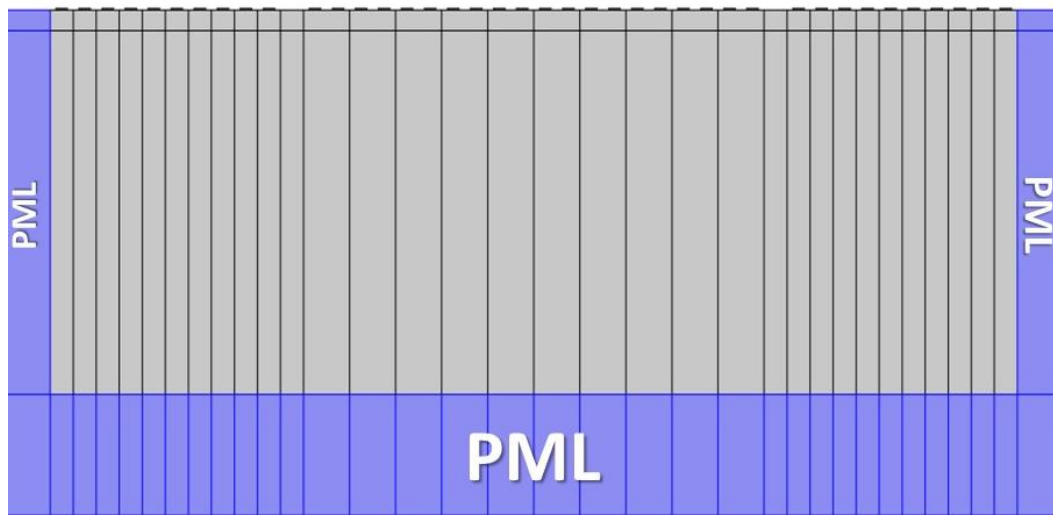


**Figure 3.13:** Definition of the mechanical boundary conditions PML.

#### 5. Meshing of the structure:

The mesh is the division of the global domain into a finite number of subdomains/elements. Comsol Multiphysics proposes several methods for 2D meshing, including free triangular, free rectangular, extruded mesh, etc. [64]. The choice of the mesh depends on the nature of the structure, the geometry, the boundary conditions and also the physics, in our case the mesh is rectangular distributed, and the size of the mesh elements depends mainly on the wavelength of the mechanical wave propagating in the structure. The mesh in  $Y$  direction is refined more at the interface where the surface wave is localized, while in  $X$  direction we considered 16 mesh elements per wavelength.

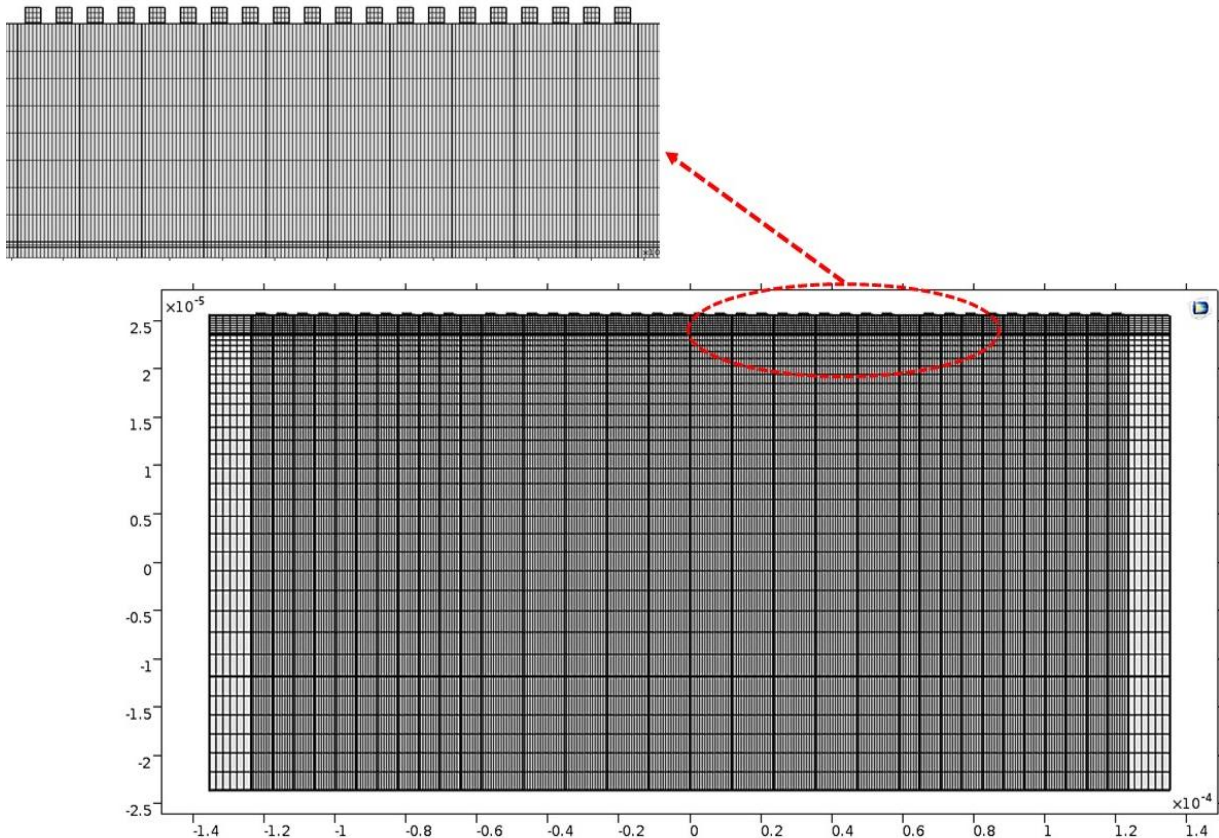


**Figure 3.14:** Mesh of the structure.

## 6. Definition of the frequency range of the study:

In this simulation the study is harmonic, it is carried out in the frequency range from 440 MHz to 600 MHz.

### Launching the calculation:

We now go to the calculation launching step (compute),

### Post processing of the results:

In this step we extract all necessary result, like electrical input admittance,  $S_{11}$  parameter, mechanical displacement field distribution, electrical field distribution, etc.

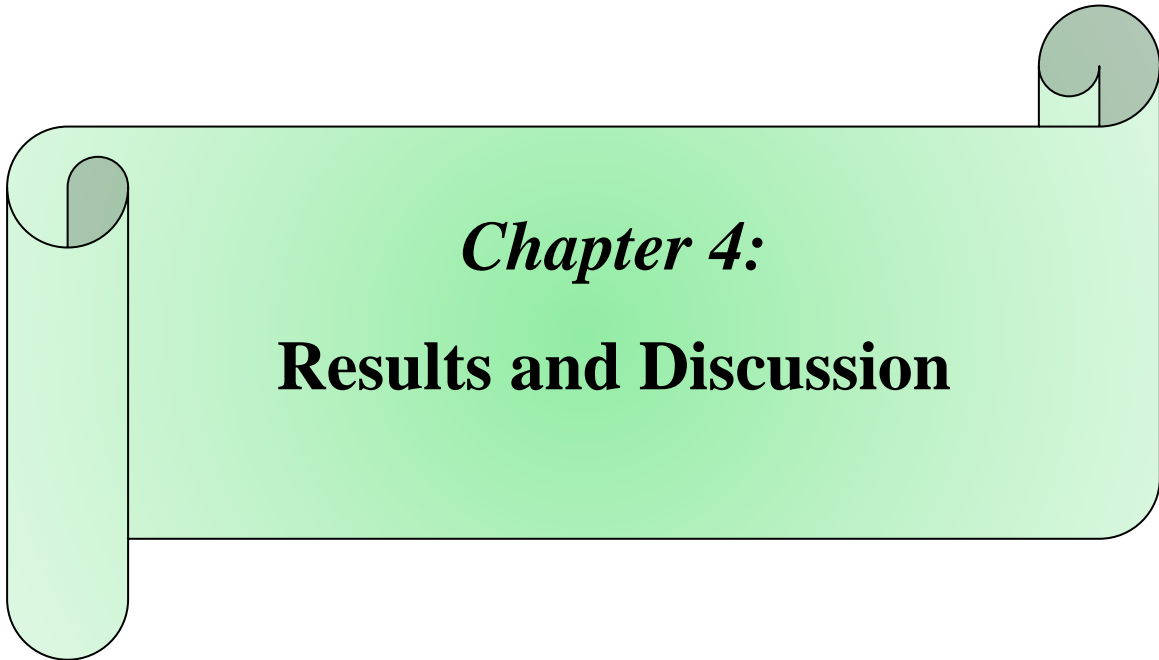
## 7. The electrical and mechanical response of SAW resonator

The main simulation parameters derived from the simulation of the piezoelectric phenomenon are the electrical charge ( $Q$ ) and the mechanical stress ( $T_{ij}$ ). All other parameters are derived from these later, especially the electrical admittance  $Y_{11}$  or scattering parameter  $S_{11}$  parameter and mechanical displacement field  $\mathbf{u}_{tot}$ . The

objective of our study is to determine the electrical admittance of the resonator, as well as the mechanical displacement field in the structure at the remarkable frequencies of the electrical response.

## **8. Conclusion**

The finite element method has become an efficiently computational tool to describe complex physical phenomena, subject to complicated boundary conditions such as the simulation of the electromechanical behavior of SAWs. We have presented in this chapter a modal study and harmonic study on a SAW cell (by considering the periodicity conditions) in order to deduce the frequencies and the eigenmodes of the structure. The design steps (Simulation procedure) and the modeling of a 2D SAW structure using the Comsol Multi-physics tool are described. Next, this simulation allowed us to faithfully reproduce the real behavior of the whole SAW structure by imposing boundary conditions such as (Electrical and Mechanical Boundary Conditions), symelary to the ones used in reality.



*Chapter 4:*  
**Results and Discussion**

## 1. INTRODUCTION :

In this chapter the results of the study are presented and discussed with we determine the center frequency of resonator at room temperature, The electromechanical coupling coefficient ( $k^2$ ) and SAW resonator quality factor ( $Q$ ), then the temperature coefficient of frequency (TCF) value. All the results will obtained for the structure with and without Pt bottom layer, our first goal is to compare our simulation result with those experimentally obtained by Chuian Li *et al.* Than, we attempte to generalize our aprouch do other new structure and pplications like SAW delay line working in time domaine for the wireless SAW sensor (with an antenna).

## 2. Structure (*Pt/AlN/Pt/Si*):

Figure 4.1 show as the final structure *Pt/AlN/Pt/Si* of the SAW sensor with  $N_B=50$ ,  $N_p=50$ , This structure is obtained by combining aproximately all the geometrical parameter the Chuian Li structure, in order to obtain the same situation and compare the results.

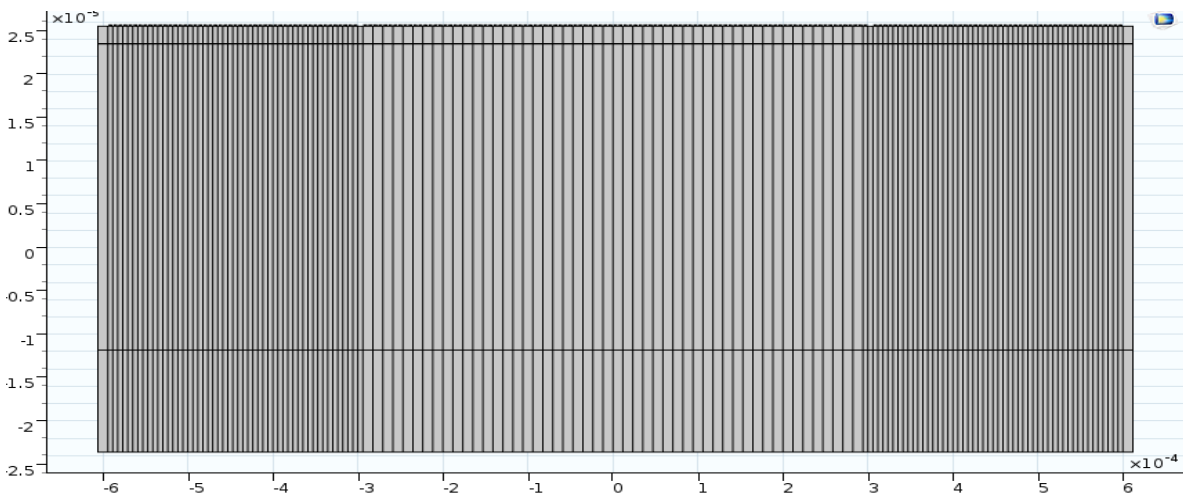
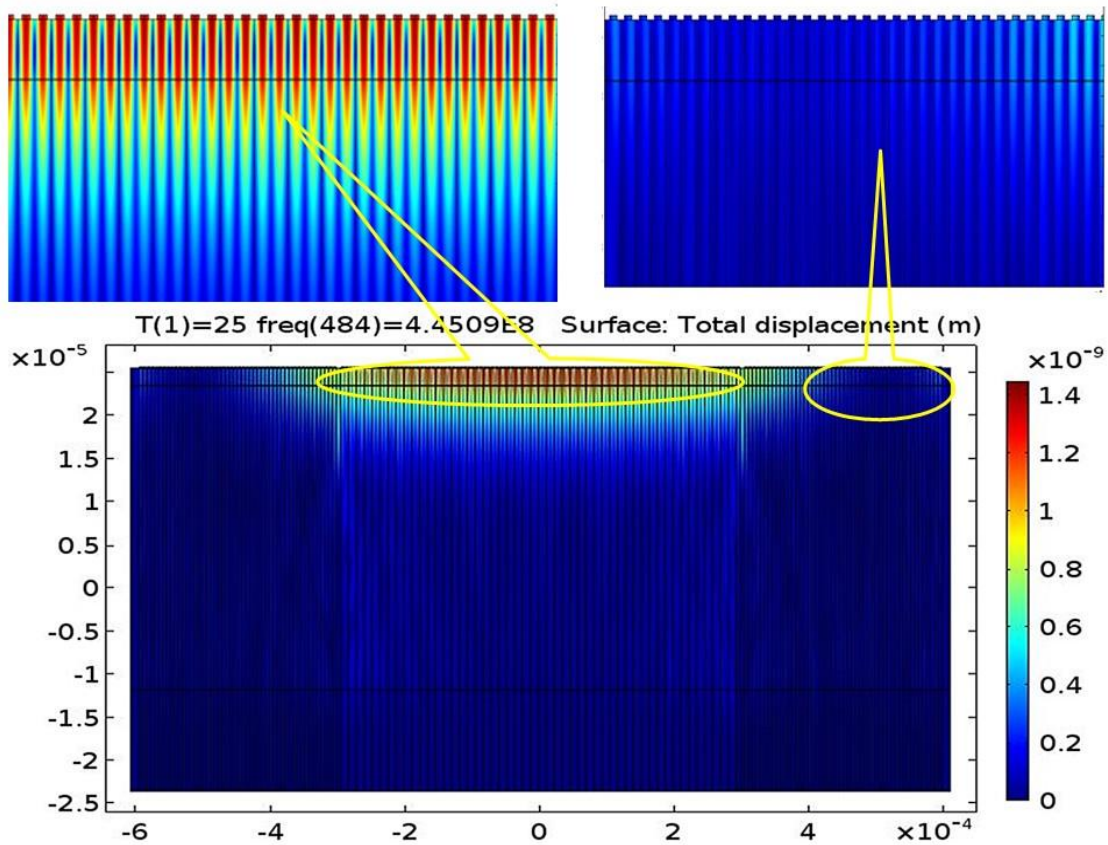


Figure 4.1: Geometry the SAW structure *Pt/AlN/Pt/Si*, ( $N_p=50$ ,  $N_B=50$ )

### 2.1. Total mechanical displacement field:

At the resonance frequency  $f_0=445.09$  MHz, the mechanical displacement field is maximum in the center of the SAW structure because of the use of the bragg reflectors the mechanical displacement field is confined in the center of the structure, all mechanical energy of the SAW waves is localized on the IDT system, so reflectors act as bragg mirror which prohibit the mechanical loss forming thus an acoustic resonance cavity.



**Figure 4.2:** Mechanical displacement field of the SAW structure  $Pt/AlN/Pt/Si$ , with ( $N_p=50$ ,  $N_B=50$ ) at the resonance frequency of 445.09 MHz.

## 2.2. The electrical input admittance $Y_{11}$ :

The electrical input admittance noted  $Y_{11}$  or  $Y$  (expressed in "Siemens" (S) or  $\Omega^{-1}$ ) is the inverse of the electrical input impedance  $Z_{11}$  or  $Z$  ( $\Omega$ ) of the SAW device:

$$Y = \frac{1}{Z} \quad (4.1)$$

The electrical admittance is complex, its real part represents the electrical conductance ( $G$ ) and its imaginary part is the acoustic susceptance ( $B$ ), hence:

$$Y = G + jB \quad (4.2)$$

From comsol Multiphysics simulation, we can get this parameter ( $Y_{11}$ ) for different values of temperature from 25°C to 500°C for the structure  $Pt/AlN/Pt/Si$  with  $N_p=50$ ,  $N_B=50$  it's shown in [figure 4.3](#).  $Y_{11}$  present a maximum at the serie resonance frequency (electric origine) and a minimum at the parallet resonance frequency (acoustic origine).  $Y_{11}$  curve hexibits a shift toward low frequencies when the temperature increases.

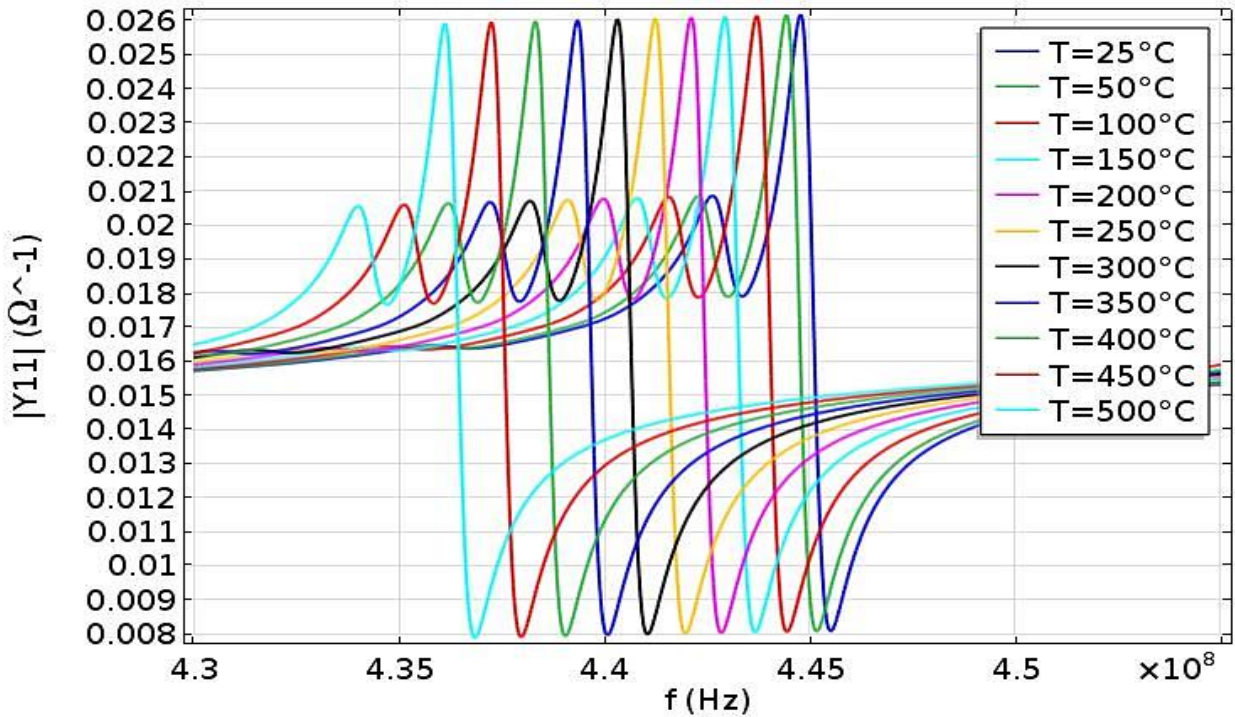


**Figure 4.3:** ( $Y_{11}$ ) Electrical input admittance amplitude of the SAW temperature sensor for different values of temperature.

### 2.3. $S_{11}$ -Scattering parameter:

$S_{11}$ -Scatterind parameter represents the reflection coefficient of the electrical power at the SAW input IDT. It is given by :

$$S_{11} = \frac{Z_{11} - Z_0}{Z_{11} + Z_0} \quad (4.3)$$

Where,  $Z_{11}$  represents the electrical input impedance of the SAW device and  $Z_0$  is electrical input impedance of the generator,  $S_{11}$  can be extracted directly from simulation when using electrical terminals with electrical power excitation (as the case of the Vectorial Network Analyser, VNA). But, it can also be deduced directly from  $Y_{11}(f)$  as explained in the figure 4.4.

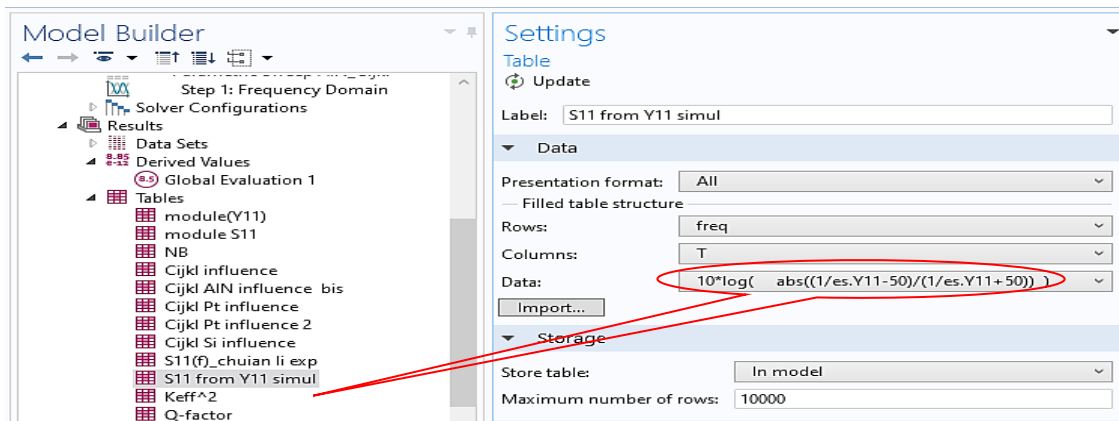


**Figure 4.4:** Extraction of  $S_{11}(f)$  from  $Y_{11}(f)$ .



The variation curves  $S_{11}(f)$  for different values of the temperatures (T), ranging from 25°C to 500°C with a step of 25°C are shown in figure 4.5.  $S_{11}$  present a minimum value at the resonance frequency of the device at  $f=445.09$  MHz for  $T=25^\circ\text{C}$ , the same as the corresponded  $Y_{11}$ . The  $S_{11}$  curve exhibits, also, a shift toward low frequencies when the temperature increases.

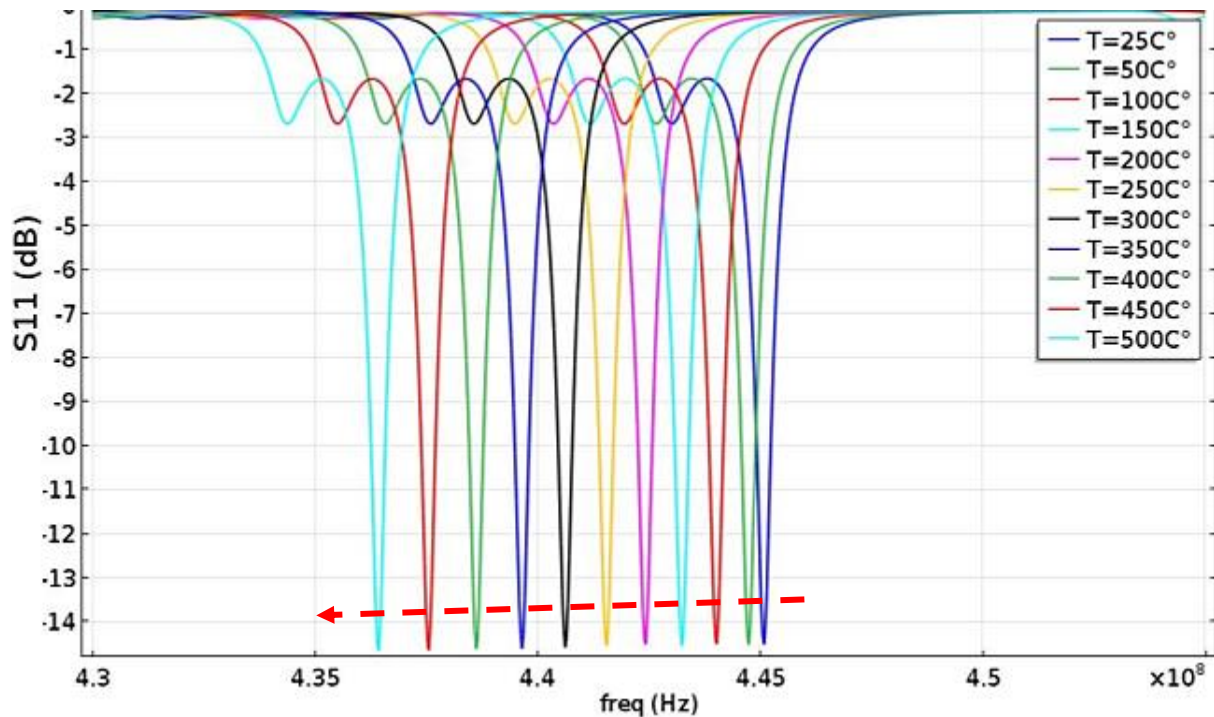


**Figure 4.5:** ( $S_{11}$ ) Electrical response of the temperature sensor in term of  $S_{11}$ -parameter for different values of temperature.

The behaviour of both  $Y_{11}(f)$  or  $S_{11}(f)$  to the temperature changing is attributed to the change in the acoustic wave velocity, and to the thermal expansion of all device materials. Obviously, thermal expansion would enlarge finger width and spacing between IDTs, this dilatation increases the value of the wave length  $\lambda$ . Since  $f_0$  is inversely proportional to the wavelength  $\lambda$  (when  $(\lambda)$  increases  $(f_0)$  decreases). the center frequency ( $f_0$ ) has significantly reduced while temperature grew up to 200 °C. The SAW resonance frequency ( $f_0$ ) shifted from 445 MHz at 25 °C to 436 MHz at 500 °C.

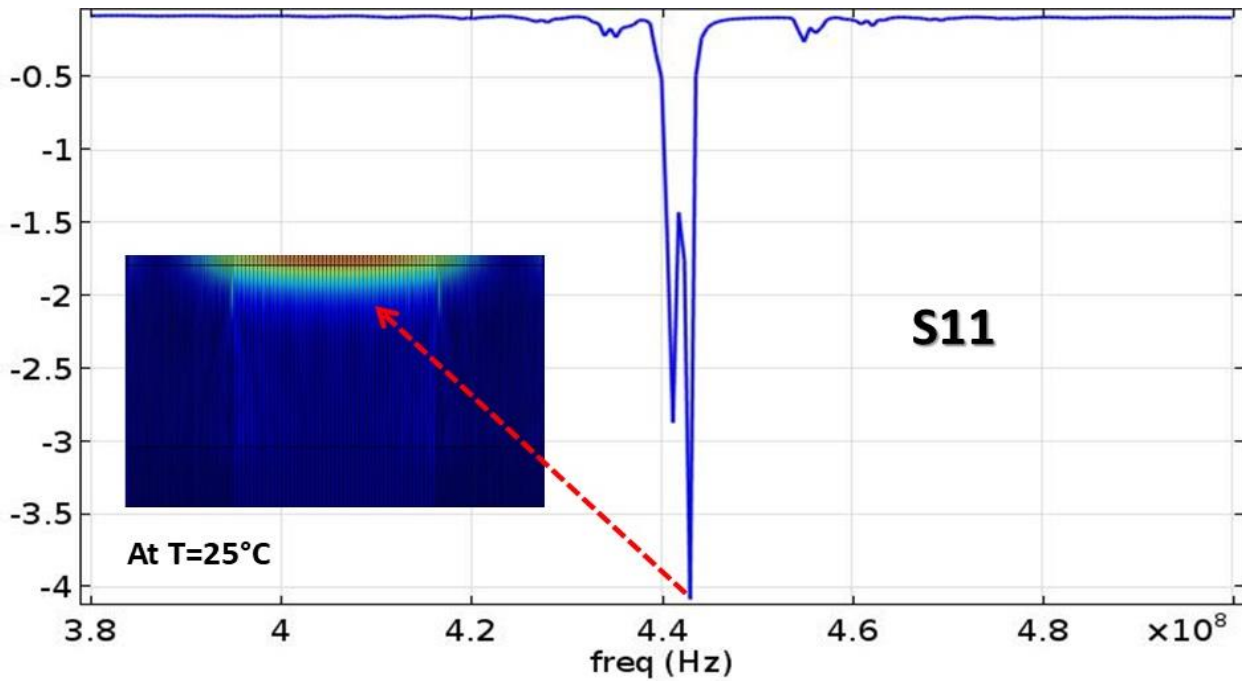


**Figure 4.6:** Characteristic of SAW resonator at room temperature.

After many adjustments using the parametric sweep on the elasticity coefficients and density of AlN, Pt and Si, available in the literature. The SAW resonance frequency ( $f_0$ ) is evaluated at 445 MHz. The swept values of these parameters are presented in the tables, (figure 4.7, 4.8 and 4.9) we've also made two crystal orientations, for Si (100) and AlN (002); where we have oriented Si in the plan system (xz) and we chose it like a fully anisotropic material and we oriented also AlN in the plan system (xz).

Parametric Sweep

Label: Parametric Sweep AlN\_Cijkl

Study Settings

Sweep type: Specified combinations

Parameter name	Parameter value list	Parameter unit
Caln11_0 (elastic cts of ALN)	3.741E11 3.788E11 4.102E11 3.7979E11 4.1E11 4.1006E11 4.1006E11 4.1006E11	Pa
Caln12_0 (elastic cts of ALN)	1.286E11 1.289E11 1.424E11 1.2041E11 1.49E11 1.0069E11 1.49E11 1.49E11	Pa
Caln13_0 (elastic cts of ALN)	1.003E11 9.61E10 1.101E11 9.002E10 9.9E10 8.382E10 1.101E11 8.382E10	Pa
Caln33_0 (elastic cts of ALN)	3.517E11 3.575E11 3.85E11 3.5739E11 3.89E11 3.8624E11 3.8624E11 3.8624E11	Pa
Caln44_0 (elastic cts of ALN)	1.116E11 1.124E11 1.229E11 1.1377E11 1.25E11 1.0058E11 1.229E11 1.25E11	Pa
RhoAlN_0	3194 3560 3560 3206.5 3300 3260 3194 3194	kg/m <sup>3</sup>

**Figure 4.7:** Parametric sweep of elasticity constants and the density of AlN.

Label: Parametric Sweep Si\_Cijkl

Study Settings

Sweep type: Specified combinations

Parameter name	Parameter value list	Parameter unit
Csi11_0 (elastic cts of SI)	165 166 166 165.7 166 166 166 166	GPa
Csi12_0 (elastic cts of SI)	34.7 64 63.9 34.7 63.9 43.15 63.9 34.7	GPa
Csi44_0 (elastic cts of SI)	65.5 80 79.6 65.5 79.6 79.69 80 80	GPa

**Figure 4.8:** Parametric sweep of elasticity constants of the Si.

Label: Parametric Sweep Pt Cijkl

Study Settings

Sweep type: Specified combinations

Parameter name	Parameter value list	Parameter unit
C11_Pt	347 227.4	GPa
C12_Pt	222 99	GPa
C44_Pt	62.5 64.2	GPa

**Figure 4.9:** Parametric sweep of elasticity constants Pt.

## 2.4. The electromechanical coupling factor ( $k^2_{eff}$ ):

The electromechanical coupling coefficient ( $k^2$ ) is an important quantity in determining the efficiency of acoustic excitation by IDTs, and it is an inherent characteristic of the acoustic wave propagation in a given piezoelectric medium which represents empirically the piezoelectric strength of the acoustic wave mode.[13] It should be noted that the  $k^2$  of SAW resonator (in %) represent the ratio conversion of the mechanical energy to the electrical energy into the piezo-material and vice versa. This parameter is determined from the real and the imaginary part of the  $S_{11}$  parameter according to the following formula:

$$k^2 = \frac{\pi G(f_0)}{4N B(f_0)} \quad (4.4)$$

where  $N$  is the number of finger pairs of IDT,  $G(f_0)$  and  $B(f_0)$  are the radiation conductance and the acoustic susceptance respectively.

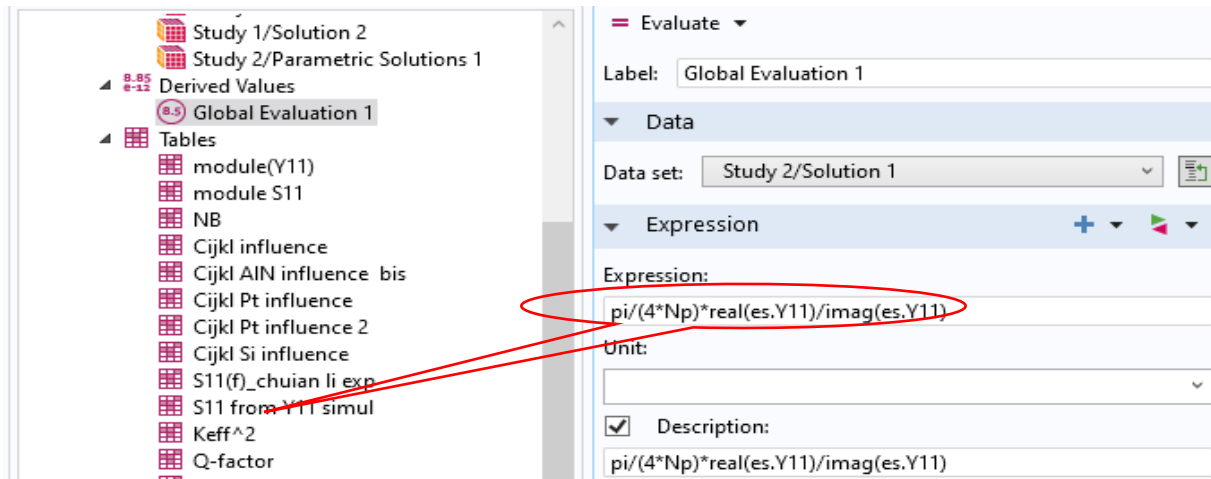


**Figure (4.10):** The electromechanical coupling coefficient formula.

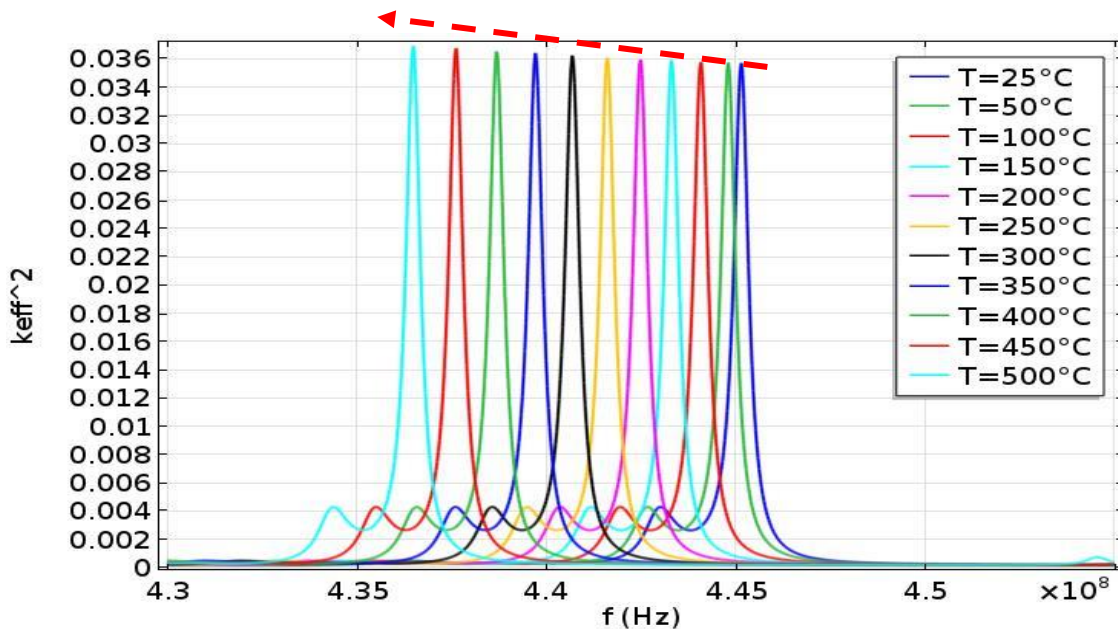


**Figure 4.11:** The electromechanical coupling coefficient of the temperature sensor for different values of temperature.

From [figure 4.11](#), we see that the  $k^2$  coefficient increases with temperature. this phenomenon is also observed in the reference [\[62\]](#).

The AlN Lamb wave resonators with the electrically floating bottom electrode provides a larger effective coupling coefficient than the grounded and open ones.[\[63\]](#) This similar phenomenon has also been found in our study. From the [figure 4.12](#) we see that The AlN resonator with the floating bottom electrode shows a  $k^2$  of 0.35%, It is considered that the floating bottom electrode could reduce the additional parasitic capacitances and increase the parallel resonance frequency and consequently enhance the  $k^2$ . Moreover, the  $k^2$  value increase from 0.35% at room temperature to

0.37% at 500°C. Interestingly, we found that the  $k^2$  coefficient quasi-linear increases with temperature. with an increase of 5.71% is observed.

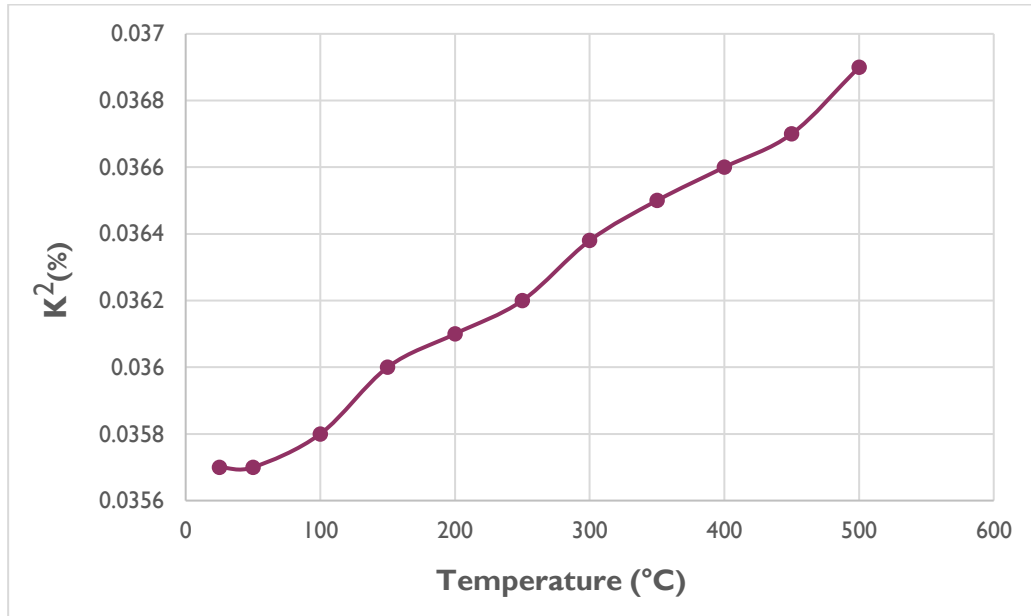


**Figure 4.12:** Variation of  $k^2$  versus temperature for the SAW resonator.

### 2.5. Quality factor (Q-factor) of Pt/AlN/Pt/Si SAW structure:

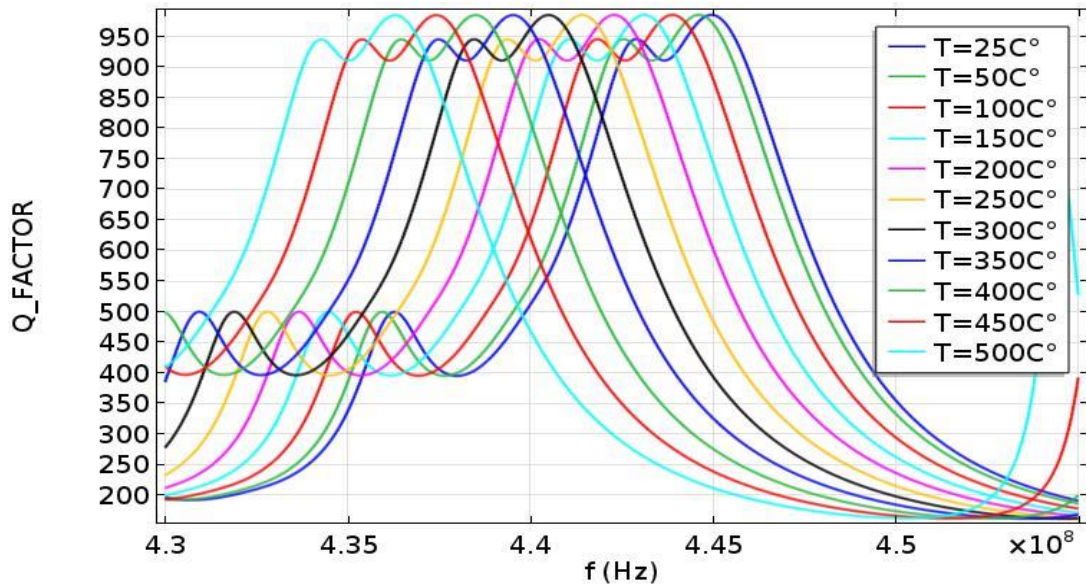


**Figure 4.13:** The Quality factor of the temperature sensor for different values of temperature.

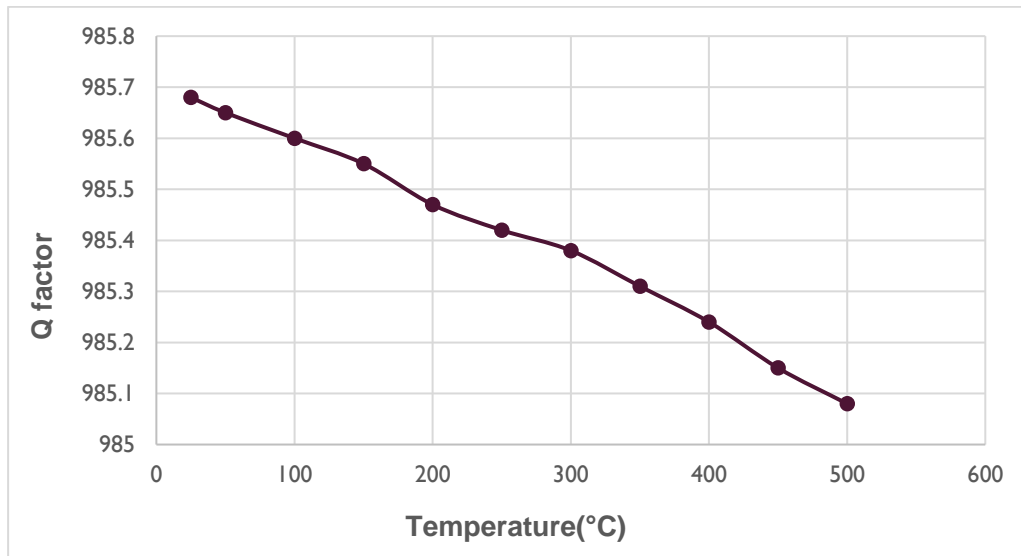


**Figure 4.14:** Quality factor variation versus temperature for SAW resonator.

The relationship between quality factor and temperature is plotted in [figure 4.14](#); a linear slightly decrease as function of temperature is observed. At 25°C Q is 985.68 and in for 500 °C it is of 985.08, which means that Q-factor still almost constant versus temperature.

## 2.6. Sensitivity of the sensor:

The relationship between frequency and temperature is plotted in [figure 4.15](#); a linear decrease as function of temperature is observed and the slope, which represents the sensitivity of the device, is given by a linear fit on the calculated values of the resonance frequency ( $f_0$ ) for each temperature. The value of the sensor sensitivity (calculated from the slope of the obtained line) is  $s = -40.54 \text{ ppm/}^\circ\text{C}$ .

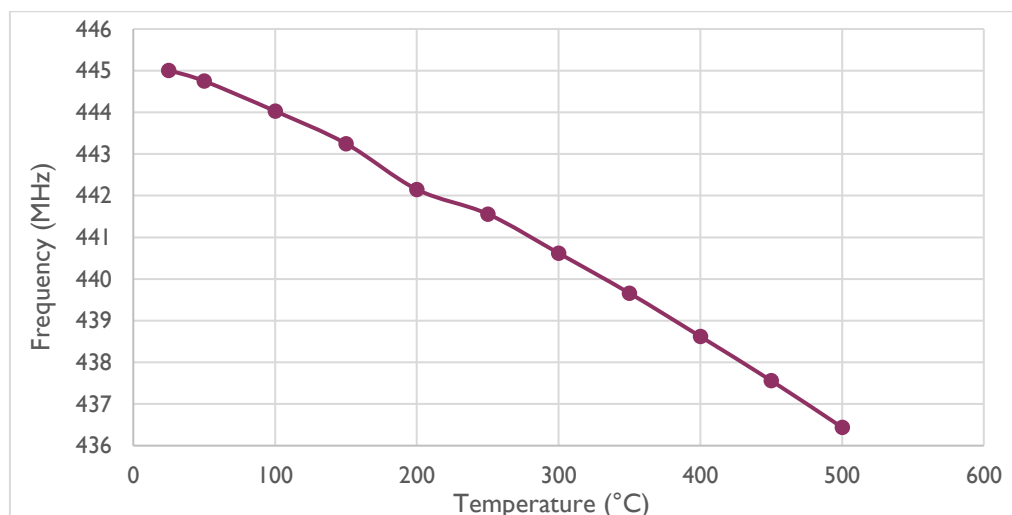


**Figure 4.15:** Resonance frequency variation versus temperature for SAW sensor.

### 3. Structure (*Pt/AlN/Si*):

In this part, we will simulate the same structure but without the Pt buffet layer, With  $N_B=50$ ,  $N_p=50$  (see, Figure 4.16).

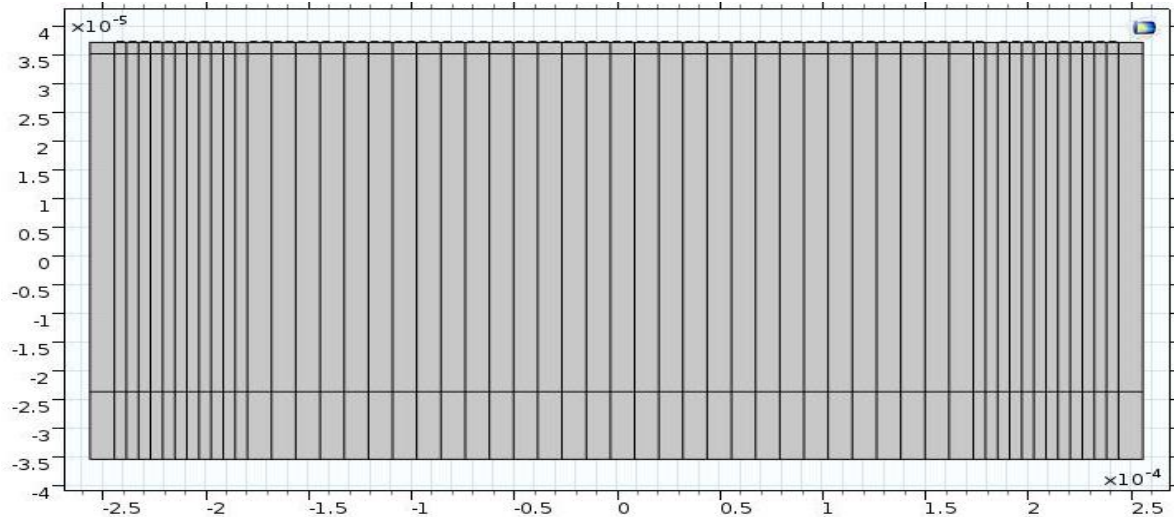


**Figure 4.16:** Geometry of the SAW structure *Pt/AlN/Si*, ( $N_p=50$ ,  $N_B=50$ )

#### Total mechanical displacement field:

The Total mechanical displacement field is presented in the figure 4.17, the resonance frequency  $f_0=418.72$  MHz, the mechanical displacement field is maximum in the center of the SAW structure, The mechanical energy of the SAW wave is localized on the IDT system because of the reflectors forming the acoustic resonance cavity.

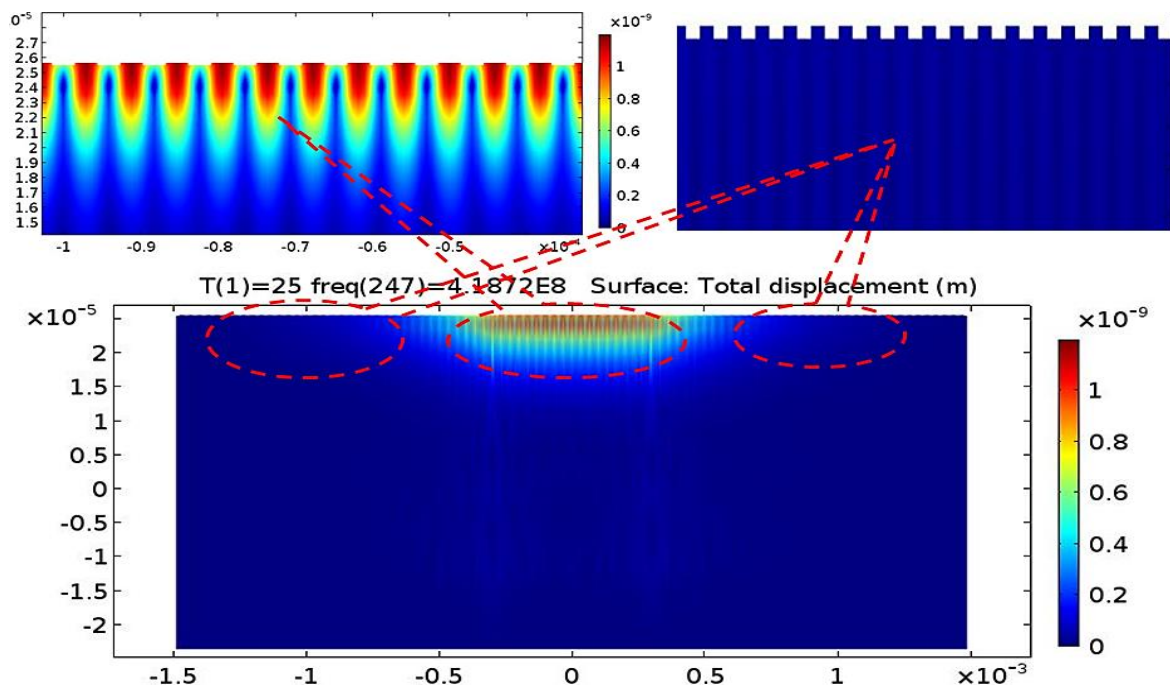


**Figure 4.17:** Mechanical displacement field of the structure *Pt/AlN/Si*, ( $N_p=50$ ,  $N_B=50$ ) at the resonance frequency of 418.7 MHz.

#### 4.1. The electrical input admittance $Y_{11}$ :

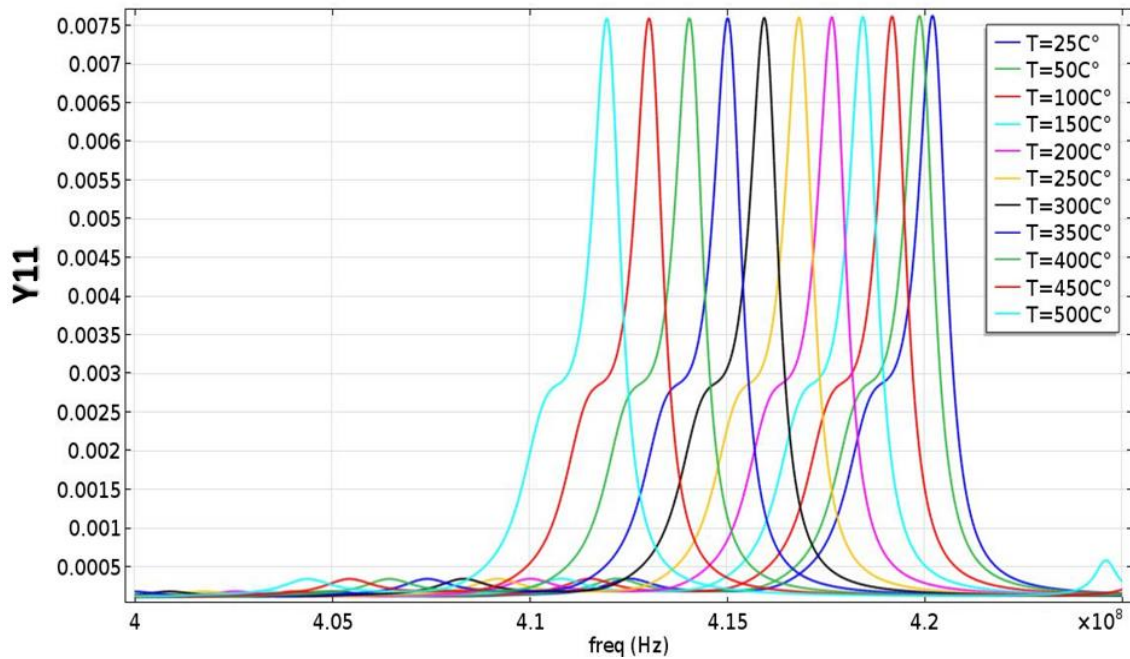


Figure 4.18: ( $Y_{11}$ ) Electrical input admittance of the temperature sensor for different values of temperature.

#### 4.2. $S_{11}$ -Scattering parameter:

The reflection coefficient variation curves  $S_{11}(f)$  versus temperatures ( $T$ ) ranging from 25°C to 500°C with a step of 25°C of the structure *Pt/AlN/Si* are shown in figure 4.19.

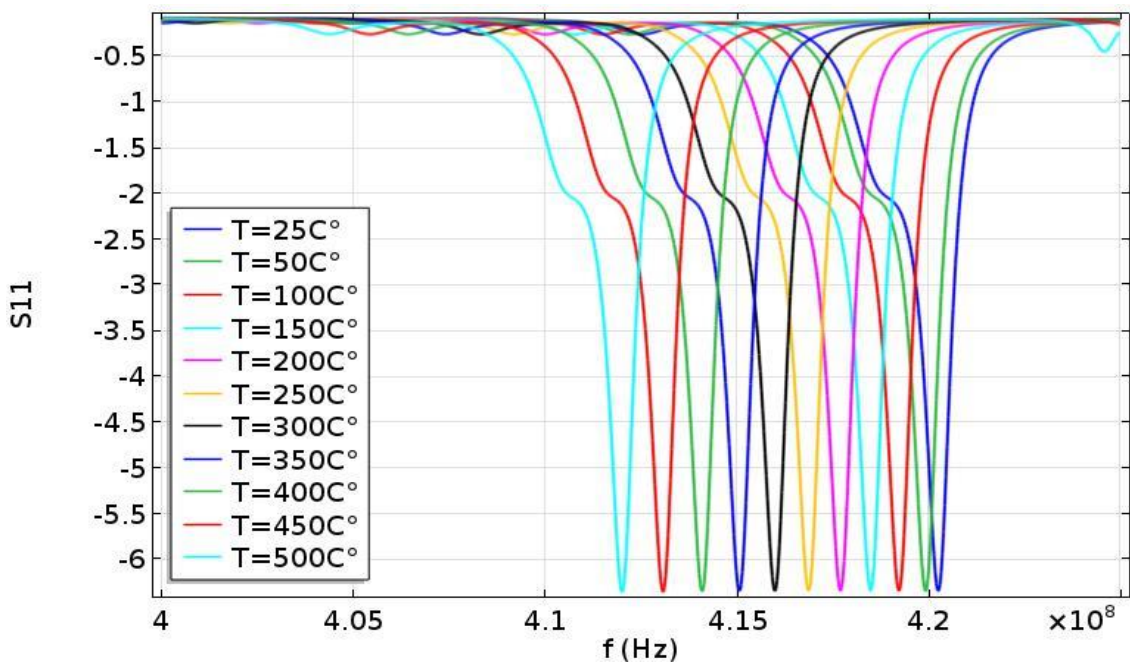
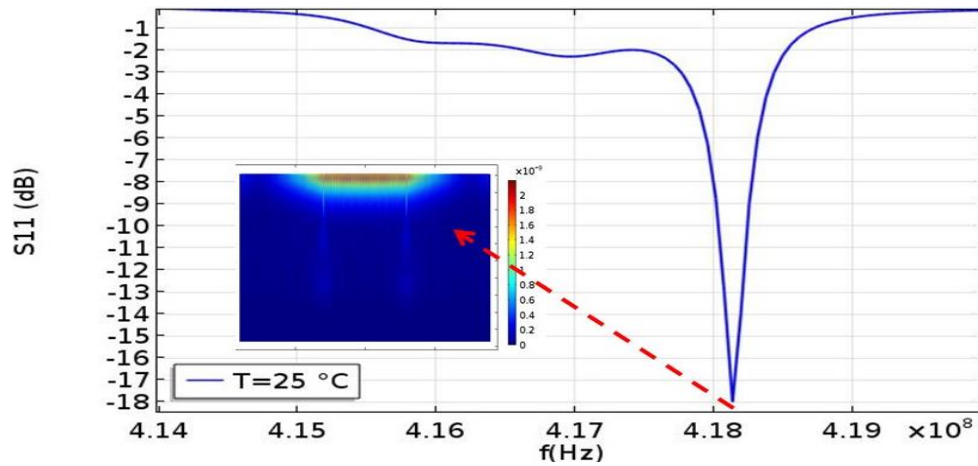


Figure 4.19: ( $S_{11}$ ) Electrical response of the temperature sensor for different values of temperature.





**Figure 4.20:**  $S_{11}$  Performance at room temperature ( $N_b=10$ ).

Figure 4.19 shows the frequency response ( $S_{11}$  magnitude) of SAW resonator at different values of temperature. The resonance frequency ( $f_0$ ) of Pt/AIN/Si configuration is 420.3 MHz.

The SAW resonant frequency is shifted from 445.01 MHz for the structure with Pt Bottom Layer to 420.3 MHz for the structure without Pt bottom layer, this confirms that SAW velocity in the structure Pt/AIN/Pt/Si is higher than the SAW speed in Pt/AIN/Si structure. The adding of the Pt layer leads to an increase in the SAW velocity and consequently in its resonant frequency.

### 4.3. The electromechanical coupling factor ( $K^2_{eff}$ ):

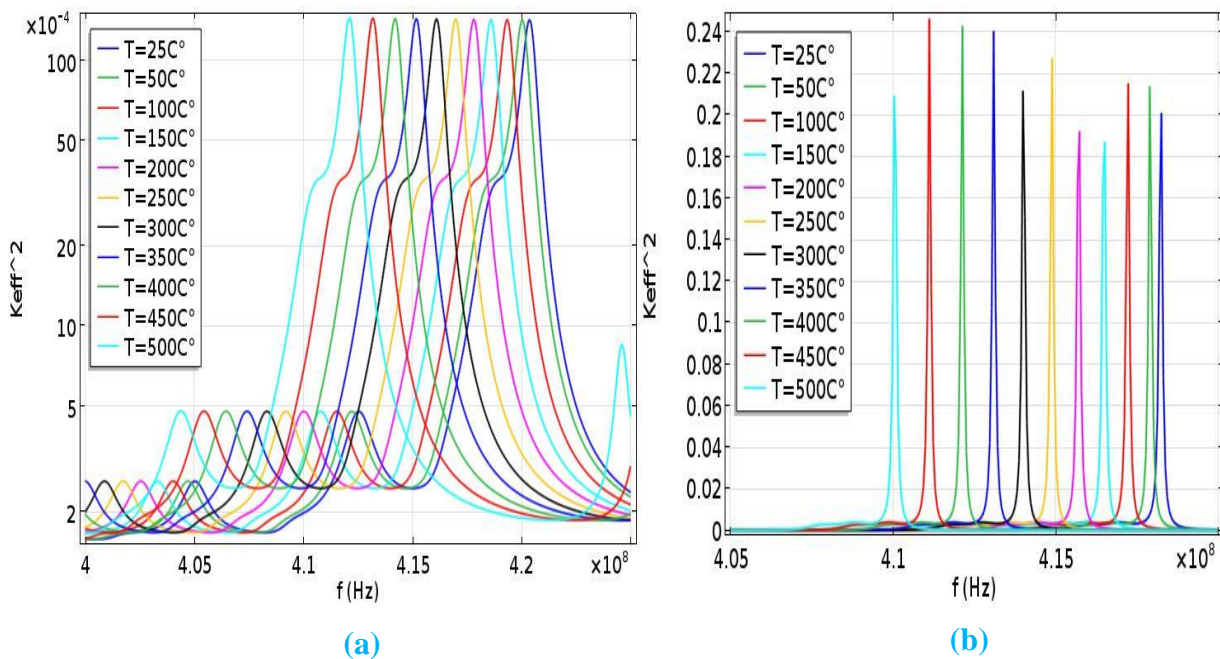


**Figure 4.21:** The electromechanical coupling factor of the temperature sensor for different values of temperature, a)-for  $N_b=50$ , b)- $N_b=100$ .

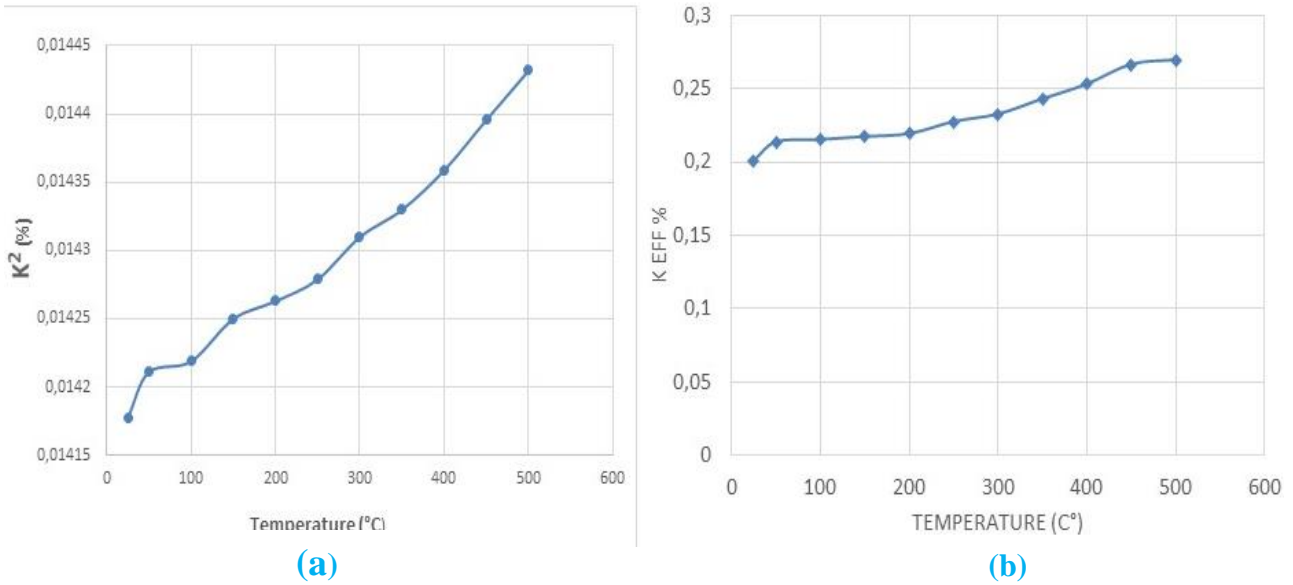


**Figure (4.22):** Relative variation of  $k^2$  versus temperature measured on SAW resonator of the structure *Pt/AIN/Si* a)-for  $N_s=50$ , b)- $N_s=100$ .

The  $k^2$  coefficient increases with temperature in this configuration. From the figure 4.22, we see that the  $k^2$  value for *Pt/AIN/Si* is 0.14 %, the *Pt/AIN/Pt/Si* configuration has larger  $k^2$  value (0.37%) than *AIN/Pt/Si*.

#### 4.4. Quality factor (Q-factor):

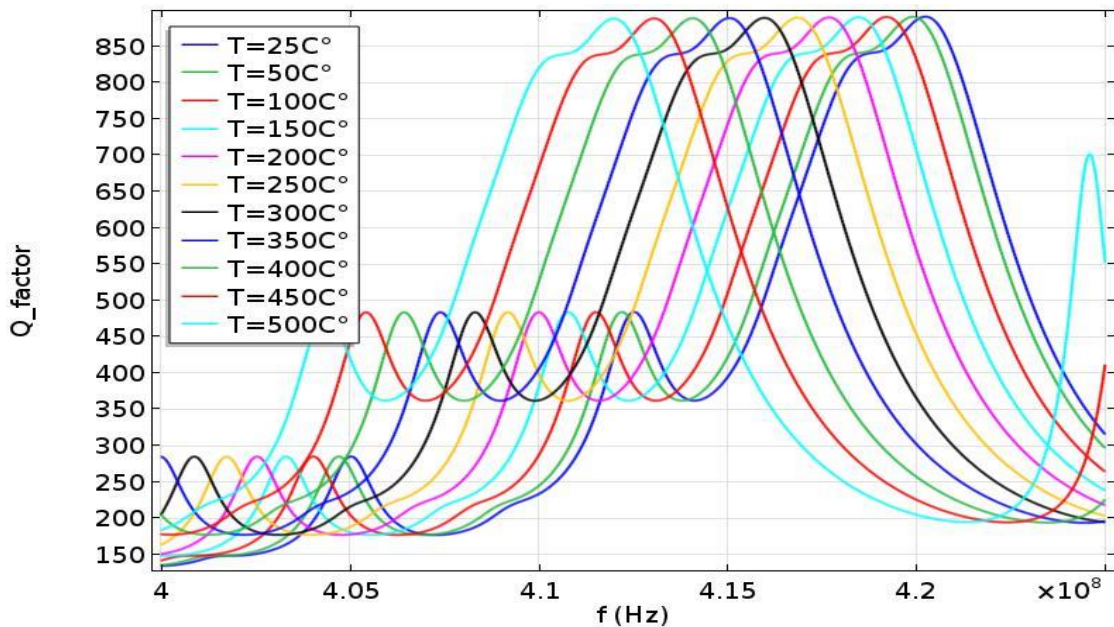


**Figure 4.23:** The Quality factor of the temperature sensor for different values of temperature.

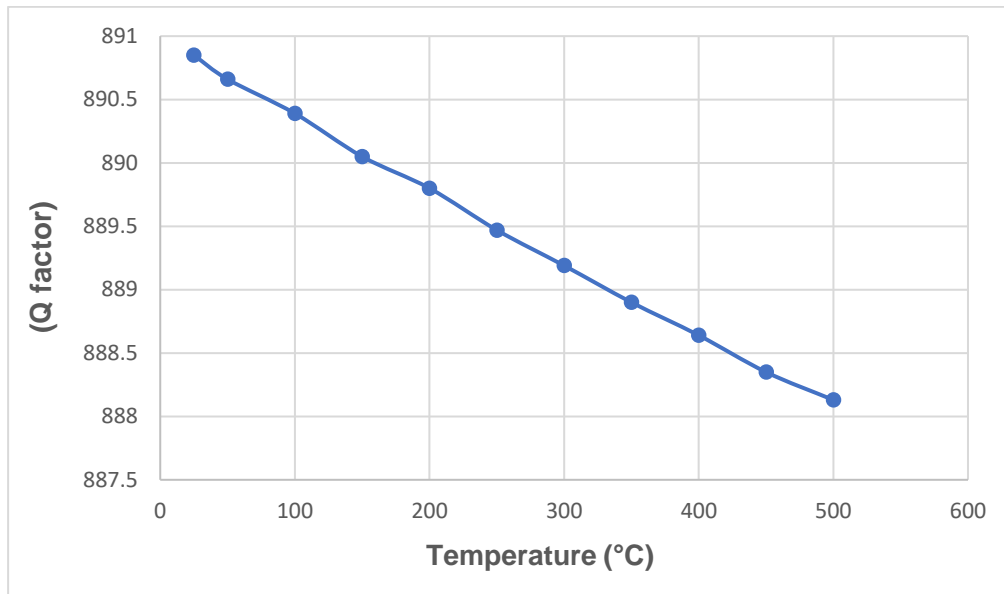


**Figure 4.24:** Quality factor variation versus temperature for SAW resonator.

The relationship between quality factor and temperature is plotted in [figure 4.24](#); a linear decrease as function of temperature is observed. from 25°C where the Q=890.85 to 500 °C where Q=888.13.

#### 4.5. Sensitivity of the sensor:

The resonance frequency variation in function of temperature is plotted in [figure 4.25](#), A linear decrease in frequency is seen as a function of temperature, a linear fit on this variation leads to the slope  $s$ , which represents the sensitivity of the device. The sensor sensitivity is  $s = - 40.32 \text{ ppm/}^\circ\text{C}$  (TCF constant of the structure).

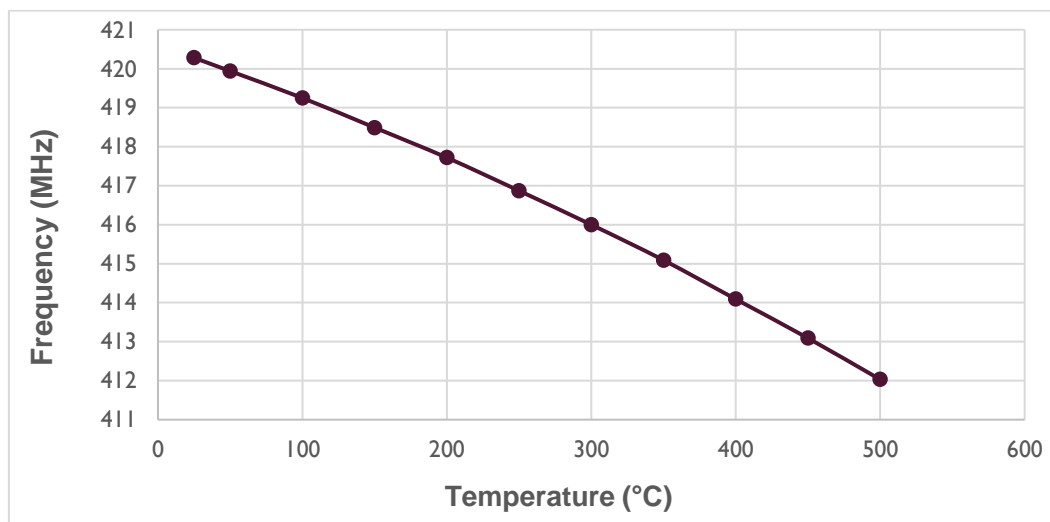


**Figure 4.25:** Resonance frequency variation versus temperature for *Pt/AlN/Si* SAW sensor.

However, the quasi-constant sensitivity to temperature makes it well suited for temperature monitor application. Compared with that of *Pt/AIN/Si* configuration, the TCF value of *Pt/AIN/Pt/Si* configuration decreases by indicating a much higher sensitivity to temperature change.

## 5. Comparison between experimental results (Chuian Li) and our theoretical results (Simulation):

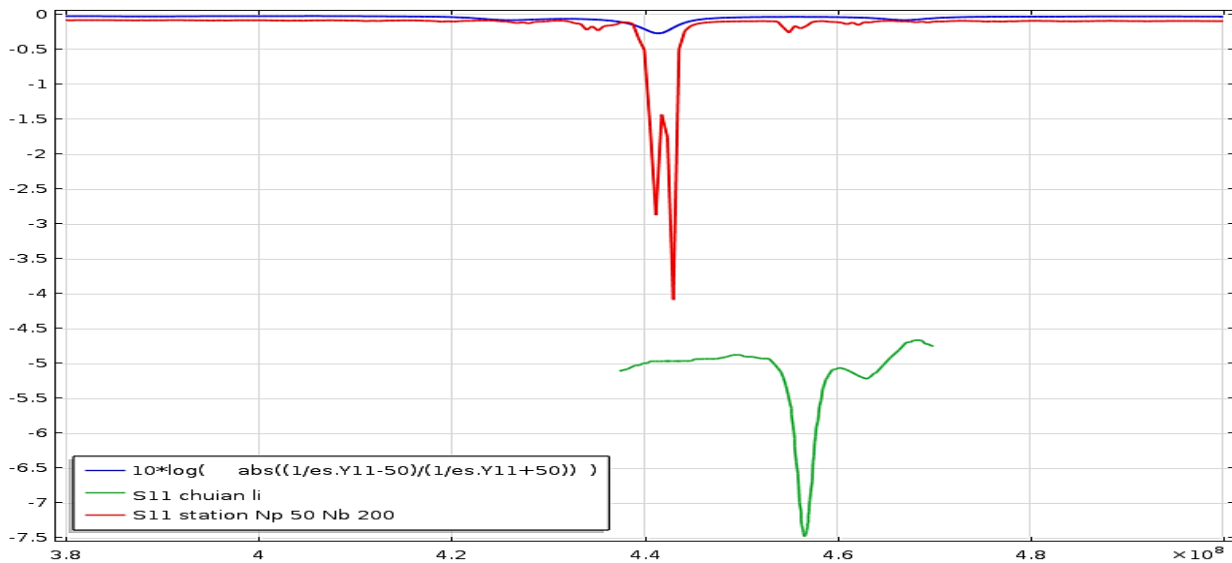
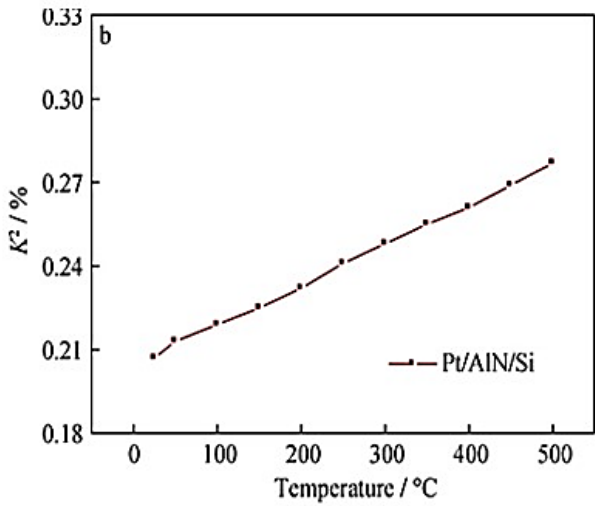


**Figure 4.26:** Comparison of our simulated results to experimental data of Chuian Li *et al.* of the structure *Pt/AIN/Pt/Si*

Figure 4.26 shows a comparison between our simulated results obtained by FEM model described previously, to the experimental data realized by Chuian Li *et al* [64], on the SAW structure, with Pt bottom electrode (*Pt/AIN/Pt/Si*). The simulated resonance frequency value deduced from  $S_{11}$  magnitude, is about 445.07 MHz, and that of the literature is about 456.6MHz. This shows that our results are in good agreement with experimental data. Because of the electrical mismatch impedance between generator and the SAW device, the level of experimental  $S_{11}$  parameter, is around -5dB.



Litterature results (Chuian Li)

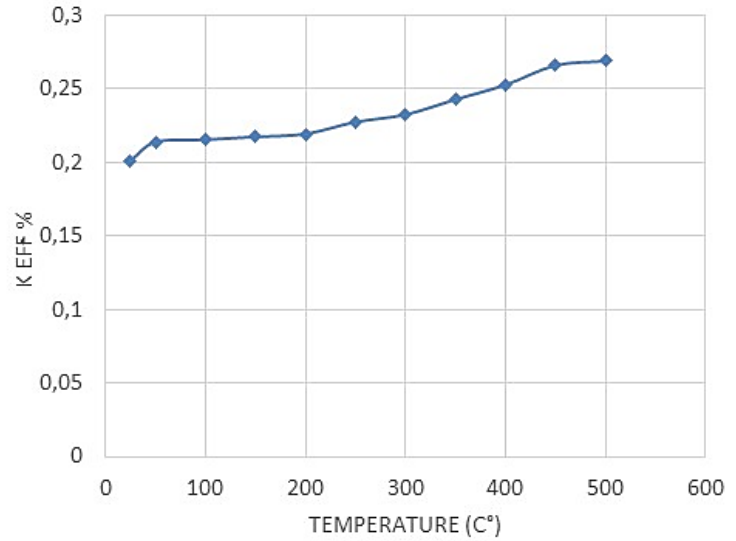
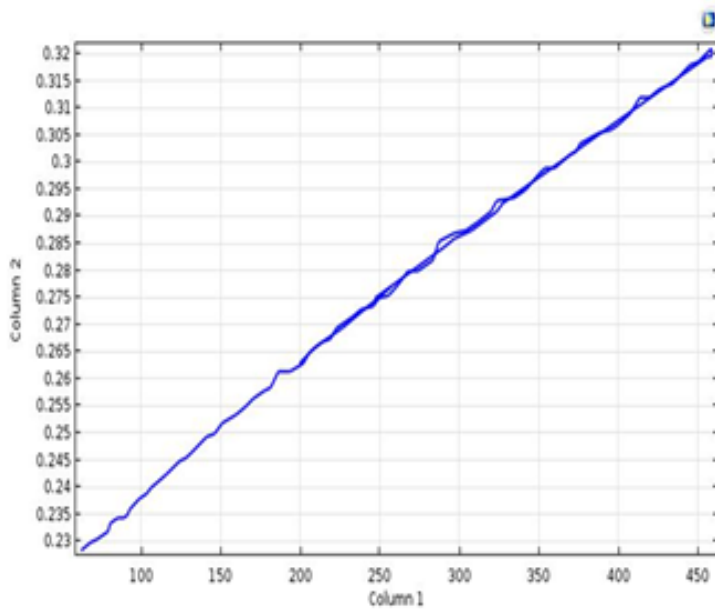
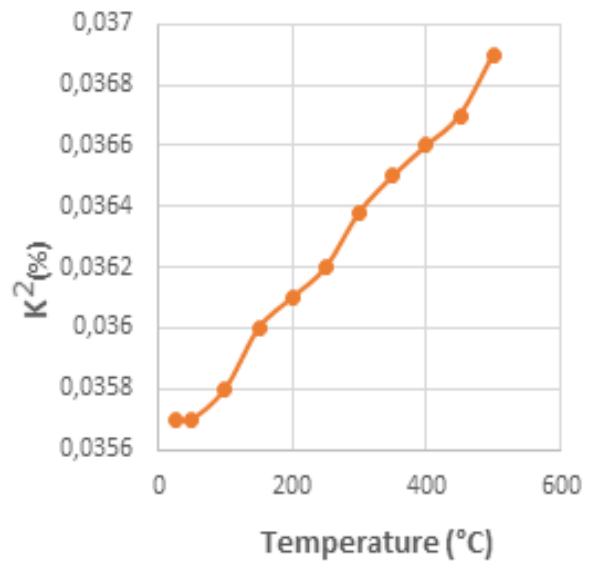


**Figure 4.27:** Influence of temperature on coupling coefficient of the structure Pt/AlN/Si.



Experimental



theoric

**Figure 4.28:** Influence of Temperature on coupling coefficient of the structure Pt/AlN/Pt/Si.

## 6. Delay line -Type SAW Sensor: (As perspectives)

In this section, and in order to optimize the applications of the SAW sensor. we present an exemple of SAW delay line type sensor. The proposed structure can be used for wireless interogation SAW sensor. The response of the sensor recorded in time domaine, deduced by the invers fast Fourier transform (IFFT) on its frequency response.

### 6.1. What does delay line mean?

A wireless delay line-type SAW sensor ([Figure 4.29.a](#)) receives an interrogation pulse through an antenna. The electromagnetic pulse is transformed into SAW with an interdigital transducer (IDT) placed on the piezoelectric material [64]. The reflectors, placed on the substrate, reflect the interrogation pulse back to the IDT, which again converts the SAW into electrical signal ([Figure 4.29.b](#)). This response signal consisting of delayed reflections is then transmitted back to the interrogation unit ([Figure 4.30](#)).

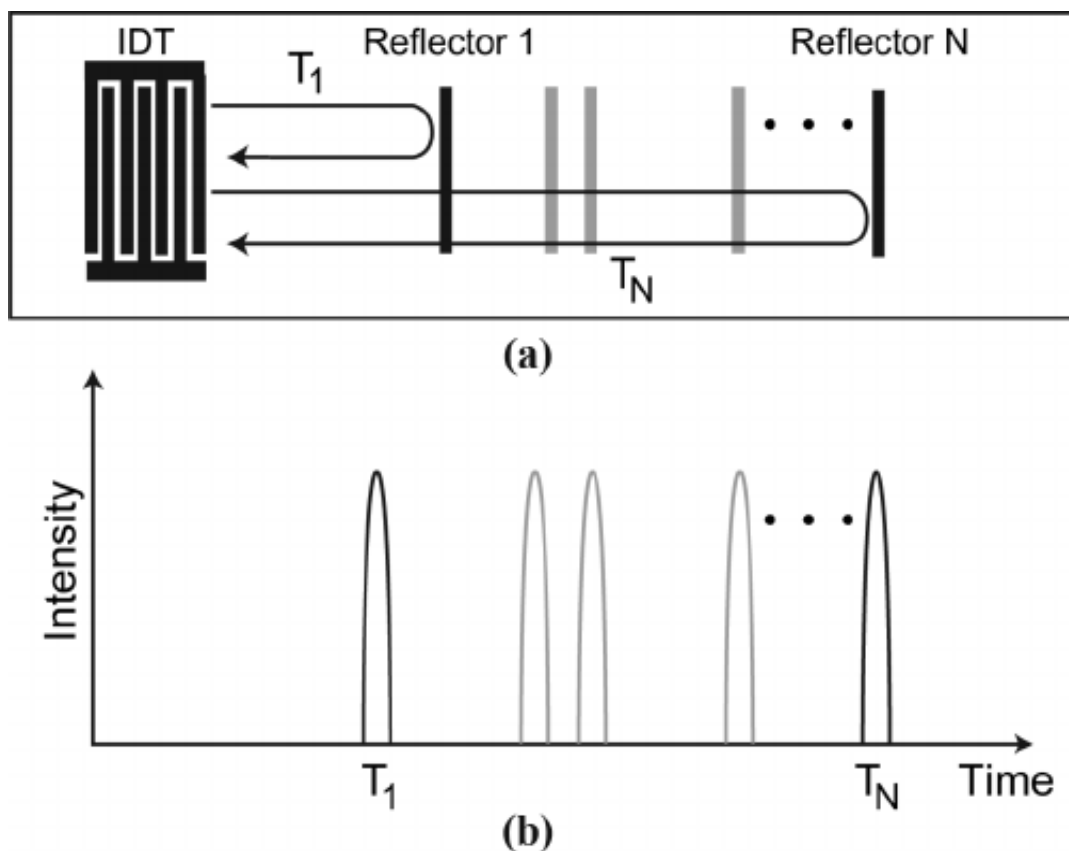


**Figure 4.29:** a schematic layout of reflective delay line surface acoustic wavesensor (a) and the corresponding impulse response of the sensor (b).

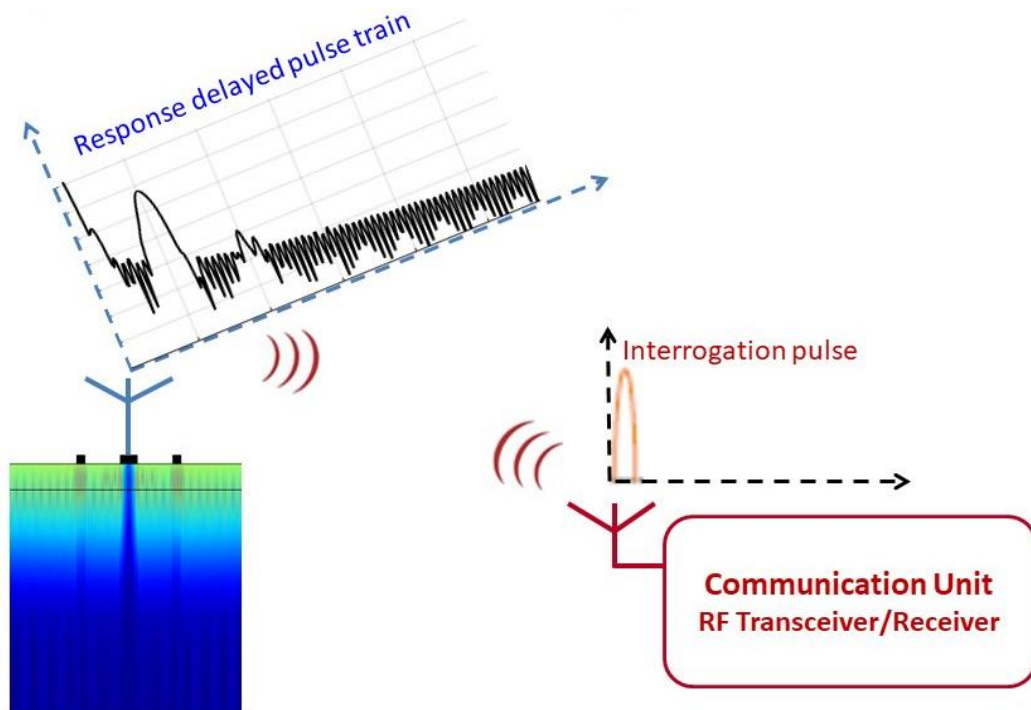


**Figure 4.30:** Intregation principle of the SAW sensor.

## 6.2. Simulation of Pt/AlN/Si SAW delay line.

We consider a two-dimensional (2D) structure, of a SAW transducer in the  $0xz$  plane, (see figure 4.31), we are interested in the excitation of the piezoelectric effect through the application of an external electric field on the input inter-digit electrodes, and than deduce the reflective signal caused by the reflector system in time domaine.

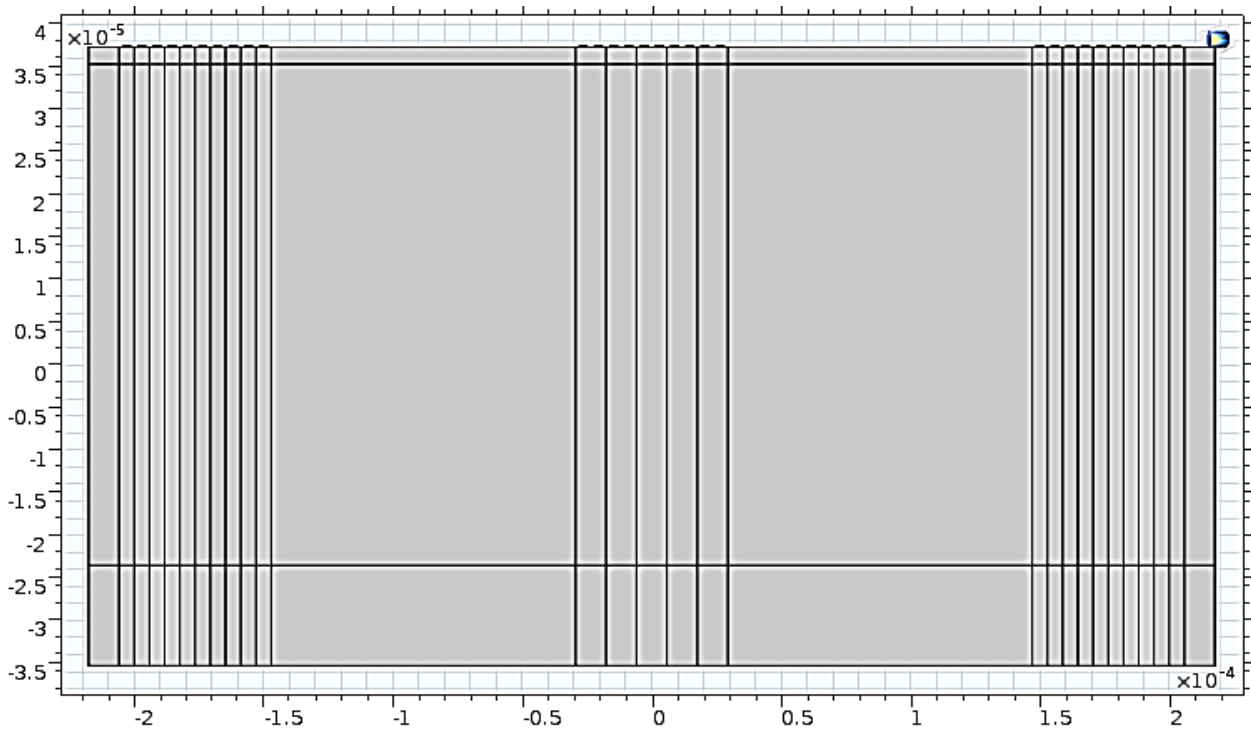


**Figure 4.31:** SAW structure Pt/AlN/Si delay line by comsol software.

The geometrical parameters used in the simulation of the delay line are illustrated in table 4.1.

**Table 4.1:** The new parameter for delay line

<b>Name</b>	<b>Expression</b>
Df	$(f_f - f_i)/200$
F <sub>f</sub>	500 MHz
F <sub>i</sub>	340 MHz
F <sub>0</sub>	440 MHz
N <sub>p</sub>	5
N <sub>B</sub>	10
L <sub>b</sub>	10*lamda

At the frequency  $f_0=439.74$  MHz, the mechanical displacement field is maximum and is confined in the reflector system and on the IDTs.



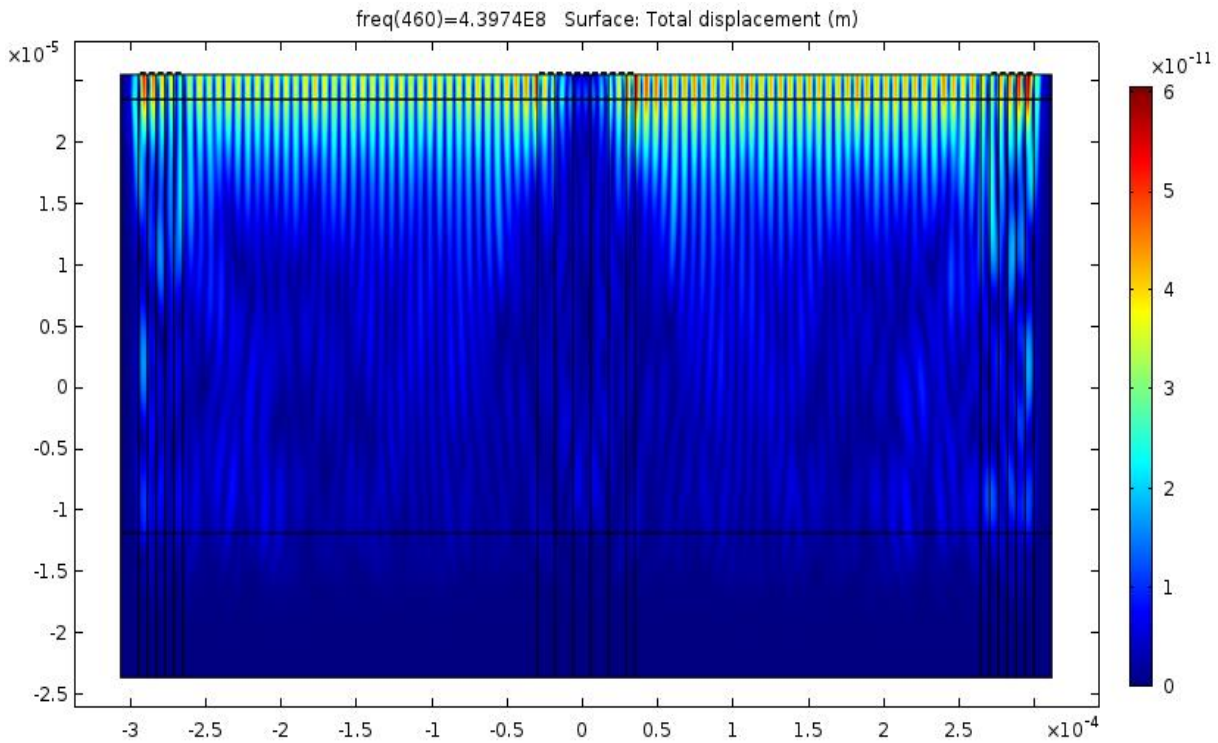


**Figure 4.32:** Mechanical displacement field of SAW delay line sensor at  $f=439.74$  MHz.

For this SAW delay line, and using COMSOL Multiphysics, the simulated  $S_{11}$  in the frequency domain is presented in figure 4.33. It presents a minimum of 0.991 dB at the frequency of 439.74 MHz, where the the mechanical displacement field is previously observed.  $S_{11}$  presents, also, some equidistant minima intensity due to the multiple reflections between transmitter/receiver IDTs and reflector systems separated by a distance of  $10\lambda$ . The representation of the  $S_{11}$  in time domain is obtained by calculating the inverse Fourier transform (IFFT) curve using Matlab program, (given in appendix A).

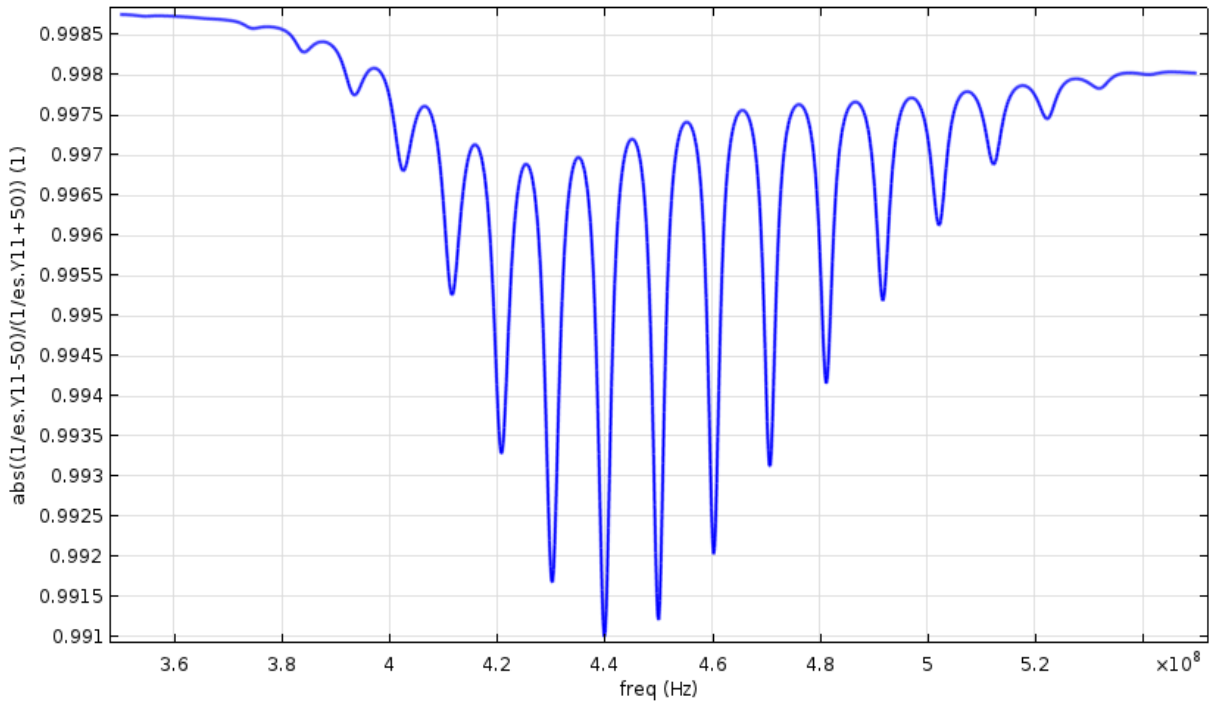


**Figure 4.33:** Simulated  $S_{11}$  in the frequency domain was obtained by comsol

The IFFT curve is obtained by calculating the Inverse Fourier transform with respect to  $x$ , the calculation program by Matlab is given in appendix A .

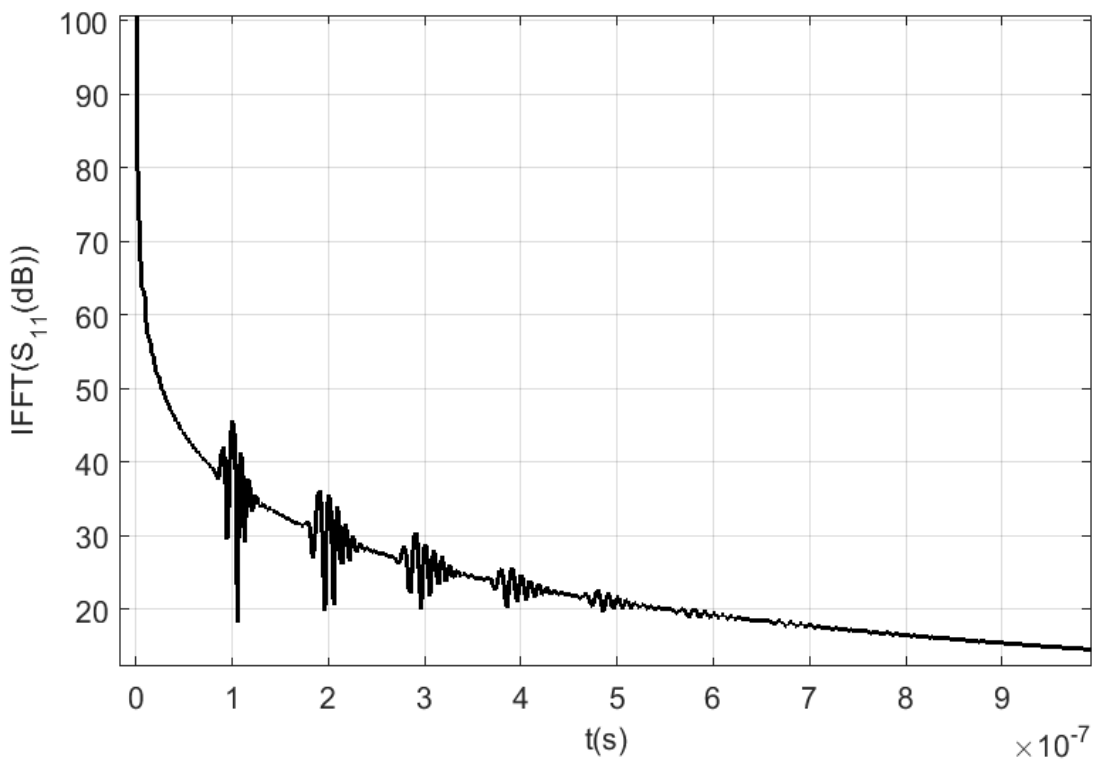


**Figure 4.34:** Simulated  $S_{11}$  in time domain using Matlab program.

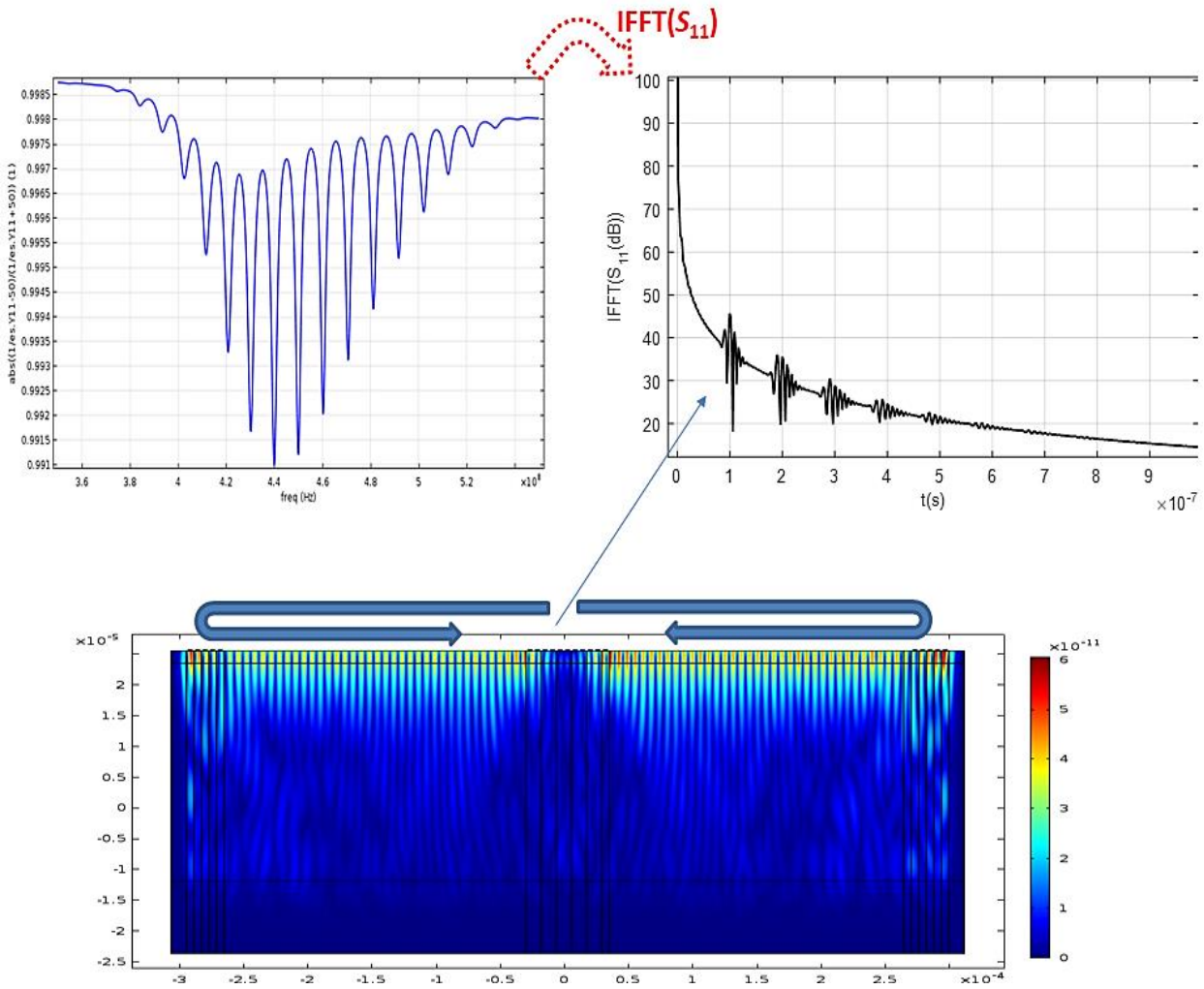


**Figure 4.35:** Resume of delay line SAW sensor.

**Important remarque:**

In our FEM mode, and in order to reduce the calculating time, we have simulated a SAW structure with  $N_b=50$  instead of  $N_b=400$  (as used in literature [60], Chuan Li *et al.*). In reality Bragg reflectors became to be efficient from  $N_b = 10$  or  $N_b=50$ , this is presented in figure 4.36, so  $N_b=50$  is sufficient for forming the acoustic resonant cavity, and it's not nessery to go up to  $N_b=400$  to get the good result.

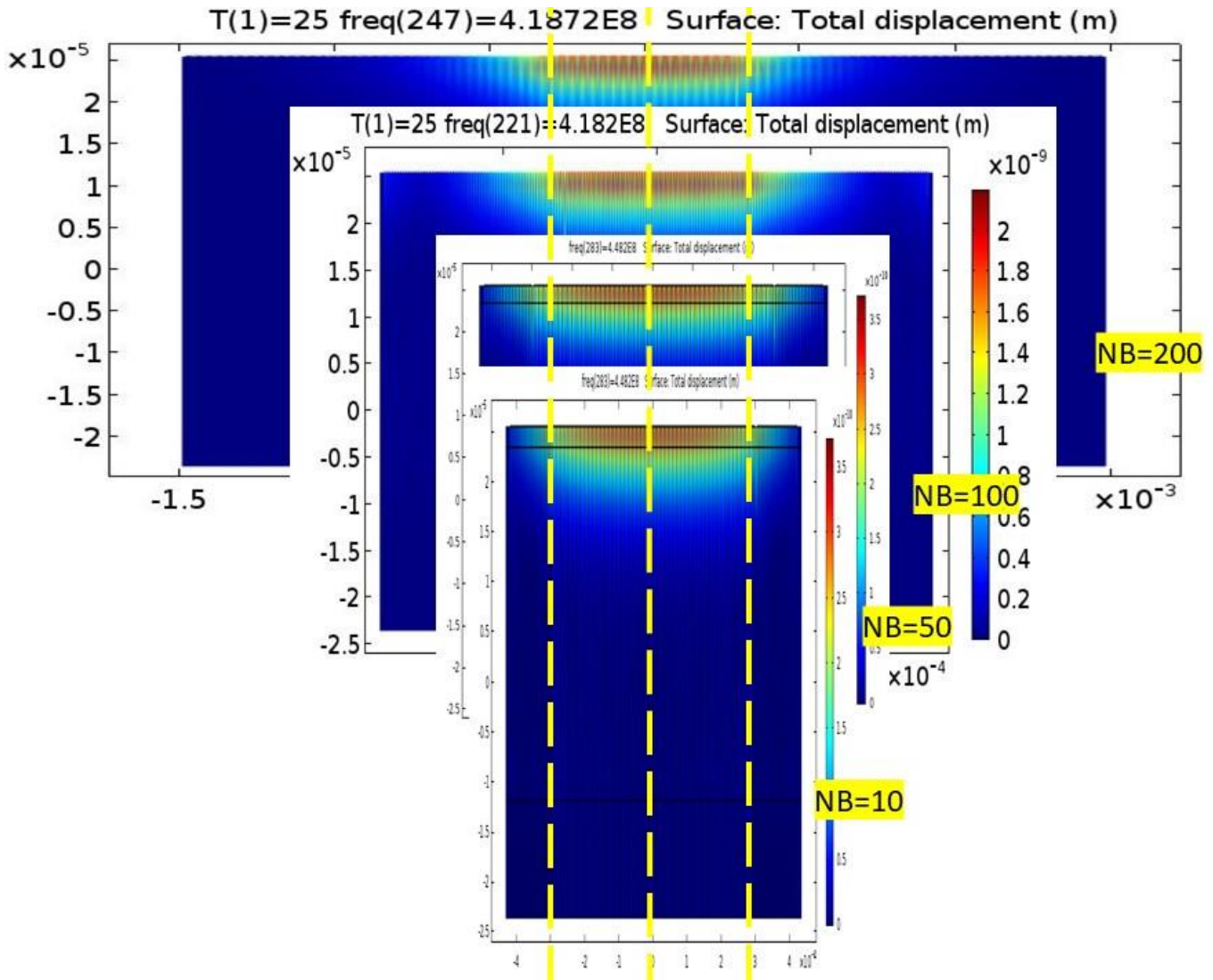


**Figure 4.36:** The mechanical displacement field for different values of Bragg relector numbers.

## 7. Conclusion:

SAW resonators with *Pt/AIN/Si* and *Pt/AIN/Pt/Si* configurations were simulated with Comsol software, we have obtained the results and we have done a comparative study on both configurations. The performances of sensors were evaluated for different values of temperature in the range of 25 to 500 °C. The center frequencies of *Pt/AIN/Si* and *Pt/AIN/Pt/Si* configuration are **420.28 MHz** and **445.01 MHz**, respectively, at room temperature. The TCF values of *Pt/AIN/Si* and *Pt/AIN/Pt/Si* are  **$-40.329 \times 10^{-6}$**  and  **$-40.54 \times 10^{-6} \text{ C}^{-1}$** , respectively. As a result, the SAW resonator with Pt Bottom Layer has good performance for temperature sensor applications.

The comparison made on the results, obtained by our theoretical FEM model and by the experimental results of Chuian Li, shows that they are in a good agreement, and this confirms the validity and the reliability of our FEM model.

## General Conclusion:

In this manuscript, we have carried out a simulation, under a COMSOL multi physics environment, of a temperature sensor based on a SAW transducer. We started this work with a brief summary on SAW sensors, we also present the main theoretical foundations, necessary to understand their operating principle and their main characteristics.

Our contribution, focused on the study of the center frequency shift of resonator due to the temperature changes, the electromechanical coupling coefficient, the quality factor, and the temperature coefficient of frequency (TCF), which represent the sensitivity of the sensor.

First, we recalled the theoretical approach of SAW device, we gave some generalities on the piezoelectric phenomenon, its governing equations, the main piezoelectric materials used in MEMS domain, and on the propagation of surface acoustic waves in piezoelectric materials. We have also presented the operating principle of SAW transducers.

Secondly, we have presented the procedure and steps of the FEM simulation using COMSOL multi physics environment. Then, we performed the 2D simulation of a SAW sensor, this gives a good approximation for the problem resolution. This FEM model is coupled to the theoretical temperature effect model to get the response of the SAW temperature sensor.

The obtained results are in a good agreement with those established in the works of Chuin Li et al. and allowed the validation of our FEM model. We have considered in this work, two types of SAW sensor, a multilayer **Pt/AlN/Pt/Si** and **Pt/AlN/Si** SAW resonators operating respectively at 445.01 and 420.28 MHz, and tested for different values of temperature, in the range of 20°C to 500°C. The electrical measurements revealed a piezoelectric response with a quality factor  $Q_r$  of 985 at resonance frequency. The electromechanical coupling coefficient ( $k_{\text{eff}}^2$ ) was estimated to be 0.32% at 500°C, and the temperature coefficient of frequency (TCF) value is -40.50 ppm/°C.

As perspectives, it would be interesting to extend the study on the SAW delay line working in time domain, in order to optimize their performances and to use it as a tag in wireless radio frequency (RF) sensors and communication.

# Appendix (A)

Matlab program to plot the  $S_{11}$  in the frequency domain

```
clear all
close all
clc
data=load('real_imag_S11.txt');
f=data(:,1);
real_S11=data(:,2);
imag_S11=data(:,3);
S11=real_S11+1i*imag_S11
plot(f,10*log(abs(S11)), 'LineWidth',2)
% Create xlabel
xlabel('f(Hz)', 'FontSize',16);
% Create ylabel
ylabel('S_1_1 (dB)', 'FontSize',16);
df=f(2)-f(1);
add_zero=fix(f(1)/df)
S11_extend= [ S11(1)*ones(add_zero,1) ; S11];
f_extend=0:df:(length(S11_extend)-1)*df
hold on
plot(f_extend,10*log(abs(S11_extend)), 'r', 'LineWidth',1)
Ne=length(f_extend);
fe=(Ne-1)*df;
dt=1/fe;
t=0: dt:(Ne-1)*dt;
IFFT_S11=(ifft(S11_extend))*df;
figure(2)
% subplot(311)
plot(t(1:Ne/2),10*log(abs(IFFT_S11(1:Ne/2))), 'k', 'LineWidth',2)
% subplot(312)
% plot(t,real(IFFT_S11), 'k', 'LineWidth',2)
% Create xlabel
xlabel('t(s)', 'FontSize',16);
% Create ylabel
ylabel('IFFT(S_1_1 (dB))', 'FontSize',16
```

## **Bibliographical Reference**

- [1] Lord Rayleigh, "On Waves Propagated Along the Plane Surface of an Elastic Solid," Proc. London Math. Soc., vol. s1-17, No. 1, pp.4–11, 1885.
- [2] JIANG, Xiaoning, KIM, Kyungrim, ZHANG, Shujun, *et al.* High-temperature piezoelectric sensing. *Sensors*, 2013, vol. 14, no 1, p. 144-169.
- [3] LI, Chuan, LIU, Xingzhao, SHU, Lin, *et al.* AlN-based surface acoustic wave resonators for temperature sensing applications. *Materials Express*, 2015, vol. 5, no 4, p. 367-370.
- [4] LIU, Yi et CUI, Tianhong. Power consumption analysis of surface acoustic wave sensor systems using ANSYS and PSPICE. *Microsystem technologies*, 2007, vol. 13, no 1, p. 97-101.
- [5] DHILLON, S. S., VITIELLO, M. S., LINFIELD, E. H., *et al.* The 2017 terahertz science and technology roadmap. *Journal of Physics D: Applied Physics*, 2017, vol. 50, no 4, p. 043001.
- [6] SATYANARAYANA, T., SRINIVAS, G., PRASAD, MVVK Srinivas, *et al.* Design and analysis of MEMS based composite piezoelectric ultrasonic transducer. *Electrical and Electronic Engineering*, 2012, vol. 2, no 6, p. 362-373.
- [7] CAMARILLO, David B., KRUMMEL, Thomas M., et SALISBURY JR, J. Kenneth. Robotic technology in surgery: past, present, and future. *The American Journal of Surgery*, 2004, vol. 188, no 4, p. 2-15.
- [8] WILSON, William C. et JUAREZ, Peter D. Emerging needs for pervasive passive wireless sensor networks on aerospace vehicles. *Procedia Computer Science*, 2014, vol. 37, p. 101-108.
- [9] STRASHILOV, Vesseline L. et YANTCHEV, Ventsislav M. Surface transverse waves: properties, devices, and analysis. *IEEE transactions on ultrasonics, ferroelectrics, and frequency control*, 2005, vol. 52, no 5, p. 812-821.
- [10] BUCHWALD, V. T. et DAVIS, A. Surface waves in anisotropic elastic media. *Nature*, 1961, vol. 191, no 4791, p. 899-900.
- [11] FARNELL, Waves GW. Types and properties of surface. *Acoustic surface waves*, 1978, p. 13-60.
- [12] COLLET, Bernard, DESTRADE, Michel, et MAUGIN, Gérard A. Bleustein–Gulyaev waves in some functionally graded materials. *European Journal of Mechanics-A/Solids*, 2006, vol. 25, no 5, p. 695-706.
- [13] AVRAMOV, Ivan D. High-performance surface transverse wave resonators in the lower GHz frequency range. *International journal of high speed electronics and systems*, 2000, vol. 10, no

03, p. 735-792.

- [14] F. Arduini et G. Palleschi, "Screening and confirmatory methods for the detection of heavy metals in foods", in *Persistent Organic Pollutants and Toxic Metals in Foods*, Elsevier, p. 81–109, 2013
- [15] FARRÉ, Marinella, KANTIANI, Lina, PÉREZ, Sandra, *et al.* Sensors and biosensors in support of EU Directives. *TrAC Trends in Analytical Chemistry*, 2009, vol. 28, no 2, p. 170-185.
- [16] FARRÉ, Marinella, KANTIANI, Lina, PÉREZ, Sandra, *et al.* Sensors and biosensors in support of EU Directives. *TrAC Trends in Analytical Chemistry*, 2009, vol. 28, no 2, p. 170-185.
- [17] Hashimoto et Ken-Ya. "Surface Acoustic Wave Devices in Telecommunications", Springer: Berlin/Heidelberg, Germany, 2000.
- [18] R. Guldiken, M. C. Jo, N. D. Gallant, U. Demirci, et J. Zhe, "Sheathless Size-Based Acoustic Particle Separation", *Sensors*, vol.12, n° 1, p.905–922, 2012.
- [19] T. Wang, Q. Ni, N. Crane, et R. Guldiken, "Surface acoustic wave based pumping in a microchannel", *Microsystem Technologies*, vol. 23, n° 5, p. 1335–1342, 2017.
- [20] J.R. Gell, M.B. Ward, R.J. Young, R.M. Stevenson, P. Atkinson, D. Anderson, G. A.C. Jones, D.A. Ritchie, et A.J. Shields, "Modulation of single quantum dot energy levels by a surface-acoustic-wave", *Applied Physics Letters*, vol. 93, n° 8, p. 081115, 2008.
- [21] R. Aigner, "SAW and BAW technologies for RF filter applications: A review of the relative strengths and weaknesses", In *Proceedings of the 2008 IEEE Ultrasonics Symposium*, p. 582–589, Beijing, China, 2008.
- [22] O. Onen, A. Sisman, N. D. Gallant, P. Kruk, et R. Guldiken, "Urinary Bcl-2 Surface Acoustic Wave Biosensor for Early Ovarian Cancer Detection", *Sensors*, vol. 12, n°6, p.7423–7437, 2012.
- [23] A. Marcu et C. Viespe, "Surface Acoustic Wave Sensors for Hydrogen and Deuterium Detection", *Sensors*, vol. 17, n° 6, p. 1417, 2017.
- [24] A. Hachigo et D. C. Malocha, "SAW dispersive equivalent circuit modeling for diamond layered structures", *Proceedings IEEE Ultrasonics Symposium*, vol.1, p. 151-154, San Antonio, Texas, USA, 1996.
- [25] K.-Y. Hashimoto, "Simulation of Surface Acoustic Wave Devices", *Japanese Journal of Applied Physics*, vol.45, p.4423–4428, 2006.
- [27] KAŽYS, R., VOLEIŠIS, Algirdas, et VOLEIŠIENĖ, Birutė. High temperature ultrasonic transducers. *Ultragarsas/Ultrasound*, 2008, vol. 63, no 2, p. 7-17.
- [28] ELMAZRIA, Omar et AUBERT, Thierry. Wireless SAW sensor for high temperature applications: Material point of view. In : *Smart Sensors, Actuators, and MEMS V*. SPIE, 2011. p. 19-28.



- [29] A. Kateb, “Analyse du signal micro-onde acoustique via la transformée en ondelettes”, Mémoire de Magister, Université de Batna, (2013).
- [30] C. Zimmermann, “Conception réalisation et études de microcapteurs a ondes de love pour applications en milieu gazeux cas de la détection de composes organophosphoré”, Thèse de Doctorat, Université de Bordeaux 1, (2002).
- [31] XU, Runjie Lily, MUÑOZ ROJO, Miguel, ISLAM, S. M., et al. Thermal conductivity of crystalline AlN and the influence of atomic-scale defects. *Journal of Applied Physics*, 2019, vol. 126, no 18, p. 185105.
- [32] TANIYASU, Yoshitaka, KASU, Makoto, et MAKIMOTO, Toshiki. An aluminium nitride light-emitting diode with a wavelength of 210 nanometres. *nature*, 2006, vol. 441, no 7091, p. 325-328.
- [33] STRITE, a S. et MORKOÇ, Hy. GaN, AlN, and InN: a review. *Journal of Vacuum Science & Technology B: Microelectronics and Nanometer Structures Processing, Measurement, and Phenomena*, 1992, vol. 10, no 4, p. 1237-1266.
- [34] C-Y. Yeh, Z. W. Lu, S. Froyen, and A. Zunger. Zinc-blende-wurtzite polytypism in semiconductors. *Physical Review B*, 46(16) :10086, 1992.
- [35] CLAUDEL, Arnaud. Elaboration et caractérisation de couches de nitrure d'aluminium AlN par CVD haute température en chimie chlorée. 2009. Thèse de doctorat. Institut National Polytechnique de Grenoble-INPG.
- [36] T. Goto, J. Tsuneyoshi, K. Kaya, and T. Hirai. Preferred orientation of AlN plates prepared by chemical vapour deposition of AlCl<sub>3</sub> + NH<sub>3</sub> system. *Journal of Materials Science*, 27(1):247,254, 1992.
- [37] A. Dollet, Y. Casaux, M. Matecki, and R. Rodriguez-Clemente. Chemical vapour deposition of polycrystalline AlN lms from AlCl<sub>3</sub>-NH<sub>3</sub> mixtures: II Surface morphology and mechanisms of preferential orientation at low-pressure. *Thin Solid Films*, 406(1-2):118,131, 2002.
- [38] Y. Pauleau, J.J. Hantzpergue, and J.C. Remy. Les couches minces de nitrure d'aluminium. *Bulletin de la Societe Chimique de France, Partie I* (n 5-6) :199 214, 1979.
- [39] Y. G. Roman and A. P. M. Adriaansen. Aluminium nitride lms made by low pressure chemical vapour deposition: Preparation and properties. *Thin Solid Films*, 169(2) :241248, 1989.
- [40] Theoretical Interpretation of Impulse Response Tests of Embedded Concrete Structures *Journal of Engineering Mechanics*, Vol. 130, No. 9, September 1, 2004. ©ASCE,

## ISSN.

- [41] <https://onscale.com/the> impulse response.
- [42] E. A. Guillemin, *theory of linear physical systems*. New York Wiley, ch. 16, 1963
- [43] Machui, et al, a New low loss SAW filter structure with extremely wide bandwidth for mobile communication systems. In *Microwave Symposium Digest, 1993. IEEE MTT-S International*, pages 1501–1504. IEEE, 1993.
- [44] <http://www.rfm.com/products/SAWfilters.php>.
- [45] L. Reindl et W. Ruile, "Programmable reflectors for SAW-ID-tags. In *Ultrasonics Symposium, 1993. Proceedings, IEEE, volume 1, p. 125–130, 1993*.
- [46] M. Mohamed, El Gowini and Waled A. Moussa, « A Reduced Three Dimensional Model for SAW Sensors Using Finite Element Analysis », *Sensors*, 9, 9945-9964, 2009.
- [47] H. Wohltjen, « mechanism of operation and design considerations for surface acoustic wave device vapour sensors », *Sensors and Actuators*, 5, 307- 325, 1984.
- [48] J. O. Kim, "The effect of a viscous fluid on Love waves in a layered medium", *The Journal of the Acoustical Society of America*, vol. 91, n° 6, p. 3099–3103, 1992.
- [49] F. Herrmann, D. Hahn, et S. Büttgenbach, "Separate determination of liquid density and viscosity with sagittally corrugated Love-mode sensors", *Sensors and Actuators A: Physical*, vol. 78, n° 2-3, p. 99–107, 1999.
- [50] J. Comput, Bérenger. *Phys.* 114, 185 (1994).
- [51] J. Zhao, C. Jiang, Y. Chen, H. Li, et S. He, "A study of Love wave sensors with SU-8 guiding layers", *IEEE Ultrasonics Symposium*, p. 1120–1123, Beijing, China, 2008.
- [52] W. Wang et S. He, "Sensitivity Evaluation of a Love Wave Sensor with Multi-guidinglayer Structure for Biochemical Application", *Sensors & Transducers Journal*, vol. 96, n°9,p.32-41, 2008.
- [53] E. Gizeli, C. R. Lowe, M. Liley, et H. Vogel, "Detection of supported lipid layers with the acoustic Love waveguide device: application to biosensors", *Sensors and ActuatorsB: Chemical*, vol. 34, n° 1–3, p. 295–300, 1996.
- [54] O. Tamarin, S. Comeau, C. Déjous, D. Moynet, D. Rebière, J. Beziau, J. Pistré, "Real time device for biosensing: design of a bacteriophage model using love acousticwaves", *Biosensors and Bioelectronics*, vol. 18, n° 5-6, p. 755-763, 2003.
- [55] N. Moll, E. Pascal, D.H. Dinh, J-P. Pillot, B. Bennetau, D. Rebière, D. Moynet, Y. Mas, D. Mossalayi, J. Pistré, et C. Déjous, "A Love wave immunosensor for whole E. colibacteriadetection using an innovative two-step immobilisation approach",

Biosensors and Bioelectronics, vol. 22, n° 9-10, p. 2145-2150, 2007.

[56] S. Lee, K.-B. Kim, et Y.-I. Kim, "Love wave SAW biosensors for detection of antigen-antibody binding and comparison with SPR biosensor", Food Science and Biotechnology, vol. 20, n° 5, p. 1413–1418, 2011.

[57] H. J. Lee, K. Namkoong, E. C. Cho, C. Ko, J. C. Park, et S. S. Lee, "Surface acoustic wave immunosensor for real-time detection of hepatitis B surface antibodies in whole blood samples", Biosensors and Bioelectronics, vol. 24, n° 10, p. 3120–3125, 2009.

[58] P. Tang, Y. Wang, J. Huo, et X. Lin, "Love Wave Sensor for Prostate-Specific Membrane Antigen Detection Based on Hydrophilic Molecularly-Imprinted Polymer", Polymers, vol. 10, n° 5, p. 563, 2018.

[59] L. Rana, R. Gupta, M. Tomar, et V. Gupta, "Highly sensitive Love wave acoustic biosensor for uric acid", Sensors and Actuators B: Chemical, vol. 261, p. 169-177, 2018.

[60] LI, Chuan, LIU, Xingzhao, SHU, Lin, *et al.* AlN-based surface acoustic wave resonators for temperature sensing applications. *Materials Express*, 2015, vol. 5, no 4, p. 367-370.

[61] Richter, D.; Fritze, H. High-temperature Stable Electrodes for Langasite Based Surface Acoustic Wave Devices. In Proceedings of the Sensor+Test Conferences 2011, Nürnberg, Germany, 9 June 2011; pp. 532–537. ]

[62] C. M. Lin, T. T. Yen, V. V. Felmetger, M. A. Hopcroft, J. H. Kuypers, and A. P. Pisano; Thermally compensated aluminum nitride lamb wave resonators for high temperature applications; *Appl. Phys. Lett.* 97, 083501 (2010).

[63] C. M. Lin, V. Yantchev, J. Zou, Y. Y. Chen, and A. P. Pisano; Micromachined one-port aluminum nitride lamb wave resonators utilizing the lowest-order symmetric mode; *J. Microelectromech. Syst.* 23, 78

[64] r. M. White and F. W. Voltmer, "direct piezoelectric coupling to surface elastic waves," *Appl. Phys. Lett.*, vol. 7, pp. 314–316, 1965. .